Ultra-Large-Pore Ordered Mesoporous Organosilicas and Related Hollow Nanoparticles

By

Manik Mandal

A dissertation submitted to the graduate Faculty in Chemistry in partial fulfillment of the requirement for the degree of Doctor of Philosophy, The City University of New York

2010

This manuscript has been read and accepted for the Graduate Faculty in Chemistry in satisfaction of the dissertation requirement for the degree of Doctor of Philosophy

Prof. Michal Kruk

_____ _____

Date Chair of Examining Committee

Prof. Mahesh K. Lakshman

_____ _____

Date Executive Officer

Prof. Glen R. Kowach

_____

Prof. Krishnaswami Raja

_____

Supervisory Committee

THE CITY UNIVERSITY OF NEW YORK

Abstract

Ultra-Large-Pore Ordered Mesoporous Organosilicas and Related Hollow Nanoparticles

By

Manik Mandal

Advisor: **Professor Michal Kruk**

My dissertation describes the synthesis of ultra-large-pore ordered mesoporous organosilicas and related hollow nanoparticles. In the first part, we developed a versatile approach through which a series of periodic mesoporous organosilicas (PMOs) with 2-dimensional hexagonal structure and different bridging groups can be synthesized. The bridging groups are methylene (-CH_2-), ethylene (-CH_2CH_2-), ethenylene (-CH=CH-), and phenylene (-C_6H_4-). For this purpose, a combination of a commercially available triblock copolymer Pluronic P123 ($EO_{20}PO_{70}EO_{20}$) with judiciously chosen micelle swelling agent (cyclohexane, or 1,3,5-triisopropylbenzene) was used as a miceller template, and the initial step of the synthesis was performed at temperature between 10 and 18 ^{o}C, followed by hydrothermal treatment at 100-150 ^{o}C. The PMOs were characterized using small-angle X-ray scattering (SAXS), nitrogen adsorption, transmission electron microscopy, and solid-state ^{29}Si NMR. For all PMO compositions, the formation of 2-D hexagonal structures with (100) interplanar spacing, d_{100}, up to 21-26 nm was achieved, which is at least seven nanometers larger than d_{100} reported earlier for any PMO with 2-D hexagonal structure. The nominal (BJH) pore diameters up to 20-

27 nm were achieved for the considered compositions of PMOs with with 2-D hexagonal ordering, while even larger pore sizes were sometimes attained for disordered or weakly ordered structures. The mesopores exhibited constrictions or narrow entrances that were widened by increasing the hydrothermal treatment temperature. The pore diameter tended to increase as an initial synthesis temperature decreased, allowing for the pore size adjustment, but the useful temperature range depended on the bridging groups. The present work suggests that the low-temperature micelle-templated synthesis with judicious selected swelling agents is a general pathway to ultra-large-pore 2-D hexagonal PMOs with both aliphatic and aromatic bridging groups.

In the second part, we have demonstrated the synthesis of large-pore ethylene-bridged periodic mesoporous organosilica with face-centered-cubic structure. This was achieved by the use of judiciously chosen swelling agents and Pluronic F127 block copolymers at sub-ambient temperature (~ 15 ^{o}C). While our work confirmed that 1,3,5-trimethylbenzene (TMB) which was already employed by other researchers, is a facile swelling agent for Pluronic F127-templated ethylene-bridged PMOs with cubic Fm3m structure and our optimization of the synthesis afforded hitherto unreported unit-cell size and pore size for this PMO, it was also demonstrated that swelling agent predicted to have a higher extent of solubilization in Pluronics than TMB provide vast new opportunities. In particular, xylene was found to afford highly ordered materials with large unit-cell size and pore diameter, and a wide range of moderately or weakly ordered materials with very large unit-cell parameters (up to ~ 50 nm) and some with very large pore diameters (up to ~ 20 nm). In this case, the pore size and unit-cell size was tunable by adjusting the amount of inorganic salt (KCl) in the synthesis mixture. The use toluene

allowed for the increase in the primary mesopore volume and also afforded large-pore PMOs in the absence of an inorganic salt. The use of the latter was also not required when benzene was used as a swelling agent. The identification of new swelling agents for ethylene-bridged PMO with spherical mesopores is likely to be extendable on PMOs of other framework compositions and for other related materials.

In the third part, based on understanding of the condition for the formation of ordered mesoporous organosilicas, we were able to synthesize hollow nanoparticles with different organic bridging groups. Different organic bridging groups such as methylene, ethylene, ethenylene, and phenylene were incorporated in the organosilica walls of the hollow nanoparticles. Further, we were able to synthesize hollow nanotubules comprising of these bridging groups in the walls.

I dedicate this dissertation
to my parents
Shikha Mandal and Binoy Kumar Mandal

ACKNOWLEDGEMENTS

I would like to express my sincere gratitude to Dr. Michal Kruk, for his guidance, expertise, supports throughout my research career, and willingness to explore the sport of science freely.

My grateful thanks are due to thesis committee members: Dr. Michal Kruk, Dr. Glen R. Kowach, City College (CUNY), and Dr. Krishnaswami Raja, College of Staten Island (CUNY) who mentored the progression of my research work annually.

I also would like to thank the other group members: Dr. Liang Cao, Ms. Liang Huang, Ms. Tiffany Man, Ms. Kristina Foulias, and Mr. Abhisek Roka for their help and encouragement and also for maintaining friendly atmosphere in the laboratory.

I also acknowledge Professor Bradley F. Chmelka, and his student Mr. Robert J. Messinger, University of California (Santa Barbara), for analyzing some of my samples using two dimensional NMR technique and providing profound insight into their molecular-scale structures. I also owe thank to scientists of College of Staten Island for their help with various analytical techniques.

I sincerely acknowledge Dr. Jianqin Zhuang (CSI) for assistance with NMR measurements. The imaging facility at CSI is acknowledged for providing access to transmission electron microscope.

The continuous source of inspiration has been my family members and friends, who enabled me to complete this long expedition.

Lastly I would like to acknowledge support from National Science Foundation (CHE-0723028, and DMR-0907487); American Chemical Society Petroleum Research Fund (Award PRF #49093-DNI5); and Doctoral Students Research Grants.

M. Mandal

Table of Contents

List of Tables

List of Figures

1. Introduction

The sol-gel process is an important method through which inorganic materials are formed through hydrolytic polycondensation. Sol-gel technique uses molecular chemistry approach to synthesize new materials in contrast to classical high-temperature approach for the synthesis of solid state materials.[1,2] Among the materials accessible through the sol-gel process, materials containing Si-O-Si chemical linkages (silicas and their derivatives) are very attractive. The most common precursor used for synthesizing such materials is tetraalkoxysilane, such as tetraethylorthosilicate (TEOS), and tetramethylorthosilicate (TMOS). Sol-gel polymerization of tetraalkoxysilane involves hydrolysis and condensation to form silica gel, and is catalyzed by acid or base. During the polymerization, the silica precursor hydrolyses and condenses to form silica polymer until it attains a critical size at which it starts forming gel and precipitates out. The final morphology of the materials depends upon the conditions of hydrolysis and condensation and subsequent drying and processing.[1]

The potential of inorganic polymers, such as silica, can be greatly extended by the introduction of organic groups in silica-based frameworks to form inorganic-organic hybrid materials.[1,3] The resulting hybrids, which are derived from bis(trialkoxysilyl)organic or multi(trialkoxysilyl)organic precursors, can be considered as derivatives of silica in which some of the siloxane (Si-O-Si) bridges are replaced by Si-R-Si bridges, where R is an organic group. This architecture offers a wealth of opportunities in tailoring physical and chemical properties of materials due to the possibility of incorporation of a variety of bridging organic groups. Some of the representative precursors with various organic bridging groups are shown below:

AROMATIC

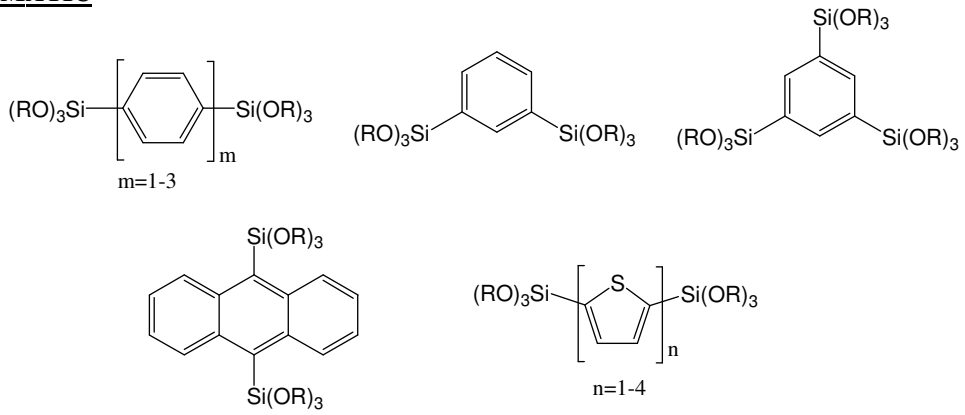

ALKYNE

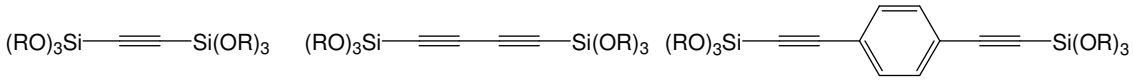

ALKENE

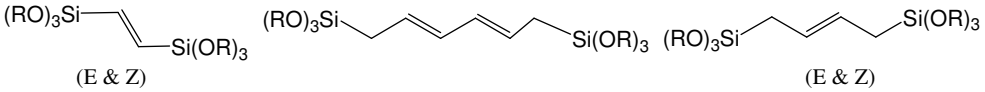

ALKANE

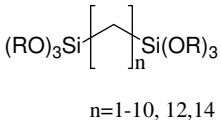

FUNCTIONALIZED

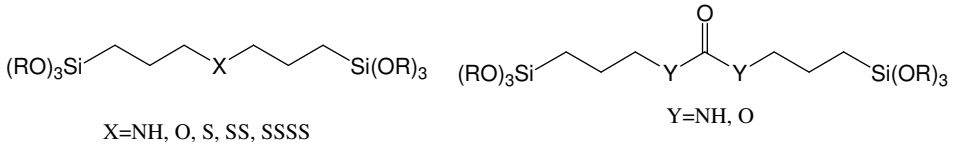

ORGANOMETALLIC

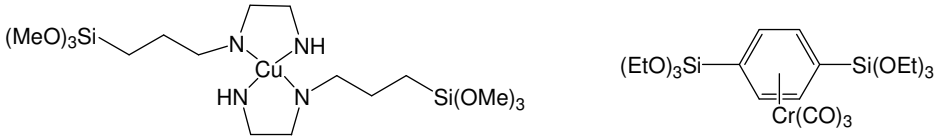

Figure 1.1 Representative molecular precursors used in sol-gel processing to form silica-based inorganic-organic hybrid materials (adapted from reference 4).

The molecular precursors include siloxanes containing aliphatic (such as alkane, alkene, alkylene), and aromatic bridging groups (such as benzene, biphenylene). In some cases, these precursors contain functional groups, such as amine, thiol, ether, polysulphide, ketone, and carboxy. In addition, metals may form the part of the bridging

group, or be included in a pendant group. These precursors undergo sol-gel polymerization to form polymers (or gels) with inorganic-organic hybrid network. Initial work using these precursors to form microporous materials was carried out by mostly Loy and Shea, as well as the Corriu group with additional contribution from others.[4-28] The organic content in the framework could be as high as 40-60 wt% of the material.[29] These required precursors are known from as early as early nineteen forties. At the beginning, these precursors were used in surface modifications, coatings, coupling agents, or adhesives. Although the silica prepared by sol-gel method is amorphous, the inorganic-organic hybrid materials synthesized using the same method can feature short range ordering.[30-34]

The discovery in early nineteen nineties of the micelle-templating approach to the synthesis of well-defined mesoporous materials led to another breakthrough in the synthesis of the silica-based materials, endowing them with periodic nanopore structures of well-defined morphology, and uniform pore diameter.[35-47] The resulting materials are commonly referred to as ordered mesoporous silicas (OMS) and periodic mesoporous organosilicas (PMOs). The materials synthesis involves the formation of surfactant-(solid-framework) nanoscale composites. The solid framework could be either inorganic,[48-50] or inorganic-organic hybrid in nature.[51,52] Initially, it was envisioned that the formation of silica-surfactant nano-composites involves the formation of a liquid crystal phase, that is the silica precursor forms a nanoscale composite with preformed liquid crystalline phase of micelles, such as arrays of micelles arranged in two-dimensional hexagonal structure.[36] But soon, it was realized that the actual mechanism is usually far from that involving the formation of a true liquid crystalline structure of

surfactant.[35] Later, it was found that liquid crystal templating mechanism indeed could be operative under certain conditions which are not so typical in the formation of silica-surfactant nanoscale composites.[53,54]

In late nineteen ninetees, oligomer and block-copolymer surfactants were found to be attractive alternatives[55-61] of alkylammonium surfactants[35,36] and neutral amine surfactants.[62,63] Amphiphilic block copolymers, such as Pluronics, are known to form micelles of uniform size.[64,65] Pluronics are poly(ethylene oxide)-poly(propylene oxide)-poly(ethylene oxide) (PEO-PPO-PEO) block copolymers and are commercially available with different molecular weight and PEO/PPO weight fraction. The micelles formed could be several nanometers to tens of nanometers in size with well-defined shape, such as spherical and cylindrical. PEO-PPO-PEO block copolymer has hydrophobic PPO block and hydrophilic PEO blocks. In aqueous solutions, these surfactants form micelles where PPO forms the core and PEO forms the corona surrounding the core. The silica or organosilica precursor interacts with the PEO chains of the micelles,[66-68] although in the case of organosilica, the interaction of precursor could extend further to the PPO block.[68,69] The inclusion of PEO blocks into the silica and organosilica frameworks was used to explain the generation of microporosity in the materials after block-copolymer removal.[70,71] The condensation of the silica precursors takes place in the proximity of PEO chains without having any direct ionic or covalent linking between PEO chains and silica precursor. In contrast, in the case of alkylammonium (cationic) surfactant templated materials, there exist ionic interactions between the silica or organosilica precursor and the surfactant ions. This difference in interaction between two different kinds of surfactants has some implications. First, the amount of precursor could be varied to a

significant amount without changing the structure type in the case of PEO-based surfactants,[72] while in the case of alkylammonium (cationic) surfactants, the amount of precursor required is fully dependent on charge matching between the alkylammonium surfactant and precursor.[73] The stoichiometry of silica precursor with respect to the surfactant is not strictly defined in the case of PEO-based surfactant, the excess amount of precursor (such as tetraethylorthosilicate, TEOS or perhaps bis(trialkoxysilyl)organosilane)) may form constrictions or "plugs" in the main mesopores.[74,75] The plugs appear due to the solubilization of the hydrophobic silica/organosilica precursor with the hydrophobic PPO block.[68,75] The use of low precursor/surfactant ratio is considered to be the cause of thinning of the pore walls,[72] but no further structural implications were envisioned until recently. In the cases described above, the surfactant micelles are covered with framework precursor that occludes hydrophilic PEO blocks. While this is a common scenario in case of materials with ordered structure, there could be another possibility of formation of individual micelles covered with the framework precursor, that is, the formation of isolated nanoobjects.

Since their discovery, OMSs[35,36,56,57] and PMOs[44-47] have attracted much attention of the scientific community due to their high prospect of applications.[49] Particularly, periodic mesoporous organosilicas (PMOs), in which the organic groups are homogenously distributed in the silica-based framework, are appealing compared to mesoporous silicas, because it is easier to tailor the physical and chemical properties in case of PMOs. Initial reports on the synthesis of large-pore PMOs indicate that using block-copolymers, large-pore PMOs can be obtained. Froeba et al. and Dutartre et al. reported large-pore PMOs in 2001 which were prepared using Pluronic P123 block

copolymers as template.[76,77] While Dutartre et al. obtained highly ordered materials, PMOs obtained by Froeba et al. much less ordered ones, as seen from XRD patterns. A careful investigation of the synthetic routes indicates that while the first group used highly concentrated solution of block copolymers, the latter used dilute solution of block copolymers for the PMO synthesis. This indicates that the formation of organosilica-precursor/block-copolymer nanostructured composites is very much dependent on the mutual interaction between the components. Presumably, use of concentrated solution of amphiphilic block copolymer reduced interaction between the organosilica precursor and PPO blocks of copolymers, allowing for the retention of the original ordered liquid-crystalline arrangement and thus making the obtained materials highly ordered. Matos et al. used poly (ethylene oxide)-poly(butylene oxide)-poly (ethylene oxide) (PEO-PBO-PEO) surfactant, where the core of the micelle contains much more strongly hydrophobic PBO block, presumably reducing interaction between the PBO of block copolymer template and the organosilica precursor. They obtained ordered material with large cage-like pores of size ~ 10 nm.[78] The above mentioned explanation regarding reduced interaction between the hydrophobic core and the precursor can be further verified from the fact that the use of salt in block copolymer solution when used in combination with organosilica precursors produces ordered PMOs. For example, Guo et al. obtained large-pore ordered 3D PMOs using salt while absence of salt produces much less ordered materials.[79] The addition of salt in the block copolymer solutions dehydrates both hydrophobic and hydrophilic blocks, thereby making the overall micelle formed by the block copolymers in solution more hydrophobic. It is not fully clear why this helps in

forming well-defined PMOs. Anyway the use of large hydrophobic domain in block copolymer or use of salt typically helps in obtaining ordered PMOs.[78-80]

So far, PMOs have been synthesized with a variety of organic bridging groups,[68] including short saturated aliphatic linkages (methylene, $-CH_2-$, ethylene, $-CH_2-CH_2-$ and their mono- or disubstituted derivatives)[44-46,81-83] and unsaturated carbon chains (ethenylene, -CH=CH-),[45,46] longer chain-like bridges with heteroatoms,[84] as well as aromatic bridges (including 1,4-phenylene, $-C_6H_4-$, biphenylene, $-C_6H_4-C_6H_4-$ and their derivatives, as well as 2,5-thiophene, $-C_4H_2S-$).[47,85,86] In addition to the above two-point-attachment bridges, a variety of more complicated structural units, including aromatic,[87] heteroatom-containing cyclic and multicyclic,[88-91] branched[92] and dendritic moieties,[93] were successfully incorporated in PMOs. An additional structural diversity was achieved through co-condensation of bridged-organosilanes with one another,[94] or with non-bridged organotrialkoxysilanes (the resulting materials were referred to as bi-functional PMOs, BPMOs).[95-98] Moreover, the co-condensation of the bridged organosilanes with silica precursors opened an opportunity to "dilute" organic groups in the framework[45] or to incorporate bridging groups that are not suitable (or not envisioned) to afford a sustainable porous structure.[99-101] However, in the case of the latter co-condensation strategy, the presence of organic groups in the periodic framework (rather than on the surface of the pure-silica framework or in separate non-mesostructured domains) is difficult to ascertain.[51] PMOs can also be doped with heteroatom (Al,[102] Ti,[103,104] V[105]) in a manner similar to that for pure-silica materials.

In addition to different chemical composition, a variety of nanoscale structures with ordered geometry have been achieved for PMOs,[68] including 2-dimensional hexagonal

structure with cylindrical pores,[44,68] 3-dimensional hexagonal ($P6_3/mmc$),[44] cubic Pm3n,[82] body-centered cubic (Im3m),[79] and face-centered cubic (Fm3m)[106-108] structures with spherical pores as well as gyroidal (Ia3d)[109] structure of approximately cylindrical pores with intersections. The structure type can be controlled to an appreciable extent by the selection of suitable single surfactant or mixed surfactant template.[110,111]

While the framework composition of PMOs can be varied over wide range, their pore size was found much less adjustable[68] compared to their pure-silica counterparts.[56,112-116] The pore size of PMOs was tailored by using surfactant molecules of different size, for instance, alkylammonium surfactant of different chain length,[117-120] oligomeric surfactants,[121] and block copolymers[76-78,122-131] (in which case a hydrothermal treatment was also found suitable to tune the pore size[78,130]), affording cylindrical or spherical mesopores of diameters from ~ 2 to 10 nm.[78,102,123] In comparison, the templating with commercially available and custom-made surfactants affords ordered mesoporous silicas with cylindrical pores of diameter from 2 to at least 16 nm,[35,56,112,132,133] and spherical pores of diameter up to 31 nm.[113,114,134] Moreover, the use of micelle swelling agents, which in the case of ordered mesoporous silicas allows one to obtain cylindrical and spherical pores of diameter up to 26-36 nm,[115,116,135] typically afforded organosilicas that had disordered (or poorly ordered) enlarged pores,[106,136-140] or heterogeneous mesoporous structures with a fraction of ordered large-pore domains.[141] A successful swelling-agent-based low-temperature synthesis of well-ordered large-pore PMO with Fm3m structure of spherical mesopores of diameter up to ~15 nm is notable exception,[107] while other well-ordered PMOs synthesized in the presence of swelling agents had moderate pore diameters.[111,142-144] Our literature survey indicates that in the case of PMOs with well-

ordered 2-D hexagonal structure of cylindrical mesopores, the largest pore diameter was ~ 10 nm,[123,125] and the largest (100) interplanar spacing, d_{100}, was 13-14 nm.[90,93] It should be noted that d_{100} multiplied by 1.155 provides the unit-cell parameter that is equal to the distance between the pore centers in 2-D hexagonal structure. In contrast, 2-D hexagonal silicas with pore diameters and d_{100} interplanar spacings up to 26 nm were reported.[116,145] Likewise, pore sizes reported for PMOs with spherical mesopores were much lower than those for pure-silica materials. Therefore, there is a clear need for new approaches to the pore size engineering for PMOs to overcome the limitations dicussed above.

Recently, new opportunities emerged in the micelle-expander-based synthesis of large-pore ordered mesoporous silicas.[68] The use of appropriate swelling agents (hexane and TMB) at sub-ambient initial temperature (~ 15 ^{o}C) afforded large-pore SBA-15 silica (LP-SBA-15) with cylindrical mesopores up to ~ 15 nm[146] and LP-FDU-12 silica with Fm3m structure of spherical mesopores of diameter up to ~ 27 nm.[115] In the latter case, the pore diameter was found to increase as the initial synthesis temperature decreased from 23 to 14-15 ^{o}C, thus allowing one to adjust the pore diameter through the control of the initial synthesis temperature. The TMB-based low-temperature synthesis of Fm3m structures of spherical mesopores was extended on ethylene-bridged PMO, and in particular, the temperature lowering led to the increase in the unit-cell parameter and pore size,[107] but in comparison to LP-FDU-12 silica, the PMO had somewhat smaller unit-cell size and much smaller pore diameter (~ 15 nm). The studies of LP-SBA-15 and LP-FDU-12 silicas[147,148] indicated that the amounts of the swelling agents (hexane or TMB) solubilized in the block copolymer micelles were quite small. This stimulated the search for swelling agents that would solubilize in micelles to a more significant extent than the

swelling agents mentioned above, yet not in excessive amount,[116] which is known to lead to foam-like[149] or otherwise disordered products.[150] Based on earlier studies[151,152] of solubilization of organic compounds in micelles and on their extrapolation within families of similar compounds, 1,3,5-triisopropylbenzene (TIPB) and cyclohexane were identified[116] as promising swelling agents in conjunction with commercially available Pluronic P123 ($EO_{20}PO_{70}EO_{20}$) triblock copolymer surfactant, which is the most common copolymer template for 2-D hexagonal materials, including SBA-15 silica[56,57] and PMOs.[77,122,128,130] Cyclohexane is particularly interesting, because it is a cost-effective, common reagent and solvent. The use of a moderate amount of cyclohexane afforded well-ordered large-pore SBA-15 with d_{100}= ~ 13 nm, whereas the use of its large amount led to a disordered large-pore (~20 nm) product, confirming that cyclohexane is a potent swelling agent. The use of TIPB afforded SBA-15 silica with pore diameters from 10 to 26 nm,[116] thus achieving a major advance in the synthesis of this important material.

In the first part of this dissertation,[68] it is shown that the application of cyclohexane and TIPB in combination with Pluronic P123 provides a simple and versatile route to families of 2-D hexagonal ultra-large-pore PMOs with aliphatic and aromatic bridging groups in the framework and with nominal (BJH) pore diameters from 12 nm to 20-27 nm, which corresponds to actual pore diameters approaching 20 nm.

Another topic of interest is the formation of ordered spherical mesopores arranged in 3-dimensional structure.[108] First, PMOs were synthesized using bis(trialkoxysilyl)organic precursors and cationic alkylammonium surfactants as templates[44-47,82] and a remarkable tendency to the formation of highly ordered structures with spherical mesopores was observed.[44,82] More specifically, common alkylammonium surfactants

(cetyltrimethylammonium, octadecyltrimethylammonium) known from their tendency for templating 2-D hexagonal structures of silicas (MCM-41,[35] FSM-16[39]) afforded 3-D hexagonal ($P6_3/mmc$) and cubic Pm3n organosilica structures. Since then, a variety of alkylammonium surfactants were successfully used to template the aforementioned and other PMO structures with spherical mesopores, including face-centerd cubic (Fm3m) structure.[111,153-155] The resulting materials showed pore sizes up to ~ 7 nm.[111,156] Oligomeric surfactants also afforded PMOs with spherical mesopores of size comparable to that achievable with alkylammonium surfactants.[157]

The introduction of block copolymes as templates for PMO synthesis[76-78] opened new opportunities in engineering of ordered arrays of spherical mesopores.[108] However, the block-copolymer-templated synthesis of PMOs with spherical pores proved to be challenging. An initial work with Pluronic copolymers indicated that the use of commercially available Pluronic F127 ($EO_{106}PO_{70}EO_{106}$) affords well defined organosilica structures when the bridged organosilane precursor is mixed with a substantial amount of the silica precursor.[158] It was argued[158] that the properties of the hydrophobic block of the copolymer template have a crucial effect on the synthesis of well-defined PMOs. This contention was soon confirmed with the successful synthesis of PMO with with spherical mesopores template by poly(ethylene oxide)-poly(butylene oxide)-poly(ethylene oxide) triblock copolymer (PEO-PBO-PEO),[78] whose middle block was more hydrophobic than the PPO blocks in Pluronics. The resulting PMO had large mesopores (~ 10 nm) with narrow size distribution, and a periodic structure, as seen from small-angle X-ray scattering (SAXS) and TEM. Although the structure was originally not assigned,[78] the reported SAXS reflections correspond to the interplanar spacing ratios of

1 : 1.64 : 2.60 : 2.88, which can be identified as (111), (220), (331), and (422) reflections of Fm3m structure, matching reflections observed later[107] for ethylene-bridged PMO synthesized at low initial temperature in the presence of TMB. On the basis of the identification as Fm3m structure, the unit-cell parameter of the PEO-PBO-PEO-templated PMO was 24 nm. However, block copolymer templates with suitable hydrophobic blocks (such as PBO) are not readily available commercially. Therefore, an important breakthrough in the synthesis of copolymer-templated PMOs with spherical mesopores was the use of inorganic salts to facilitate the formation of the periodic nanostructure, which first led to ethylene-bridged PMO with body-centered cubic (Im3m) structure and pore diameter ~ 10 nm templated by Pluronic F127.[79,80] A similar synthesis approach afforded ethylene-bridged PMO with Fm3m structure under somewhat lower acid concentration.[106,159] Subsequent synthesis of phenylene- and thiophene-bridged PMOs with Im3m structure[160] proved that the use of inorganic salts is not necessary for the formation of highly-ordered Pluronic-templated PMOs with spherical mesopores. Phenylene-bridged PMO with spherical pores was also synthesized by Inagaki et al.,[161] but the structure was not assigned. Mixed-phase ethenylene-bridged PMO with very large pores (18.5-28.3 nm) containing a fraction of Fm3m structure was also reported, although in this case, Pluronic P123 ($EO_{20}PO_{70}EO_{20}$) was used as a template in the presence of 1,3,5-trimethylbenzene (TMB) as a swelling agent.[141]

A recently developed low-temperature approach to the copolymer template synthesis of ordered mesoporous materials[68,107,115,116,145-148,162-164] brought new opportunities in the synthesis of PMOs with spherical mesopores.[68,107,108] As was originally demonstrated on large-pore FDU-12 (LP-FDU-12) silica with Fm3m symmetry (unit-cell parameter up to

44 nm),[115] the low initial synthesis temperature (~ 15 °C) in combination with the addition of a suitable swelling agent (for instance, TMB for LP-FDU-12) allows one to appreciably increase the unit-cell size and pore diameter of FDU-12[165] materials. A judicious selection of a swelling agent (such as xylene for LP-FDU-12) led to a further increase in the unit-cell size achievable at low temperature for LP-FDU-12 (unit-cell parameter up to 56 nm).[135] The low temperature procedure originally developed for silicas has been extended on ethylene-bridged PMO with Fm3m structure (unit-cell parameter up to 37 nm),[107] and more recently on a variety of 2-D hexagonal PMOs (d_{100} up to at least 20 nm) as already mentioned.[68] The realization that the use of a more strongly solubilized swelling agent can improve the TMB-based synthesis of LP-FDU-12 led to the identification of xylene and toluene as swelling agents for ultra-large-pore FDU-12 synthesis.[135]

Large-pore mesoporous materials are important for practical applications. In particular, PMOs are suitable as catalysts or catalysts supports,[166] immobilization media for biomolecules,[142] templates for nanostructures,[167] precursors for ceramics,[159] and adsorbents.[168] For the application point of view, materials with three-dimensionally connected cage-like mesopores have some advantages over the two-dimensional pore structures, because the differences in the molecular transport phenomena and avoidance of pore blocking. The ability to design large-pore materials is also an important problem from the point of view of fundamental materials research. While PMOs and related materials with very large mesopores are known,[68,107,137,139,141] most of them are appreciably disordered, while highly ordered PMO with very large spherical mesopores

was reported only in the case of the use of Pluronic F127 and TMB in the low-temperature synthesis procedure.[107]

In the second part of this dissertation,[108] it is shown that the large-pore ethylene-bridged PMOs with unprecedented structural properties can be achieved through our low-temperature synthetic route, which involves either TMB, which was used by others in a similar synthesis,[107] or other judiciously selected swelling agents, namely xylene, toluene, and benzene. The use of selected swelling agents, combined with the optimization of the amount of the inorganic salt, afforded highly-ordered Fm3m PMOs with the unit-cell parameter ~ 40 nm, and a range of materials with even larger unit-cell size (up to 50 nm and beyond) with gradually diminished degree of structural ordering. Highly ordered products had the pore diameter of ~ 14-17 nm, where as the less-well-ordered counterparts reached the pore size of ~ 20 nm. To the best our knowledge, these are the largest unit-cell sizes and pore diameters achieved for well ordered PMOs with spherical mesopores.

While lot of research interest has been focused on the formation of periodic, surfactant-templated consolidated structures which were discussed above, much less is known about the formation of individual inorganic nanoobjects, such as nanoparticles and nanotubules. So far, different nanoparticles and nanotubules consisting of carbon, boron nitride and silica have been synthesized.[169-174] These nanoobjects are mostly synthesized under drastic conditions such as very high temperature. Since the discovery of consolidated surfactant-templated nanotubules consisting of silica by Mobil scientists in early nineteen nineties,[35,36] a wide range of consolidated inorganic materials has been synthesized as discussed above. These materials resemble bundles of nanotubules arranged in 2-D

hexagonal pattern (honeycomb structure, although there is no void between the tubules). It appears that the same strategy should afford individual micelle-templated nanotubules, but surprisingly little is known on generating isolated micelle-templated objects, and known examples are primarily hollow spheres.[175-191] It appears that single nanotubules are not available due to the lack of understanding of formation mechanism of these materials.

In many cases, single nanotubules or nanoparticles potentially could be more useful than their condensed counterparts, as the former can act as building blocks for making more complicated architectures. Moreover, this single building block can be filled with other materials to form composite materials or functionalized with other groups to change the properties. Hollow nanoparticles and nanotubules could be used as drug delivery vehicles, and contrast agents.[174-191]

Recently, we studied the use of block copolymer as templates to obtain ordered mesoporous organosilica materials with cylindrical and spherical mesopores.[68,108] These mesoporous organosilica materials were prepared by hydrolyzing bis(trialkoxysilyl)silane precursors, where the organic group can be a short aliphatic (methylene, ethylene) chain, or unsaturated chain (ethenylene) or aromatic ring (phenylene). In some cases, we observed the formation of hollow nanoparticles. The formation of these nano-structures was achieved through a particular selection of the block copolymer template and the composition of the synthesis medium. There arises a question why certain conditions (such as low precursor/surfactant ratio) lead to individual particles. Normally, it was observed in numerous studies that surfactant interacts with silica/organosilica sources to form consolidated structures, such as ordered mesoporous silicas or organosilicas. In one

case, the individual particles were stabilized using an agent that would suppress cross-linking between the particles, so that a consolidated structures would not form.[175] It was suggested that isolated particles form at lower silica-surfactant ratio while a larger relative amount of silica precursor leads to the formation of consolidated structures,[182,183] but the transition was not fully understood.

Our literature survey shows that so far only ethylene-, phenylene-, and 1,4-diethylphenylene-bridging groups have been introduced in case of hollow nanospheres with walls comprising of organosilica.[177-180] Phenylene-bridged hollow nanospheres can be easily chemically modified, but ethylene-bridged organosilicas are less amenable to chemical functionalization. In this regard, it would be desirable to introduce other organic groups, which can be easily chemically modified for prospective applications. Other groups, including unsaturated ones, could give rise to more applications. So it is desirable to obtain materials with functionalizable organic bridging groups, including saturated, unsaturated and aromatic bridges.

Our generalized synthesis of hollow micelle-templated nanoparticles is based upon understanding of the formation of organosilica/block copolymer nano-composites. We proposed a general mechanism based on understanding on the interaction between organosilica precursors and block-copolymers,[68,69] which can be used as a guideline for the synthesis of hollow nanospheres and nanotubules. This unique approach was realized by suitable choice of Pluronic block coplymer and suitable precursors under acidic media. Unlike any other route available so far, our approach is more versatile and general in that this method can be used for wide range of organosilica as well as silica precursors, such as those with aliphatic saturated bridging groups (methylene, and ethylene),

unsaturated bridges (ethenylene), and aromatic rings (phenylene) in the silica-based frameworks. This work highlights to the following aspects: synthesizing large-pore mesoporous organosilica hollow nanospheres and nanotubules, direct conversion of organosilica hollow particles to silica hollow particles, and the control of the pore size of the hollow nanospheres.

2. Materials and Methods

2.1.1 Synthesis of methylene-bridged PMO.[68] In a typical experiment, 2.40 g of Pluronic P123 was dissolved in 84 ml of 1.30 M HCl solution followed by mechanical stirring until the whole polymer dissolves completely at 15.00 ^{o}C (or other temperatures selected from 12.00-17.00 ^{o}C range). Then premixed bis(triethoxysilyl)methane, BTEM (Gelest Inc.) and 13 ml cyclohexane were added at once. The molar composition of the reaction mixture was BTEM/P123/cyclohexane/HCl/H_2O = 0.5+x/0.0168/4.88/4.42/186, where x=0.2, 0.3 (preferred composition) or 0.4. The whole solution was stirred for 1 day. Then the product was treated hydrothermally at 100 ^{o}C for 2 days (in closed polypropylene bottle) or at higher temperatures (130 or 150 ^{o}C) for 2 days. For hydrothermal treatment at higher temperatures, the solution was transferred to Teflon-lined autoclaves. The resulting as-synthesized materials were then filtered, washed with deionized water and dried at ~ 60 ^{o}C under vacuum. Finally, the materials were calcined under air (or nitrogen) at 300 ^{o}C for 5 h (heating ramp 2 ^{o}C min^{-1}). The surfactants were also removed by calcination under nitrogen or extracted using ethanol. In some cases, the materials were treated with NH_4OH and NH_4Cl buffer solution. For this purpose, 0.3 g of extracted material was treated with equal volume of each solution (total 18 ml of buffer solution) and heated at selected temperature (100, 130 or 150 ^{o}C) in a autoclave for 1 day. Then the sample was filtered, and dried in a vacuum oven at ~ 60 ^{o}C. Then the material was calcined under nitrogen at 300 ^{o}C for 5 hr (heating ramp 2 ^{o}C min^{-1}).

2.1.2 Synthesis of ethylene-bridged PMO.[68] 0.60 g of Pluronic P123 was dissolved in 21 ml of 1.3 M HCl solution using mechanical stirring until the whole polymer dissolved completely at 15.00 ^{o}C. Then premixed bis(trimethoxysilyl)ethane, BTME (Gelest Inc. or

Aldrich) or bis(triethoxysilyl)ethane, BTEE (Gelest Inc.) and 3.25 ml cyclohexane were added at once. The molar composition of the reaction mixture was BTME (or BTEE)/P123/cyclohexane/HCl/H_2O = 0.5+x/0.0168/4.88/4.42/186, where x=0.40, 0.60 (preferred composition), 0.70, 1.00, and 1.50 for BTME and 0.40 for BTEE. The whole solution was stirred for 1 day. Then the reaction mixture was treated hydrothermally at 100 ^oC for 2 days. The resulting as-synthesized materials were then filtered, washed with deionized water and dried at ~ 60 ^oC under vacuum. Finally, the materials were extracted with ethanol using Soxhlet apparatus and were dried.

2.1.3 Synthesis of ethenylene-bridged PMO.[68] 0.6 g of Pluronic P123 was dissolved in 21 ml of 1.3 M HCl solution using mechanical stirring until the whole polymer dissolved completely at 15.00 ^oC. Then premixed bis(triethoxysilyl)ethylene, BTEEn and 3.25 ml of cyclohexane were added at once. The molar composition of the reaction mixture was BTEEn/P123/cyclohexane/HCl/H_2O = 0.5+x/0.0168/4.88/4.42/186, where x=0.40, (or 0.70, if so noted). The whole solution was stirred for 1 day. Then the reaction mixture was treated hydrothermally at 100 ^oC for 2 days. The resulting as-synthesized materials were then filtered, washed with deionized water and dried at ~ 60 ^oC under vacuum. Finally, the materials were extracted with ethanol using Soxhlet apparatus and were dried.

2.1.4 Synthesis of material using $(CH_3O)_3Si\text{-}CH_2\text{-}C(=CH_2)\text{-}CH_2\text{-}Si(OCH_3)_3$ as precursor.[68] 0.6 g of Pluronic P123 was dissolved in 21 ml of 1.3 M HCl solution followed by mechanical stirring until the whole polymer dissolved completely at 15.00 ^oC. Then premixed bis(trimethoxysilylmethyl)ethylene, BTMSME (Gelest Inc.) and 3.25 ml cyclohexane were added at once. The molar composition of the reaction mixture was

BTSME/P123/cyclohexane/HCl/H_2O = 0.5+x/0.0168/4.88/4.42/186, where x=0.00, 0.30, 0.40, and 0.50. The whole solution was stirred for 1 day. Then the reaction mixture was treated hydrothermally at 100 ^oC for 2 days. The resulting as-synthesized materials were then filtered, washed with deionized water and dried at ~ 60 ^oC under vacuum. Finally, the materials were extracted with ethanol using Soxhlet apparatus and were dried.

2.1.5 Synthesis of phenylene-bridged PMO.[68] 0.60 g of Pluronic P123 was dissolved in 21 ml of 1.30 M HCl solution followed by mechanical stirring until the whole polymer dissolved completely at initial synthesis temperature selected in the range from 14.00-18.00 ^oC. Then premixed bis(triethoxysilyl)benzene, BTEB (Gelest Inc. or Aldrich) and 1.2 ml (or 0.6 ml) 1,3,5-triisopropylbenzene (TIPB) were added at once. The molar composition of the reaction mixture was BTEB/P123/TIPB/HCl/H_2O = 0.5+x/0.0168/0.79 (or 0.40)/4.42/186, with x=0.30. For optimization of the synthesis condition, the amount of BTEB was varied from x=0.00, -0.10, -0.15, -0.20, -0.30 (for 0.6 ml TIPB). The whole solution was stirred for 1 day. Then the reaction mixture was treated hydrothermally at 100 ^oC (or higher temperature up to 170 ^oC in a autoclave) for 2 days. The resulting as-synthesized materials were then filtered, washed with deionized water and dried at ~ 60 ^oC under vacuum. Finally, the materials were either extracted with ethanol using Soxhlet apparatus followed by drying and calcination under air at 250 ^oC[130], or calcined under nitrogen at 300 ^oC.

2.1.6 Synthesis of ethylene-bridged PMO with spherical pores.[108] In a typical experiment, 0.50 g of Pluronic F127 ($EO_{106}PO_{70}EO_{106}$) was dissolved in 30 g of 2.0 M HCl solution under mechanical or magnetic stirring at 15 ^oC. Then, 0.50 g (or 1.00 g, see below) of the swelling agent (TMB, 1,3,5-triisopropylbenzene (TIPB), 1,3,5-

triethylbenzene (TEB), xylene-mixture of isomers, toluene or benzene) and 2.50 g (or other amount) of KCl was added (except for benzene, in which case no salt was used). It should be noted that for TMB, TEB, TIPB, a mechanical stirrer set at a moderate stirring speed was used and the reaction mixture was prepared in a polypropylene (PP) bottle with its mouth taped with parafilm leaving a small hole for the stirrer. For xylene, toluene, and benzene, a magnetic stirrer (set at 300 rpm) was used and the reaction mixture was in a glass container whose mouth was taped with parafilm. After two hours, 2.90 g of bis(trimethoxysilyl)ethane (BTME) was added. The reaction mixture was stirred for one day at 15 ^{o}C (in a semi-closed container, as described above). Then, the reaction mixture was treated hydrothermally at 100 ^{o}C for one day in a closed PP bottle. The product was filtered out, washed with deionized water and dried at ~ 60 ^{o}C under vacuum. Finally, the surfactant was removed from the sample via the Soxhlet extraction with ethanol. One of the PMOs was calcined under argon or air at 350 and/or 400 ^{o}C (ramp 2 ^{o}C/min, dwell time 5 hours).

2.1.7 Synthesis of methylene-bridged organosilica hollow nanospheres. 0.50 g of Pluronic F127 was dissolved in 45 ml of 2 M HCl solution followed by magnetic stirring until the whole polymer dissolved completely at 15 ^{o}C. Then 0.5 g xylene and 2.5 g of KCl were added. After 2 h, 1.03 ml bis(triethoxysilyl)methane (BTEM) was added. The whole solution was stirred for 1 day. Then the reaction mixture was treated hydrothermally at 100 ^{o}C for 1 day. The resulting as-synthesized material was then filtered, washed with deionized water and dried at ~ 60 ^{o}C under vacuum. Finally, the material was calcined under nitrogen at 300 ^{o}C for 5 h with heating ramp 2 ^{o}C/min. The product was designated -CH_2-HS.

2.1.8 Synthesis of methylene-bridged organosilica nanotubules. 1.2 g of Pluronic P123 was dissolved in 42 ml of 1.3 M HCl solution followed by mechanical stirring until the whole polymer dissolved completely at 15 ^{o}C. Then, after at least 3h, a mixture of 2.15 ml BTEM and 6.5 ml cyclohexane was added. The solution was stirred for 1 day. Then the reaction mixture was treated hydrothermally at 100 ^{o}C for two days. The resulting as-synthesized material was then filtered, washed with deionized water, and dried at ~ 60 ^{o}C under vacuum. Finally, the material was calcined under nitrogen at 300 ^{o}C for 5 h with heating ramp 2 ^{o}C/min. The product was designated -CH_2-NT.

2.1.9 Synthesis of ethylene-bridged organosilica hollow nanospheres. 0.50 g of Pluronic F127 was dissolved in 30 g of 2 M HCl solution followed by magnetic stirring until the whole polymer dissolved completely at 15 ^{o}C. Then 0.5 g toluene was added. After 2 h, 0.93 ml bis(trimethoxysilyl)ethane (BTME) was added. The solution was stirred for 1 day. Then the reaction mixture was treated hydrothermally at 100 ^{o}C for 2 days. The resulting as-synthesized material was then filtered, washed with deionized water and dried at ~ 60 ^{o}C under vacuum. Finally, the material was extracted with ethanol using Soxhlet apparatus and dried. For materials with different pore sizes, the same procedure but different swelling agents (benzene, xylene, or TMB) were used. The product was designated –C_2H_4-HS.

2.1.10 Synthesis of ethylene-bridged organosilica nanotubules. 1.2 g Pluronic P123 was dissolved in 42 ml of 1.3 M HCl solution followed by mechanical stirring until the whole polymer dissolved completely at 15 ^{o}C. After at least 3h, 0.014 g NH_4F was added. Then, after another 1 h, a mixture of 2.28 ml bis(triethoxysilyl)ethane (BTEE) and 6.5 ml cyclohexane was added. The whole solution was stirred for 1 day. Then the reaction

mixture was treated hydrothermally at 100 ^{o}C for two days. The resulting as-synthesized material was then filtered, washed with deionized water and dried at ~ 60 ^{o}C under vacuum. Finally, the material was extracted with ethanol using Soxhlet apparatus and dried. The product was designated –C_2H_4-NT.

2.1.11 Synthesis of ethenylene-bridged organosilica hollow nanospheres. 0.50 g of Pluronic F127 was dissolved in 30 g of 2 M HCl solution followed by magnetic stirring until the whole polymer dissolved completely at 15 ^{o}C. Then 0.5 g xylene and 2.5 g KCl were added. After 2 h, 0.87 ml bis(triethoxysilyl)ethylene (BTEEn) was added. The solution was stirred for 1 day. Then the reaction mixture was treated hydrothermally at 100 ^{o}C for 2 days. The resulting as-synthesized material was then filtered, washed with deionized water and dried at ~ 60 ^{o}C under vacuum. Finally, the material was extracted with ethanol using Soxhlet apparatus and was dried. The product was designated –C_2H_2-HS.

2.1.12 Synthesis of ethenylene-bridged organosilica hollow nanotubules. 0.6 g Pluronic P123 was dissolved in 21 ml of 1.3 M HCl solution followed by mechanical stirring until the whole polymer dissolved completely at 15 ^{o}C. Then a mixture of 0.79 ml bis(triethoxysilyl)ethenylene (BTEEn) and 3.25 ml cyclohexane was added. The solution was stirred for 1 day. Then the reaction mixture was treated hydrothermally at 100 ^{o}C for two days. The resulting as-synthesized material was then filtered, washed with deionized water and dried at ~ 60 ^{o}C under vacuum. Finally, the material was extracted with ethanol using Soxhlet apparatus and was dried. The product was designated –C_2H_2-NT.

2.1.13 Synthesis of nanospheres using $(CH_3O)_3Si\text{-}CH_2\text{-}C(=CH_2)\text{-}CH_2\text{-}Si(OCH_3)_3$ as precursor. 0.5 g of Pluronic F127 was dissolved in 45 ml of 2 M HCl solution followed

by magnetic stirring until the whole polymer dissolved completely at 15 ^{o}C under cover. Then 0.5 g xylene and 2.5 g KCl were added. After 2 h, 0.95 ml bis(trimethoxysilylmethyl) ethylene (BTMSME) was added. The solution was stirred for 1 day. Then the reaction mixture was treated hydrothermally at 100 ^{o}C for 1 day. The resulting as-synthesized material was then filtered, washed with deionized water and dried at ~ 60 ^{o}C under vacuum. Finally, the material was extracted with ethanol using Soxhlet apparatus and was dried.

2.1.14 Synthesis of silica nanospheres using Pluronic F108. 0.5 g of Pluronic F108 ($EO_{141}PO_{44}EO_{141}$, BASF) was dissolved in 30.8 ml of 1.97 M HCl solution followed by magnetic stirring until the whole polymer dissolved completely at 15 ^{o}C. After one hour, 0.70 ml xylene and 2.5 g KCl were added. After 2 h, 0.74 ml tetraethylorthosilicate (TEOS) was added. The solution was stirred for 1 day. Then, the reaction mixture was treated hydrothermally at 100 ^{o}C for 2 days. The resulting as-synthesized material was then filtered, washed with deionized water and dried at ~ 60 ^{o}C under vacuum. Finally, the material was calcined under air at 550 ^{o}C for 5 hr with heating ramp 2 ^{o}C/min.

2.1.15 Synthesis of phenylene-bridged organosilica hollow nanospheres. 0.5 g of Pluronic F127 was dissolved in 30 g of 2 M HCl solution followed by magnetic stirring until the whole polymer dissolved completely at 15 ^{o}C. Then 0.5 g xylene and 2.5 g KCl were added. After 2 h, 0.93 ml bis(triethoxysilyl)benzene (BTEB) was added. The solution was stirred for 1 day. Then, the reaction mixture was treated hydrothermally at 100 ^{o}C for 2 days. The resulting as-synthesized material was then filtered, washed with deionized water and dried at ~ 60 ^{o}C under vacuum. Finally, the material was calcined

under nitrogen at 300 ^{o}C for 5 h with ramp 2 ^{o}C/min. The product was designated –C_6H_4-HS.

2.2 Measurements. The small-angle X-ray scattering (SAXS) patterns were recorded on Bruker Nanostar U SAXS/wide-angle X-ray scattering (WAXS) instrument equipped with a rotating anode X-ray source and a 2-D detector Vantec 2000. The instrument was in a high flux configuration and the flight path was ~ 73 cm. Samples were placed in the hole of an aluminium sample holder and secured on both sides using Kapton tape. Nitrogen adsorption measurements were carried out on Micromeritics ASAP 2020 volumetric adsorption analyzer at –196 ^{o}C. The samples were outgassed at 140 ^{o}C in the port of the adsorption analyzer before analysis. Transmission electron microscopy (TEM) images were recorded on FEI Tecnai G2 Twin microscope operated at an accelerating voltage of 120 kV. The samples were first sonicated in ethanol, and then drop-casted on carbon coated copper grid and the solvent was dried in air before analysis. Cross-polarization magic angle spinning (CP MAS) ^{29}Si NMR spectra were acquired using Varian INOVA 300 wide bore spectrometer. The operating frequency was 59.6 MHz. Samples were packed into a 5 mm zirconia rotor, loaded into a 5 mm Doty XC-5 CP/MAS probe and spun at 6~8 kHz. 1000~2000 scans were acquired based on the sensitivity of the sample. Thermogravimetric analysis was carried out under air or nitrogen from room temperature to 800 ^{o}C using Hi-Res 2950 thermogravimetric analyzer from TA Instruments.

2.3 Calculations. The BET specific surface area (S_{BET}) was determined from nitrogen adsorption isotherm in the relative pressure from 0.04 – 0.2.[192] Total pore volume (V_t) was determined from the amount adsorbed at relative pressure of 0.99.[192] Pore size

distributions (PSDs) were determined from adsorption branch of the isotherms using the Barrett-Joyner-Halenda (BJH) method.[193,194] The samples discussed herein typically exhibit large (> 10 nm) cylindrical or spherical mesopores for which the pore size calculations were not fully calibrated and validated. On the basis of earlier studies,[116] the BJH method with the Kelvin equation was used herein for PSD calculations for cylindrical mesopores, which is expected to overestimate the mesopore diameter by not more than 10-15 % for most of the considered PMOs. On the other hand, the Kelvin equation with KJS correction was used for samples with spherical mesopores, and it is expected that the pore diameter is underestimated by 10-15 %.[148,194] The micropore volume (V_{mic}) was calculated using the α_s plot method using LiChrospher-1000 silica as a reference.[195]

A brief account of the major instrumentation that was used for structural characterizations of the synthesized nanostructures materials is given below. These instruments include transmission electron microscope (TEM), small-angle X-ray scattering (SAXS), and nitrogen gas adsorption technique.

2.4 Transmission Electron Microscopy (TEM). Transmission electron microscopy (TEM) uses the same basic principle as light microscopy does. The major difference is that while the light microscope uses light as a probe, TEM uses an electron beam. Light has a wavelength of several hundred of nanometers, and because of that, light microscope can view objects that are at least several hundred nanometers in size. The electrons have much lower wavelength (as low as a few picometers, one picometer = 10^{-12} m) when compared to light. As such, TEMs are capable of imaging at significantly higher resolution than the light microscope. This allows one to look at finer details of the

materials, such as nanoscale features or even atomic planes, which are tens to thousand times smaller than the smallest object that can be observed in a light microscope. An electron source at the top of the transmission electron microscope emits electron beam. The electron beam is then focused by electromagnetic lenses and directed on the specimen. The electron beam then interacts with sample under study. The transmitted electron beam is then magnified and detected/recorded by fluorescent screen, photographic plate or CCD camera. The image that is generated is a "shadow image" of the sample, because thicker parts transmit fewer electrons than thinner areas or void spaces do.

The sample under study needs to be thin in order to be visualized. If the sample is thick, and the electron beam cannot pass through, the image is very dark (essentially no electrons transmitted) so that no information about the structure of the sample is available.

TEM gives image in two dimensions and moreover it reflects only a local structure. So it is possible to get representative information primarily when the material is homogeneous. If the sample is not homogeneous, then other techniques that give global information need to be employed. In this regard, SAXS is very helpful in combination with TEM to confirm the final structure of the materials. In our study, we used TEM to confirm structures with 2-dimensional hexagonal (p6mm), and face-centered-cubic (Fm3m) symmetry, and also the structures composed of individual nanoobjects. Typical images are shown in Figure 2.1. The images below on the top of Figure 2.1 are for materials with 2-dimensional hexagonal ordering (p6mm symmetry).

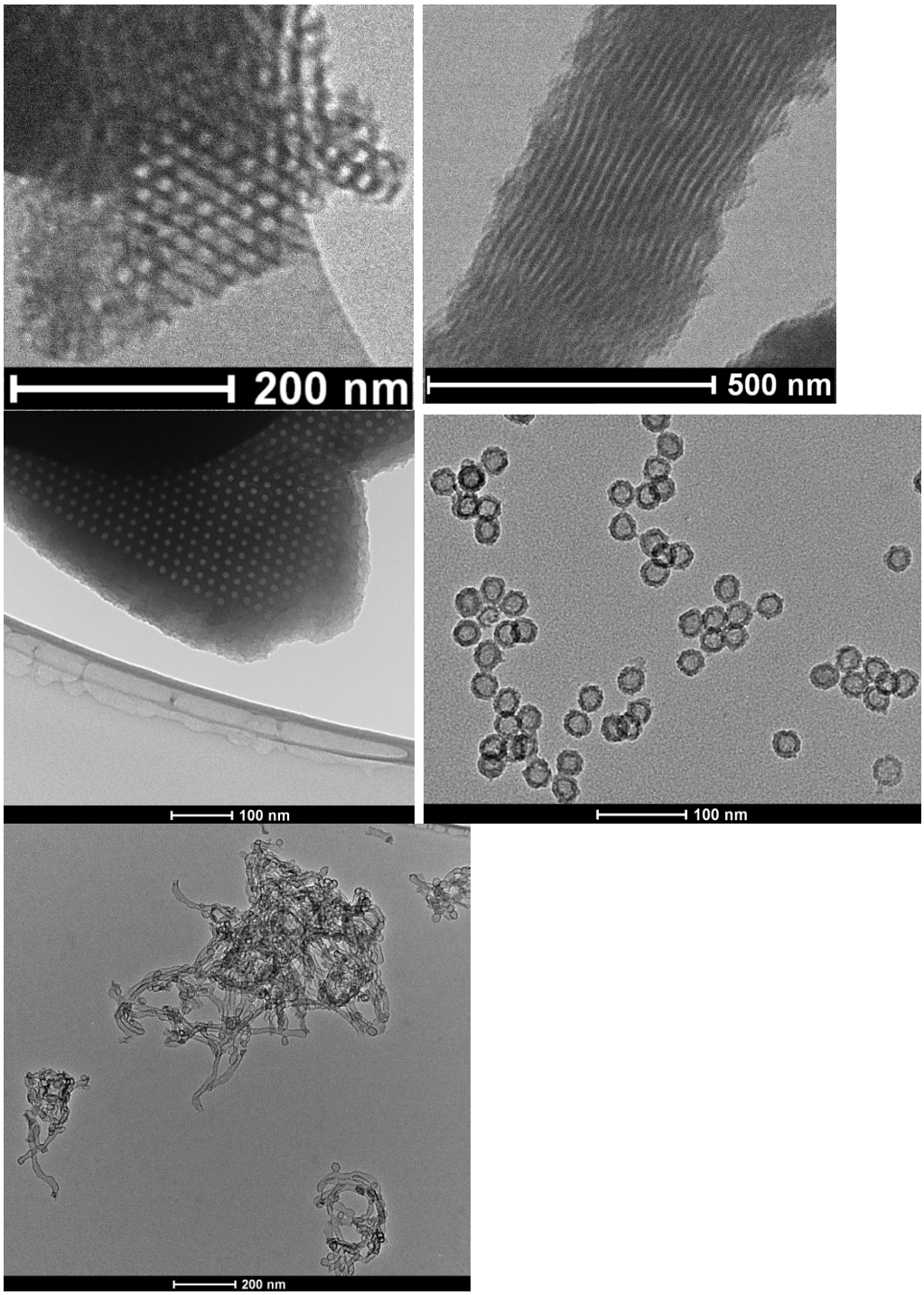

Figure 2.1 Typical TEM images of the synthesized ordered nanoporous materials and isolated nanoporous objects.

Two different kinds of images are obtained which are due to the projection of the material under electron beam, that is, along the hexagonally ordered cylinders (projection

looks like a honeycomb) or perpendicular to the cylinders (projection looks like a pattern of stripes). The image in the middle left is for a material with face-centered cubic ordering, which shows the (111) projection. The image at the middle right and bottom of Figure 2.1 is for the isolated nanoobjects (nanospheres and nanotubules).

2.5 Small-angle X-ray scattering. Small-angle X-ray scattering (SAXS) is a technique where X-ray beam is used and scattered by materials. The interaction between X-rays and the material is elastic in nature and the scattering pattern is recorded at low angles generally from ~ 0.1^{o} to several degrees. The wavelength of the X-ray source is typically 0.1 - 0.2 nm.

In our case, we used SAXS technique to determine the structure in the case of ordered or disordered nanostructured materials. Structures with 2-dimensional hexagonal and cubic Fm3m (face-centered-cubic) symmetries were identified using the SAXS technique. From the SAXS pattern, the interplanar spacing can be calculated based on the Bragg's equation:

$$\lambda = 2dsin\theta \qquad \text{Eq. 1}$$

where λ is wavelength of X-rays, which is 0.15418 nm in our case, d is the interplanar spacing, and θ is the diffraction angle of X-rays. Using the known value of wavelength (λ) and the diffraction angle (θ), the interplanar spacing (d) is calculated. In case of 2-dimensional hexagonal structure, unit cell parameter (a), that is the distance between two adjacent pore centers, is calculated from (100) interplanar spacing (d) based on following equation:

$$a = \frac{2d_{100}}{\sqrt{3}} \qquad \text{Eq. 2}$$

In the case of the face-centered-cubic structure, the unit cell parameter (a) that corresponds to the length of the edge of the unit cell, is calculated based on following equation for cubic structures:

$$a = d_{hkl}\sqrt{h^2 + k^2 + l^2} \qquad \text{Eq. 3}$$

where h, k, and l are called Miller indices. In the case of face-centered cubic structure, the most prominent peak on the scattering pattern is for (111) reflection (in which case h=1, k=1, and l=1). Therefore:

$$a = d_{111}\sqrt{3} \qquad \text{Eq. 4}$$

Typical patterns are shown below in Figure 2.2.

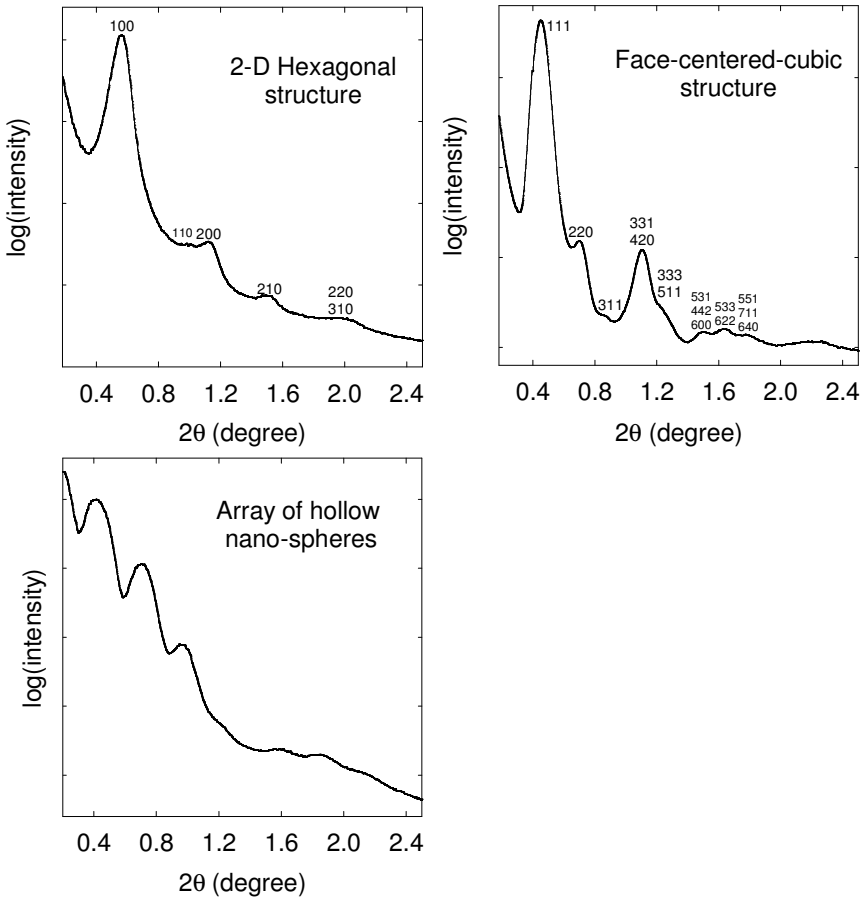

Figure 2.2 Typical SAXS patterns for materials under study.

The SAXS method is accurate and non-destructive. For SAXS, the sample preparation consists of placing of the powder in the sample holder and securing it with Kapton or Scotch tape. In the SAXS experiment, a monochromatic X-ray beam hits a sample from which X-rays scatter. Most of the X-rays go through the sample without any interaction, and the detector is screened from this intense direct beam by the beam stop. The scattered radiation forms a pattern, which is then recorded on a 2-dimensional detector located behind the sample. The scattering pattern is used to obtain information about the structure of the material.

2.6 Gas Adsorption. Adsorption is defined as enrichment or depletion of one or more componenets in an interfacial layer.[192,196]

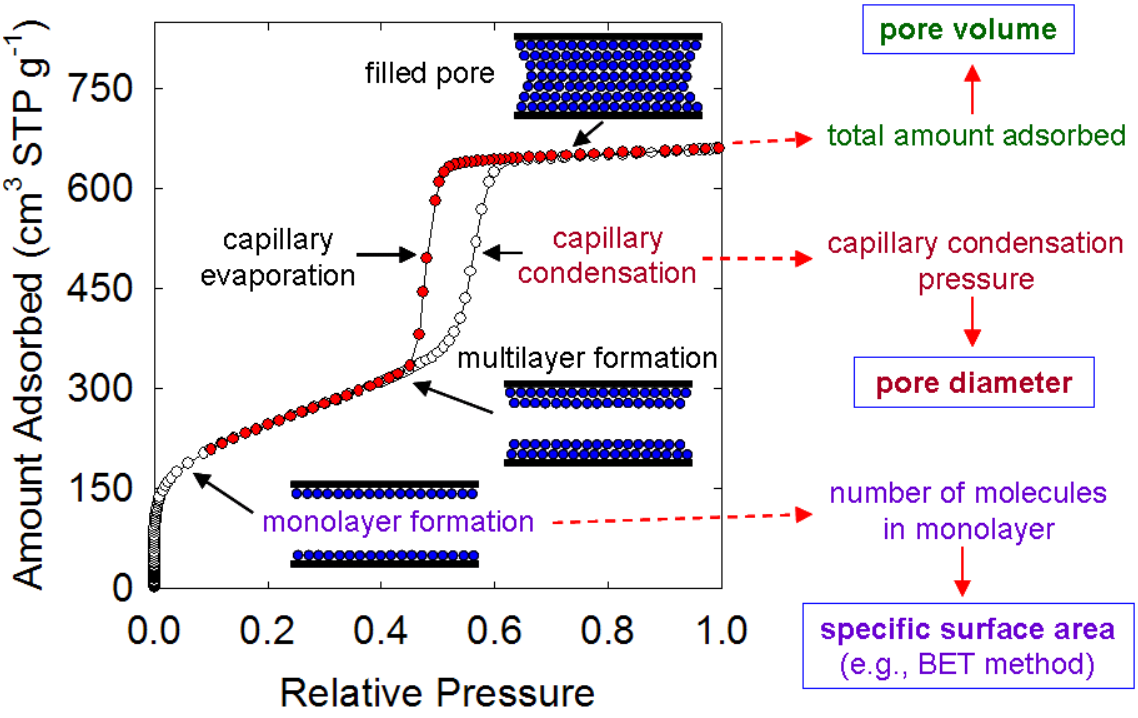

Figure 2.3 An adsorption isotherm of nitrogen at 77 K on a MCM-41 silica with uniform cylindrical pores[197] (data taken from Sayari et al.; Chem. Mater. 1997, 9, 2499). The illustration of the monolayer-multilayer adsorption process followed by capillary condensation, and the ways in which structural information is extracted from the data.

One typical adsorption process is the adsorption of a gas on a solid surface. In that case, the solid is called the adsorbent and the adsorbing gas is called the adsorbate. A typical adsorption isotherm for a mesoporous material with uniform pores is shown in Figure 2.3.

Methods to obtain physicochemical properties for porous solids from gas adsorption data

1. The Brunauer-Emmett-Teller (BET) method to calculate the specific surface area

In 1938, Brunauer, Emmett, and Teller proposed a method for determination of the specific surface area (that is, the surface area per gram of sample), which is known as the BET method. The BET method is based on the following main assumptions:

i) The adsorption is localized.

ii) The adsorption proceeds via monolayer-multilayer type adsorption.

Under these and some additional assumptions, the following equation was obtained:

$$n = n_m \frac{c\,\frac{p}{p_0}}{\left(1-\frac{p}{p_0}\right)\left[1+(c-1)\frac{p}{p_0}\right]} \qquad \text{Eq. 5}$$

Where p and p_o are the equilibrium pressure and saturation vapor pressure, respectively; and n is the amount adsorbed. Eq. 5 contains two constants: c and n_m, the latter being the monolayer capacity, that is the amount of molecules adsorbed in a monolayer (expressed in mol/g). During the measurement, both the relative pressure and the amount adsorbed are measured. Eq. 5 is used to obtain n_m and c from the experimental data. The value of n_m can be used to calculate the specific surface area (denoted here as S_{BET}):

$$S_{BET} = n_m \sigma N_A \qquad \text{Eq. 6}$$

where σ is the cross-sectional area of the adsorbate molecule and N_A is the Avogadro's number. According to the IUPAC recommendations,[192,198] nitrogen adsorption data at the temperature of 77 K and at relative pressures below 0.3 should be used in the BET calculations of the specific surface area. The cross-sectional area of the nitrogen molecule is usually assumed to be 0.162 nm^2.[192,198]

2. The single point total pore volume determination

For porous materials, the total pore volume is the summation of volumes of different kinds of pores, such as micropores, and mesopores. The total pore volume is estimated from the total volume of gas molecules adsorbed by the solid at the maximum relative pressure for which the uptake of gas can be reliably measured (usually at 0.99). In order to convert the volume of the gas adsorbed (in cm^3 STP g^{-1}) into the pore volume a conversion factor of 0.0015468 is used in the case of nitrogen adsorption at 77 K. The above method of calculation of the total pore volume is based on following assumptions. First, the density of the adsorbate is the same when it is condensed in the pores of the solid and when the bulk adsorbate is condensed. Second, the solid does not contain any appreciable amount of macropores (which are larger than 50 nm). Otherwise, most of the macropore volume is not accounted for. This is because the macropores larger than ~ 100 nm are not expected to be filled by capillary condensation at the relative pressure taken in the calculations, and thus the pore space in them is empty. Consequently, the total pore volume does not account for this space.

3. The Barrett-Joyner-Halenda (BJH) method to calculate the pore size distribution

In 1951, Barret, Joyner and Halenda proposed a method to determine the pore size distribution (PSD) which is known as the BJH method.[193] The adsorption of adsorbate

was viewed as the formation of monolayer-multilayer film on the pore surface when the pressure is increased until the capillary condensation takes place, thus filling the entire pore space. Then, further increase in pressure is assumed not to bring any further increase in the amount adsorbed. The desorption was viewed as the reverse process, involving the capillary evaporation followed by the gradual removal of adsorbate on lowering the pressure. In order to develop a method to calculate the pore size distribution under these assumptions, the relationship between: i) pore size (denoted as *r*), and the capillary condensation or evaporation pressure, and ii) monolayer-multilayer film thickness and the pressure, need to be known. For this purpose, Barrett et al. used the Kelvin equation and assumed that the statistical film thickness (t, which is function of p/p_o) is independent of the pore structure:

$$r = \frac{2\gamma V_L}{RT \ln\left(\frac{p_0}{p}\right)} + t \qquad \text{Eq. 7}$$

where r is the pore radius, γ is surface tension, V_L is molar volume of adsorbate, R is universal gas constant, and T is the absolute temperature. In case of liquid nitrogen, $\gamma = 8.88 \times 10^{-3}$ N m^{-1} and $V_L = 34.68$ cm^3 mol^{-1}.

In the BJH method, the calculation starts from the highest pressure in the adsorption-desorption isotherm. At the highest pressure, it is assumed that all the pores (micropores and mesopores) are completely filled up by the adsorbate. After filling up of all the pores, when the pressure is lowered, the pores are emptied starting from the largest pores, and gradually progressing to the pores of the smaller size. One can view the adsorption process, that is, the process taking place upon the pressure increase, as an inverse of the aforementioned scenario, which corresponded to the desorption process.

By measuring the difference in the amount adsorbed as the pressure is lowered and correlating it with the pore size via the Kelvin equation (Eq. 7), one can determine the pore volume corresponding to the particular pore size. The calculations take into account that after the capillary evaporation in pores of given size, the pore surface is still covered by the film (multilayer) of adsorbed molecules, whose thickness decreases as the pressure is decreased. The calculations described above appear to be relevant to the desorption process, but the calculation procedure can be applied to the adsorption data as well, if one processes the data "backwards" (from the highest pressures to the lowest, although they were acquired in the opposite sequence). Herein, the BJH calculations were performed from adsorption rather than desorption data.

3. Results and Discussions.

Part 1. Versatile Approach to Synthesis of 2-D Hexagonal Ultra-Large-Pore Periodic Mesoporous Organosilicas[68]

3.1.1 Methylene-bridged PMO. It was previously found that cyclohexane is a promising swelling agent in case of Pluronic-templated synthesis of large-pore SBA-15, allowing one to achieve d_{100} up to 13 nm. Herein, it is shown that cyclohexane is extremely useful for synthesizing large-pore methylene-bridged PMO. Methylene-bridged PMO synthesized under such conditions shows SAXS patterns (Figure 3.1.1), which exhibit reflections that can be identified as (100), (110), (200), and (300) peaks of 2-D hexagonal structure with interplanar spacing d_{100} of 22 nm (Table 3.1.1).

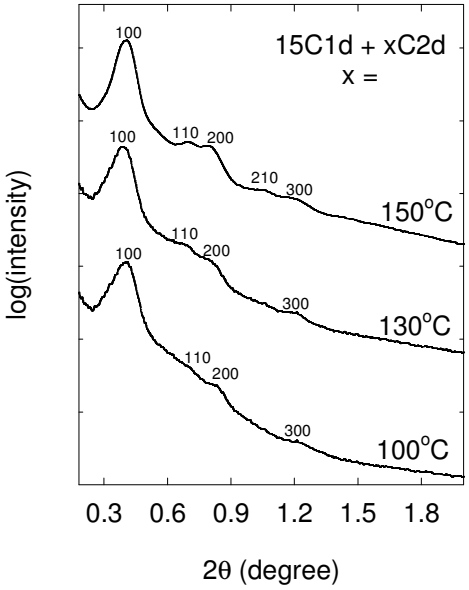

Figure 3.1.1 SAXS patterns of methylene-bridged PMO synthesized at initial synthesis temperature of 15 °C followed by hydrothermal treatment for two days at different temperatures (figure taken from reference 68).

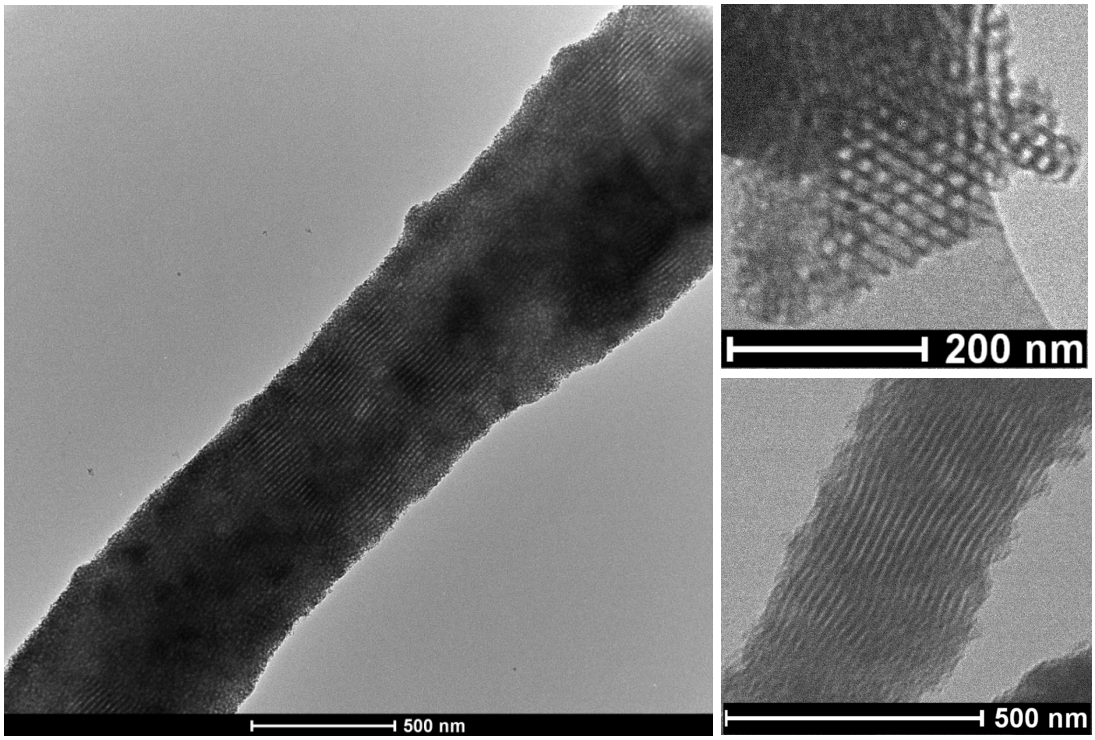

Figure 3.1.2 TEM image of calcined methylene-bridged PMO synthesized using a hydrothermal treatment at 150 °C for two days (figure taken from reference 68).

This d_{100} is more than 50% larger than the largest d_{100} reported so far for any 2-D hexagonal PMO.[68] The TEM image (Figure 3.1.2) shows that the particles of the PMO had rod-like structure with parallel stripes visible along the rods, which corresponds to the side projection of the honeycomb structure (Figure 3.1.2). Such a particle morphology makes it difficult to view the honeycomb projection, although it is visible in some places (Figure 3.1.2, top right). The surface of the rods appeared to be rough, suggesting that the rods were covered by channels circling around the rods or by some other less well defined porous structure.

Table 3.1.1 Structural properties of methylene-bridged PMOs.[a]

Sample (bridge, initial temp.)	d_{100} (nm)	S_{BET} (m^2/g)	V_t (cm^3/g)	V_{mic} (cm^3/g)	w_{BJH} (nm)
Methylene, 17 °C	21.3	1140	1.39	0.24	18.5
Methylene, 15 °C	22.1	1120	1.56	0.21	23.3
Methylene, 14 °C	22.1	1220	1.50	0.32	19.7
Methylene, 13 °C	30[b]	1180	1.27	0.35	23.9
Methylene, 12 °C	-[c]	1170	1.12	0.40	31
Methylene, 15°C, x=0.2	17.8	1197	1.28	0.26	12.0
Methylene, 15°C, x=0.3, H 100°C [d]	20.8	1230	1.61	0.28	22.2
Methylene, 15°C, x=0.3, H 130°C	22.7	1007	1.75	0.11	25.1
Methylene, 15°C, x=0.3, H 150°C	21.8	837	1.66	(-0.01)[e]	23.6
Methylene, 15°C, x=0.3, H 170°C [d]	20.5	607	1.44	e	21.7
Methylene, 15°C, x=0.4	17.2	1204	1.10	0.35	12.6

[a] Notation: d_{100}, (100) interplanar spacing for calcined sample. $S_{BET,}$ BET specific surface area; $w_{BJH,}$ BJH pore diameter; $V_{t,}$ total pore volume, $V_{mic,}$ micropore volume. [b] Estimated by tentatively assigning the first peak on SAXS pattern as (100) peak. [c] Could not be evaluated accurately due to the presence of shoulder on SAXS pattern. [d] Repeated synthesis. [e] Indicates that the micropore volume is negligible.

The methylene-bridged PMOs were further characterized by nitrogen adsorption technique to determine textural properties of the materials, such as pore size, surface area, and pore volume. The adsorption isotherm for the sample (Figure 3.1.3) shows steep capillary condensation step at high relative pressure of ~ 0.91, thus indicating the presence of very large mesopores. The material shows high BET specific surface area (1220 $m^2\ g^{-1}$) and a large pore volume of 1.56 $cm^3\ g^{-1}$. The pore size distribution (PSD) was narrow and a nominal (BJH) pore diameter was ~23 nm (Figure 3.1.3), which is

about two times larger than the largest pore size reported so far for a 2-D hexagonal PMO.[68]

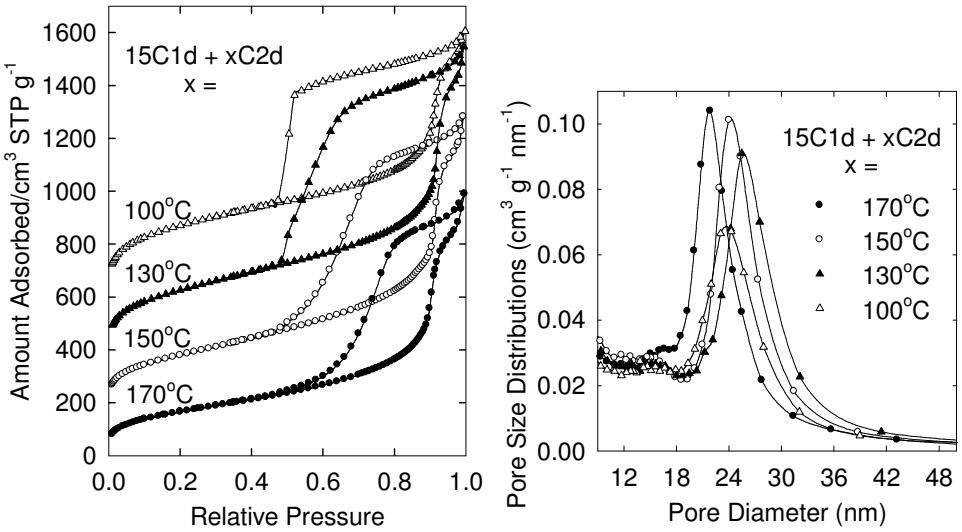

Figure 3.1.3 Nitrogen adsorption isotherm and pore size distributions for methylene-bridged PMO synthesized at initial synthesis temperature of 15 °C followed by hydrothermal treatment for two days at different temperatures. The isotherms were offset vertically by 150, 350, and 560 cm^3 STP g^{-1} for samples hydrothermally treated at 150, 130 and 100 °C.

The wall thickness for methylene-bridged PMO (in this case ~ 6 nm) was found much thicker than the wall thickness for silica-based SBA-15 material synthesized under similar conditions.[199] In case of copolymer templated 2-D hexagonal nanoporous materials, each main pore is connected by small pores, often in micropore range. In order to calculate the wall thickness more accurately, the following equation[200] was used to determine the pore size:

$$w_d = \frac{\sqrt{3}c}{2} a \sqrt{\frac{V_p}{\frac{1}{\rho} + V_p + V_{mic}}} \qquad \text{Eq. 1}$$

where a is unit-cell parameter ($a=d_{100} \times 2/\sqrt{3}$), obtained from SAXS, ρ is the density of organosilica framework, c (=1.213) is a constant for cylindrical pore shape, V_p and V_{mic}

are mesopore and micropore volume, respectively. After w_d is calculated, the pore wall thickness b is calculated by subtracting w_d from the unit-cell parameter, a: b=a - w_d.

3.1.1a Effect of hydrothermal treatment. The ultra-large cylindrical mesopores of the PMO are accessible through constrictions as seen from broad adsorption-desorption hysteresis loop (Figure 3.1.3) that closes primarily at lower limit of the adsorption-desorption hysteresis (p/p_o of 0.50), thus suggesting that the constrictions are of diameter below 5 nm.[201] In the case of considered PMO, the accessibility of the mesopores was improved by applying hydrothermal treatment at 130-170 ^oC. After hydrothermal treatment at higher temperature, the obtained material shows narrowing of the adsorption-desorption hysteresis loop (Figure 3.1.3). The pore size calculated from the position of the capillary condensation step remains almost constant, indicating that the PMO shows a slightly different hydrothermal treatment behavior compared to its pure-silica counterparts (SBA-15), whose pore diameter increases to a large extent with the increase in time or temperature of hydrothermal treatment.[147,202] Even after the treatment at such high temperatures, the hysteresis loops for PMOs were appreciably broader than those for materials with mesopores free of constrictions, indicating that it is difficult to fully eliminate the constrictions. The latter can be present either inside the mesopores (as "plugs"),[74,75] or at entrances to the mesopores.[74] In case of mesoporous pure silica materials, the unit cell parameter and pore size increases with increasing the either hydrothermal treatment temperature or duration.[147] On the other hand, for methylene-bridged PMO, unit-cell size remains almost constant, and the pore size increases to small extent (Figure 3.1.3). The synthesized organosilica material shrank little (0 to 4%) upon calcination, indicating that the material is very stable.[80]

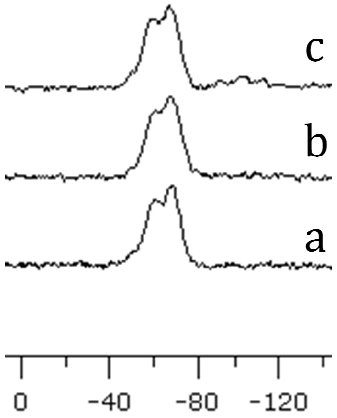

Figure 3.1.4 ^{29}Si CP MAS NMR for methylene-bridged PMOs a) as-synthesized, b) calcined at 300 ^{o}C under nitrogen, and c) calcined at 300 °C under air (scale in ppm) (figure taken from reference 68).

In ^{29}Si CP MAS NMR, for as-synthesized material, three signals are observed at 56, 62, and 69 ppm, corresponding to T sites (Si sites attached to three oxygen atoms T^n, n=1-3): T^1 [*Si*C(OH)$_2$(OSi)], T^2 [*Si*C(OH)(OSi)$_2$], and T^3 [*Si*C(OSi)$_3$] respectively (Figure 3.1.4). After calcination under air, some Q sites (Si sites attached to four oxygen atoms Q^n, n=1-4) (between -90 and -110 ppm) appear indicating the conversion of organic group to Si-O-Si linkage. However, after the calcination at 300 ^{o}C under nitrogen, no signal related to Q sites appears indicating that under these conditions, the organic-inorganic network is fully stable. The surfactant removal can also be achieved by ethanol extraction with the retention of integrity of Si-C bonds. The SAXS, adsorption and pore size distribution data for the sample from which the surfactant was removed in three aforementioned ways are shown in Figure 3.1.5. It is clear that the structural properties do not depend much on the mode of the surfactant removal. It is also determined that the hydrothermal treatment at 150 ^{o}C or even 170 ^{o}C did not lead to the cleavage of Si-C bonds (Figure 3.1.5).

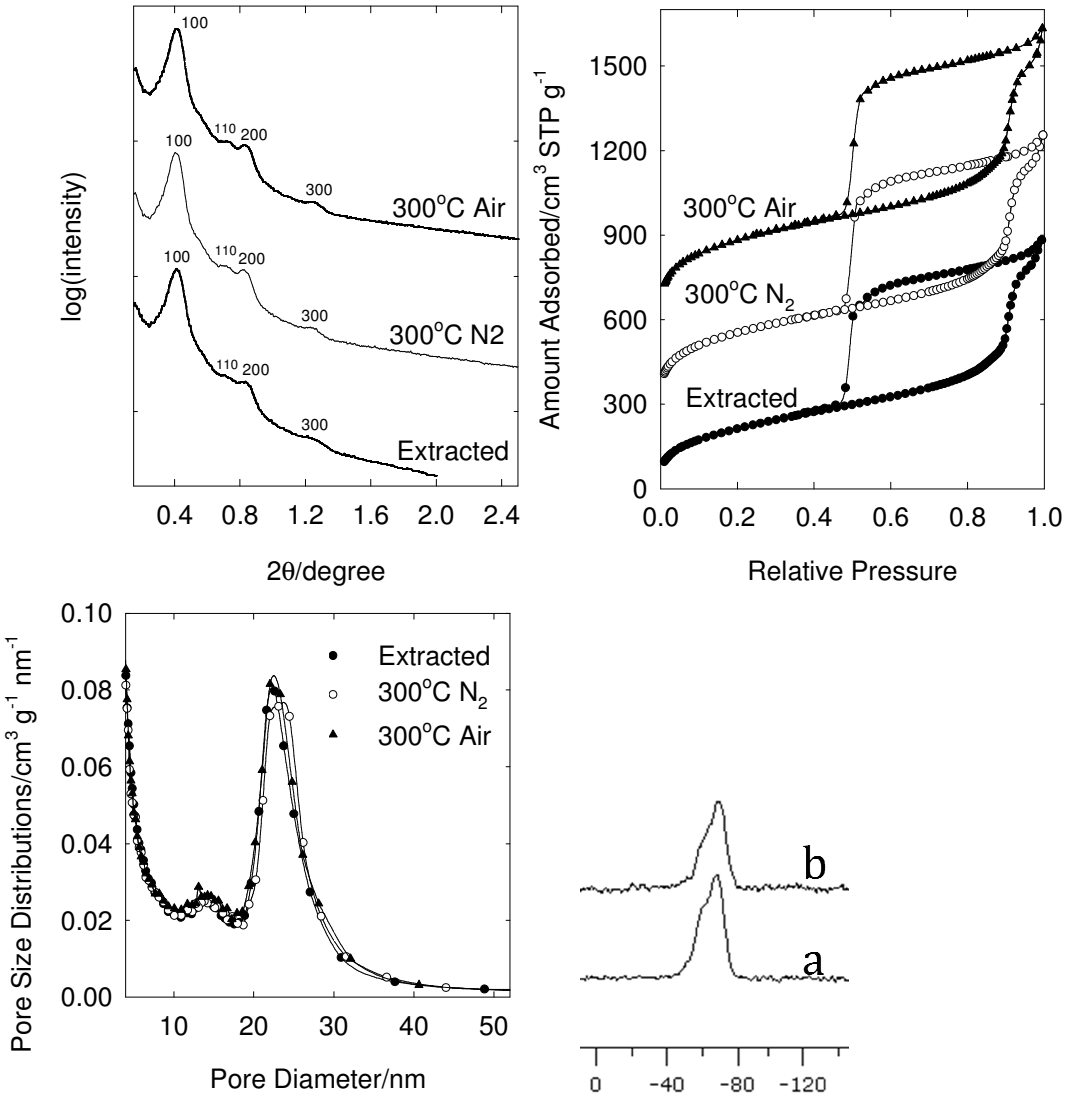

Figure 3.1.5 SAXS patterns (top left), nitrogen adsorption isotherms (top right), pore size distributions (bottom left) for methylene-bridged PMOs. Isotherms for samples calcined at 300 °C under N_2 and under air were offset vertically by 250 and 550 cm^3 STP g^{-1} for clarity. ^{29}Si CP MAS NMR for a methylene-bridged PMO hydrothermally treated at a) 150 °C and b) 170 °C for two days (scale in ppm) (figure taken from reference 68).

3.1.1b Effect of initial synthesis temperature. On the basis of the previous study of large-pore SBA-15 silica template by Pluronic P123 swollen by TIPB,[116] it was expected that the lowering of the initial synthesis temperature would lead to the unit-cell enlargement and the pore diameter increase. However, the ultra-large-pore methylene-bridged PMO was not particularly amenable to the structural adjustment. The pore

diameter and unit-cell size exhibited little variation within the 14-17 ^{o}C range (Figure 3.1.6, Table 3.1.1).

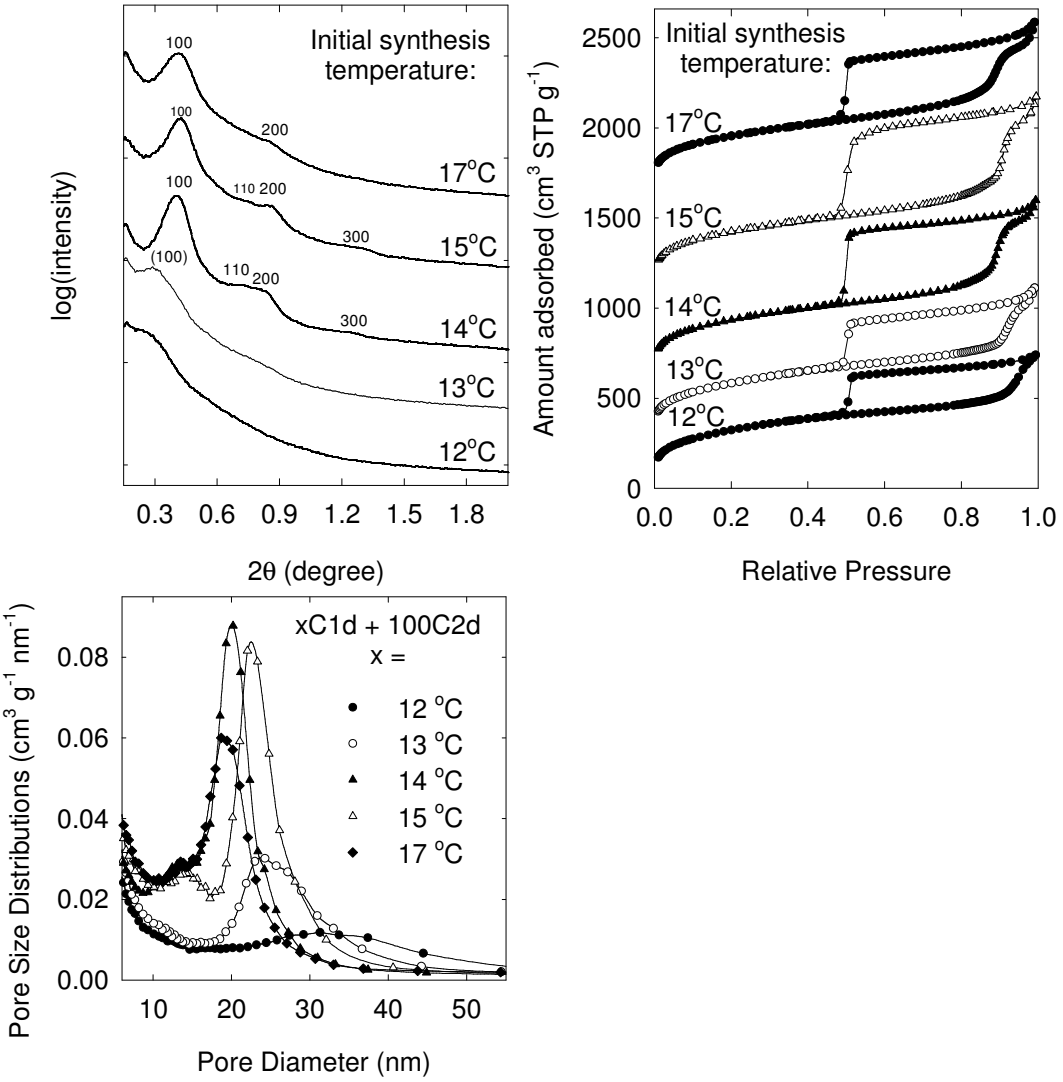

Figure 3.1.6 (top left) SAXS patterns, (top right) nitrogen adsorption isotherms and (bottom left) pore size distributions for calcined methylene-bridged PMOs synthesized at different initial synthesis temperature using cyclohexane as expander. The isotherms were offset vertically by 260, 600, 1090 and 1640 cm^3 STP g^{-1} for samples synthesized at initial synthesis temperature of 13, 14, 15 and 17 ^{o}C respectively (figure taken from reference 68).

As the temperature was decreased to 13 ^{o}C, the pore diameter somewhat increased, but the SAXS pattern became poorly resolved, having only one peak whose position corresponded to very large repeating distance of ~ 30 nm. Further temperature decrease

to 12 ^{o}C led to a marked pore diameter increase, but the SAXS pattern merely exhibited a shoulder at very low angles, showing the loss of structural uniformity.

3.1.1c Effect of amount of precursor. The amount of precursor was found to affect the unit-cell parameter and the pore size. In case of methylene-bridged PMO, the unit-cell parameter decreases with lowering or increasing the amount of the precursor (Figure 3.1.7, Table 3.1.1).

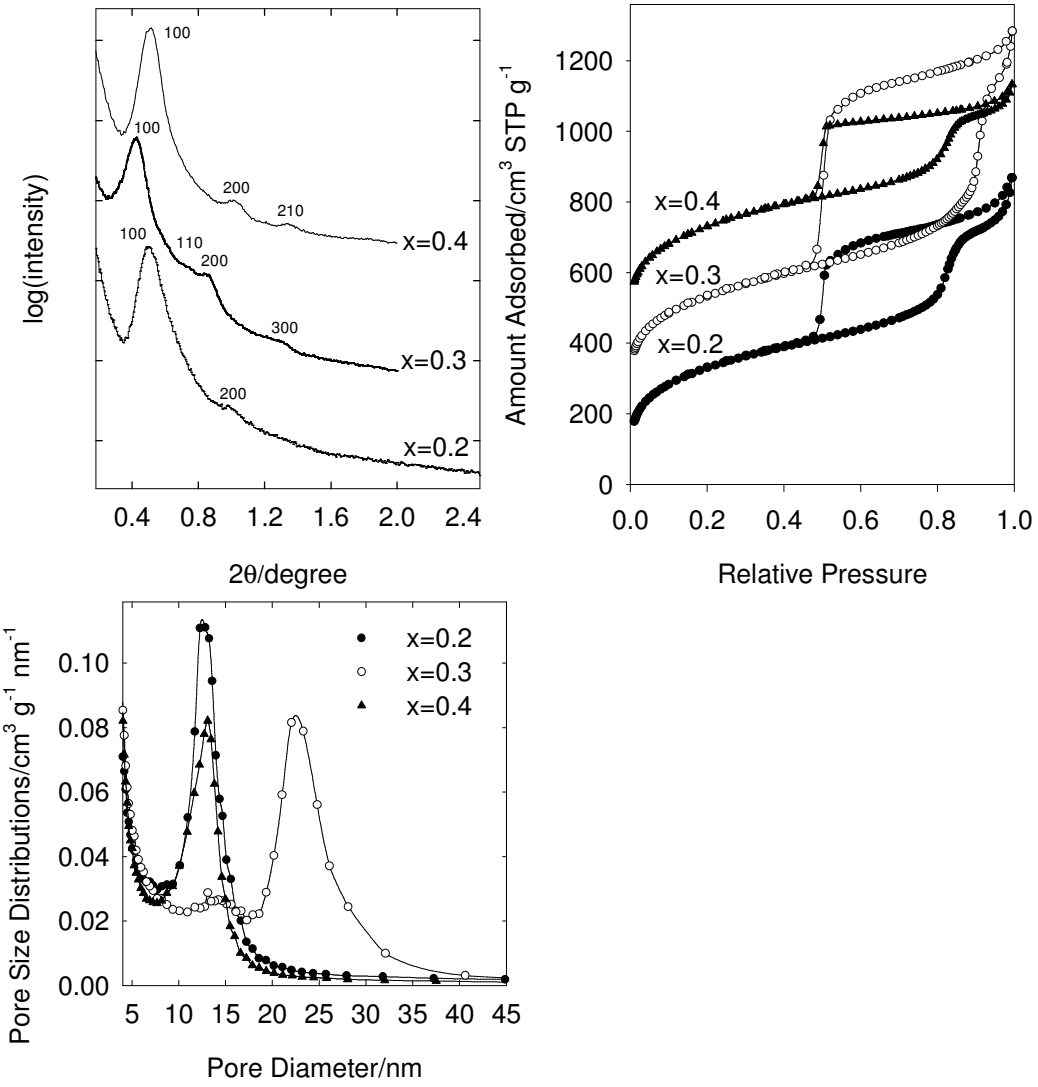

Figure 3.1.7 (top left) SAXS patterns, (top right) nitrogen adsorption isotherm and (bottom) pore size distribution of calcined methylene-bridged PMO synthesized with different amount of precursor using cyclohexane as expander. The isotherms are offset vertically by 200, and 400 cm^3 STP g^{-1} for x=0.3, and 0.4 respectively (figure taken from reference 68).

It was found that for the methylene-bridged PMO, the ultra-large-pore structure was formed at an organosilica precursor/surfactant ratio, which is 60% higher (in terms of Si/P123 molar ratio) than that typically used in the SBA-15 synthesis. Moderate deviation (e.g. ~ 12% higher or lower) in organosilica precursor/P123 ratio afforded much lower interplanar spacing (Table 3.1.1, Figure 3.1.7).

3.1.1d Effect of hydrothermal treatment on methylene-bridged PMO. As discussed above, we have synthesized large-unit-cell methylene-bridged 2-D hexagonal ordered mesostructured material. The as-synthesized and calcined samples synthesized at low-temperature only (LT, 15 ^{o}C) and with high temperature treatment (HT, 15 ^{o}C +100 ^{o}C2d, same as samples described above) were prepared from the same original synthesis mixture prepared at 15 ^{o}C, and characterized by small-angle X-ray scattering (Figure 3.1.8). The calcined material prepared with hydrothermal treatment showed well-resolved peaks, which can be indexed as (100), (110), and (200) peaks, indicating 2-dimensional hexagonal structure (as discussed above). The corresponding as-synthesized methylene-bridged organosilica-block-copolymers nanostructured composites showed one strong peak and another peak with a shoulder, which can be assigned as (100), and (110) based on peak position and comparison with the data for the calcined materials. On the other hand, the sample prepared at low temperature only showed a nearly featureless SAXS pattern for its as-synthesized (surfactant-containing) form and a single broad peak after calcination. The origin of this behavior is not fully clear, but it seems that the surfactant template (with same solubilized swelling agent and perhaps organosilica precursor or product of its partial hydrolysis) match the scattering density of organosilica framework very well. Moreover, the framework is not likely to be cross-linked sufficiently to

withstand the calcination without a major shrinkage. This can be concluded on the basis of the fact that for silicas and organosilicas templated by surfactants, the hydrothermal treatment does not change the unit-cell size, that is, the unit-cell size for as-synthesized samples before and after the treatment are about the same. This suggests that although we can not infer from SAXS, the unit-cell parameter for as-synthesized sample from LT preparation, its actual unit-cell parameter is likely to be similar to that for the corresponding hydrothermally treated sample (Table 3.1.2). If this is indeed the case, the calcination would bring a dramatic decrease (~ 20 %) in the unit-cell parameter for the LT preparation, indicating that the material has a very limited thermal stability, perhaps being cross-linked to a limited extent.

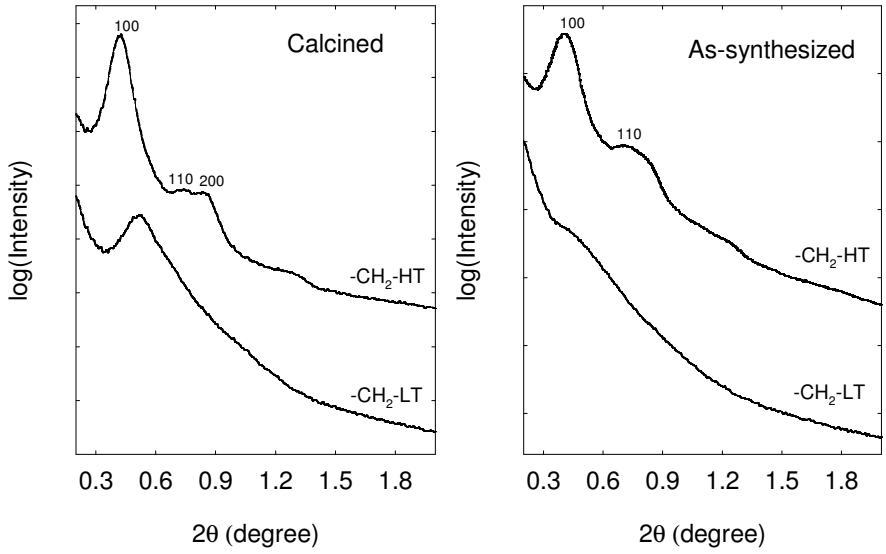

Figure 3.1.8 SAXS patterns for calcined and as-synthesized samples.

The materials were characterized by nitrogen adsorption technique (Figure 3.1.9). Both of the calcined samples show very broad hysteresis loops. The hydrothermally treated sample showed steep capillary condensation step, whereas the sample prepared at low temperature only showed a poorly pronounced capillary condensation step. This result is consistent with SAXS data and highlights poor stability of the low-temperature material.

Table 3.1.2 Interplanar spacings and physicochemical properties of the methylene-bridged PMOs.

Sample	d_{100}	d_{100}uc	d_{100}/d_{100}uc	S_{BET} (m^2/g)	w_{BJH} (nm)	V_t (cm^3/g)
PMO-CH_2-LT	14.6	NA[a]	NA	825	*b*	0.52
PMO-CH_2-HT	18.0	21.7	0.96	1212	22.5	1.68

Notation: d_{100} interplanar spacing for calcined sample, d_{100}uc, interplanar spacing for as-synthesized sample. NA, not available. [a] main peak not observable on SAXS pattern. [b] could not be obtained accurately due to broadness of pore size distribution.

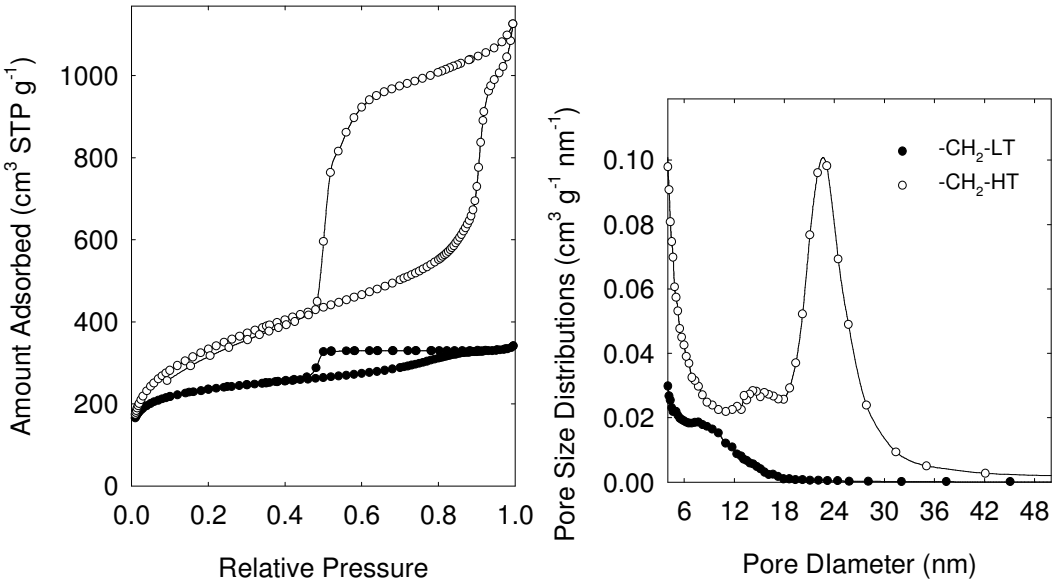

Figure 3.1.9 N_2 adsorption isotherms and pore size distribution of methylene-bridged PMO synthesized at initial synthesis temperature of 15 ^oC and further heating at 100 ^oC for two days.

3.1.1e Hydrothermal stability comparison between methylene-bridged PMO and pure-silica in a base treatment. The hydrothermal stability in basic buffer solution was compared between ordered pure silica material (SBA-15) and methylene-bridged PMO with 2-D hexagonal structure. For this purpose, a buffer solution was prepared by mixing the same volume of equimolar amount of ammonium chloride (NH_4Cl) and ammonium hydroxide (NH_4OH) solution (pH ~ 9.4). The ordered pure silica material retained the structural ordering after the basic solution treatment at 100 ^oC for 1 day, as seen from SAXS pattern (Figure 3.1.10). The intensity of the (100), (110) and (200) peaks for the

base-treated sample decreased compared to the same peaks for the sample that was not subjected to the basic treatment. This suggets that the quality of the SBA-15 material decreases upon the basic treatment. After a harsher basic solution treatment at 150 ^{o}C for 1 day, the ordered structure of SBA-15 was completely lost as seen from the SAXS pattern where no peaks are visible. This behavior is similar to the effect of 100 ^{o}C ("boiling") water treatment on MCM-41 silicas.[203] On the other hand, methylene-bridged organosilica material retained the structural ordering even after the basic solution treatment at 150 ^{o}C for 1 day. The intensities of peaks for the samples before and after the base treatment at 100 ^{o}C for 1 day remain almost the same, unlike in the case of the pure silica SBA-15 material (Figure 3.1.10, Table 3.1.3).

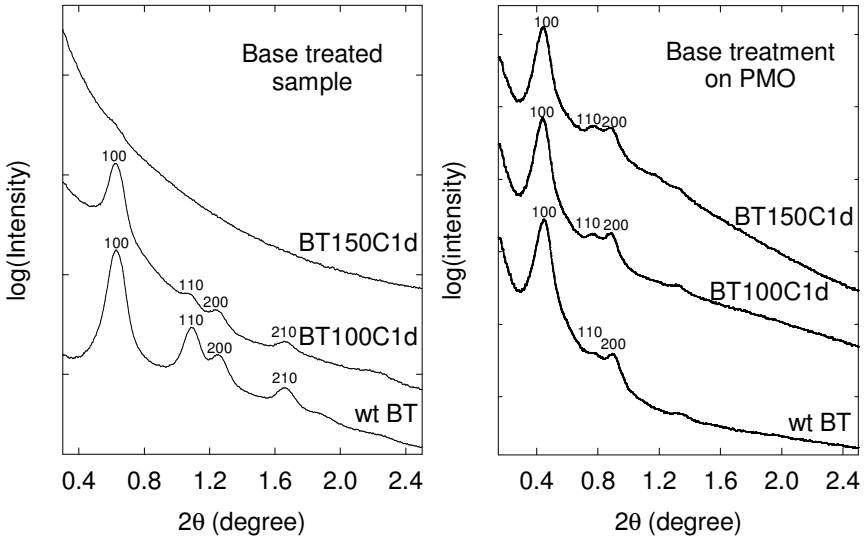

Figure 3.1.10 Comparison of SAXS patterns between silica and organosilica materials before and after the base treatment.

With increasing the basic treatment temperature to 150 ^{o}C, the intensity of (110) peak slightly increased compared to (200) peak. The increase in (110) peak intensity compared to (200) peak intensity may be related to the decrease in the wall thickness[71,204] due to the treatment, which perhaps involves dissolution of an outer layer of the wall at higher temperature. The results demonstrated that the organosilica material is much more stable

than the pure silica SBA-15 material synthesized under similar conditions. It should be noted that SBA-15 is considered as a very hydrothermally stable material.[57]

Table 3.1.3 Interplanar spacings and physicochemical properties of pure-silicas and organosilicas.

Sample	d_{100}	d_{100}uc	S_{BET} (m^2/g)	w_{BJH} (nm)	V_t (cm^3/g)
SBA-15	14.0	15.2	522	15.3	1.13
SBA-15-BT100C1d	14.2	15.2	166	13.3	0.67
SBA-15-BT150C1d	a	15.2	55	b	0.24
PMO	19.9	20.1	1132	18.9	1.45
PMO-BT100C1d	20.3	20.1	809	20.8	1.44
PMO-BT150C1d	20.1	20.1	471	22.1	1.38

Notation: d_{100} interplanar spacing for calcined sample, d_{100}uc interplanar spacing for as-synthesized sample. NA, not available. [a] main peak not observable on SAXS pattern. [b] could not be obtained accurately due to broadness of pore size distribution.

The materials were further characterized by nitrogen adsorption technique. The isotherm for pure-silica SBA-15 material after the base treatment at 150 ^oC for 1 day did not show any hysteresis loop indicating that the mesoporous structure was completely gone as also inferred from the SAXS pattern (Figure 3.1.10). After a similar treatment, methylene-bridged PMO shows a hysteresis loop with a sharp capillary condensation step indicating that the structure was preserved (Figure 3.1.11). Another interesting feature to note is that under such treatment, the desorption branch shifted considerably to higher relative pressures indicating that the entrances to mesopores became much wide. The isotherms revealed that the pore diameter of the PMO increased slightly as a result of the base treatment, but the narrow pore size distribution has been preserved.

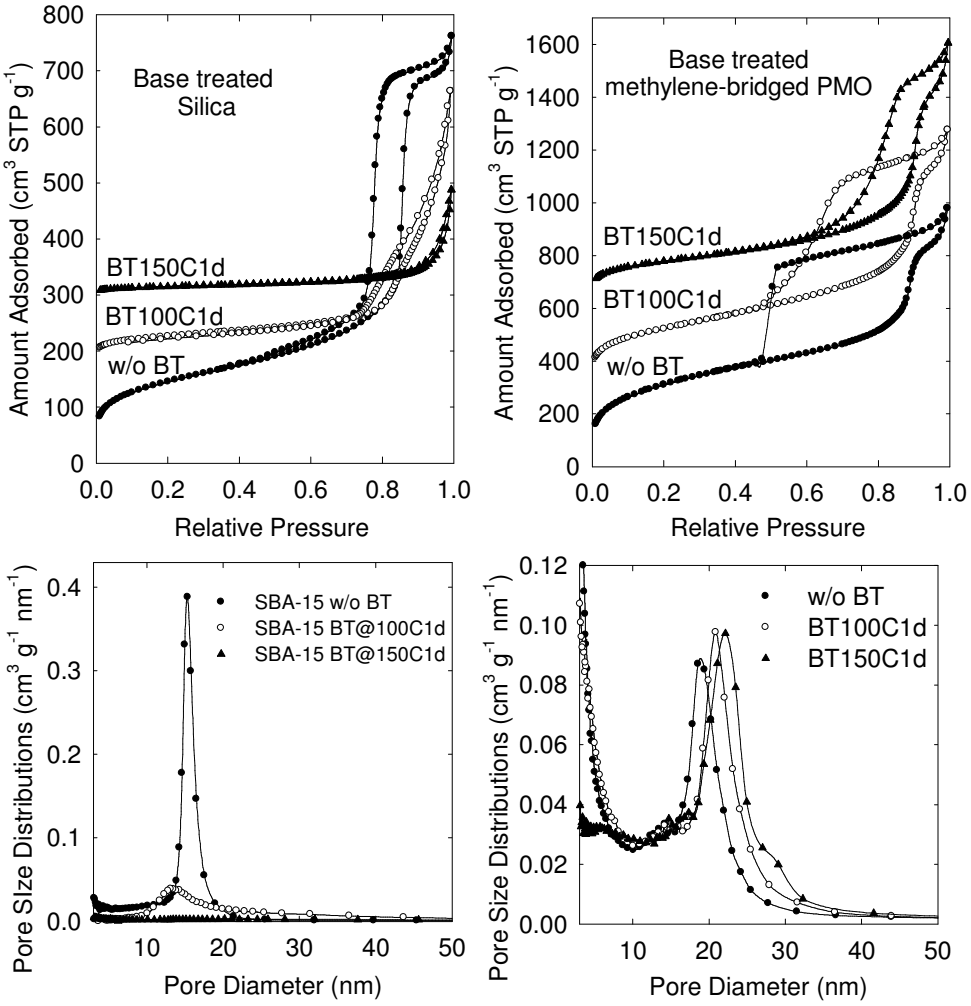

Figure 3.1.11 Nitrogen adsorption isotherms and pore size distributions comparison between pure-silica (left) and organosilica (right) material before and after base treatment.

^{29}Si CP MAS NMR (Figure 3.1.12) shows that for methylene-bridged PMO after the base treatment at 150 ^{o}C for 1 day, the material preserves Si-C bonds entirely indicating very high stability of this material, not only in terms of the nanoscale structure, but also in regard to the atomic-scale structure.

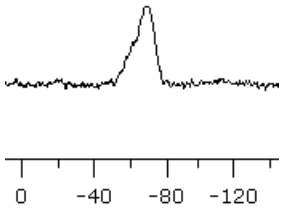

Figure 3.1.12 ^{29}Si CP MAS NMR for methylene-bridged PMOs after the base treatment at 150 ^{o}C for 1 day.

3.1.2 Ethylene- and ethenylene-bridged PMOs. Cyclohexane was also found to be very promising for obtaining 2-D hexagonal structures in case of ethylene and ethenylene-bridged PMOs. In this case, the unit-cell size was found to be readily adjustable by changing initial synthesis temperature (as discussed later) resembling the synthesis of large-pore SBA-15 silica in the presence of TIPB.[116] When the initial synthesis temperature was 15 ^{o}C, the SAXS pattern for ethylene-bridged PMO shows five well resolved peaks, which can be identified as (100), (110), (200), (210), and (220)/(310) (Figure 3.1.13, left) indicating that the material has 2-dimensional hexagonal (p6mm) pore structure with d_{100} =16.8 nm. The corresponding SAXS patterns for ethenylene-bridged PMO shows also four well-resolved peaks which can be identified as (100), (110), (200), and (220)/(310) reflections of 2-dimensional hexagonal (p6mm) pore structure with d_{100} = 14.6 nm. TEM confirmed the structures of both PMOs (Figure 3.1.14), but also suggested the presence of non-mesoporous (non-templated) domains (for ethenylene-bridged PMO) or apparently non-mesoporous envelopes around particles (for ethylene-bridged PMO).

Table 3.1.4 Structural properties of ethylene- and ethenylene-bridged PMOs.[a]

Sample (bridge, initial temp.)	d_{100} (nm)	S_{BET} (m^2/g)	V_t (cm^3/g)	V_{mic} (cm^3/g)	w_{BJH} (nm)
Ethylene, 15 °C, x=0.6, BTME	16.8	498	0.59	0.13	13.7
Ethylene, 12 °C [b], x=0.6, BTME	19.6	705	0.62	0.25	16.7
Ethylene, 11 °C, x=0.6, BTME	24.2	452	0.44	0.15	21.6
Ethylene, 10.75 °C [b], x=0.6, BTME	25.6	631	0.52	0.23	22.2
Ethylene, 10.5° C [b], x=0.6, BTME	~28[c]	626	0.47	0.26	26.0
Ethylene, 10 °C, x=0.6, BTME	-[d]	136	0.23	0.02	-[e]
Ethylene, 15°C, x=0.4, BTME	16.1	429	0.65	0.08	13.7
Ethylene, 15°C, x=0.4, BTEE	15.8	542	0.67	0.10	11.6
Ethylene, 12°C, x=0.4, BTEE	18.2	258	0.40	0.05	15.8
Ethylene, 11°C, x=0.4, BTEE	20.8	82	0.15	0.02	18.8
Ethylene, 15°C, x=0.7, BTME	16.8	534	0.56	0.16	13.8
Ethylene, 15°C, x=1.0, BTME [b]	16.7	690	0.51	0.25	13.4
Ethylene, 15°C, x=1.5, BTME	18.0	581	0.41	0.22	14.6
Ethenylene, 15 °C, x=0.4, BTEEn	14.6	263	0.50	0.03	11.9
Ethenylene, 12 °C, x=0.4, BTEEn	16.8	322	0.45	0.06	14.3
Ethenylene, 11 °C, x=0.4, BTEEn	21.3	691	0.71	0.24	20.1
Ethenylene, 10.5 °C, x=0.4, BTEEn	22.1	459	0.52	0.14	21.2
Ethenylene, 10 °C, x=0.4, BTEEn	~22[c]	69	0.17	0.01	22
Ethenylene, 15°C, x=0.7, BTEEn	14.0	139	0.27	0.00	11.1

[a] Notation: d_{100}, (100) interplanar spacing for either calcined or extracted sample. S_{BET}, BET specific surface area; w_{BJH}, BJH pore diameter; V_t, total pore volume, V_{mic}, micropore volume. [b] Sample was calcined at 300 °C under N_2. [c] Could not be evaluated accurately due to the presence of shoulder on SAXS pattern. [d] Could not be evaluated due to absence of peak on SAXS pattern. [e] No clear peak on mesopore size distribution.

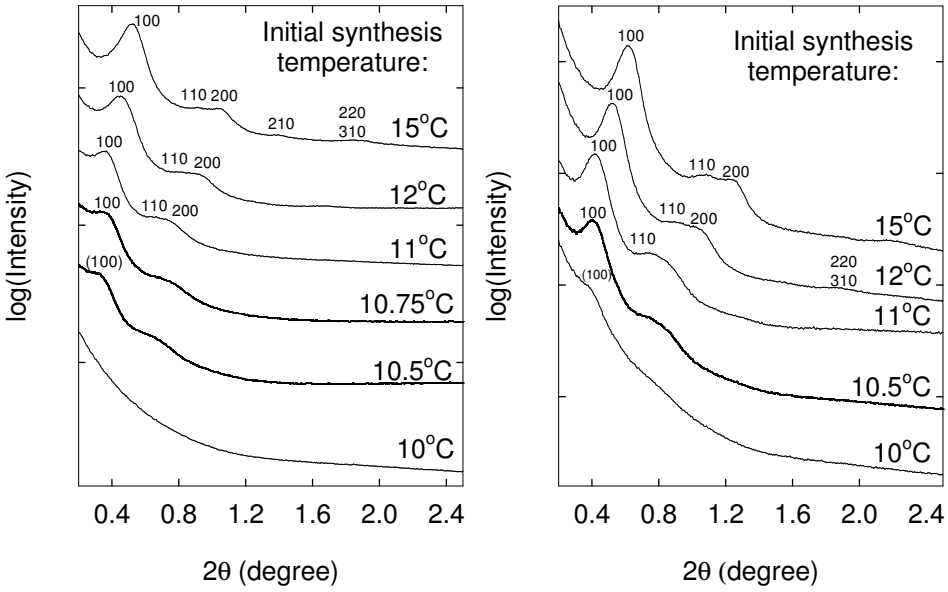

Figure 3.1.13 SAXS patterns for extracted ethylene- and ethenylene-bridged PMO samples synthesized at different initial synthesis temperature: (left) a) 10, b) 10.5, c) 10.75, d) 11, e) 12, and f) 15 ^{o}C and (right) a) 10, b) 10.5, c) 11, d) 12 and e) 15 ^{o}C using cyclohexane as a micelle expander (figure taken from reference 68).

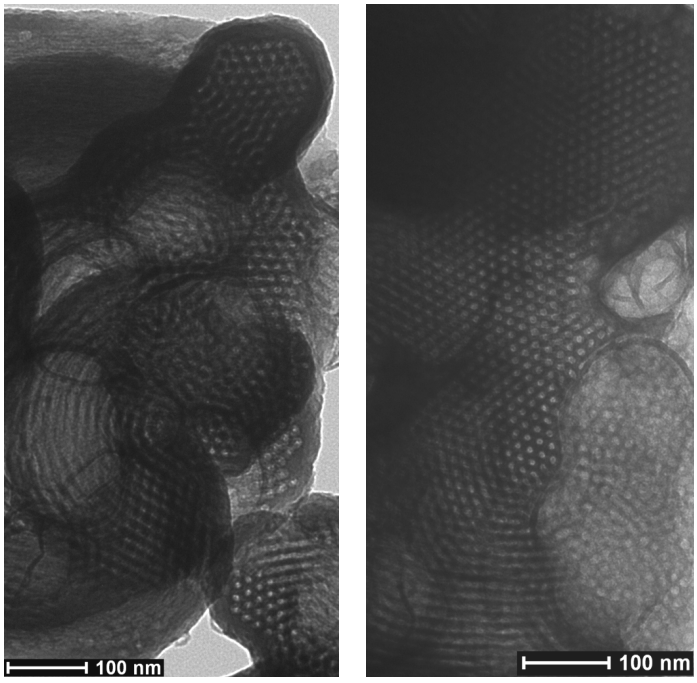

Figure 3.1.14 TEM image of (left) ethylene-bridged (as-synthesized) and (right) ethenylene-bridged PMO synthesized at initial synthesis temperature of 15 ^{o}C (figure taken from reference 68).

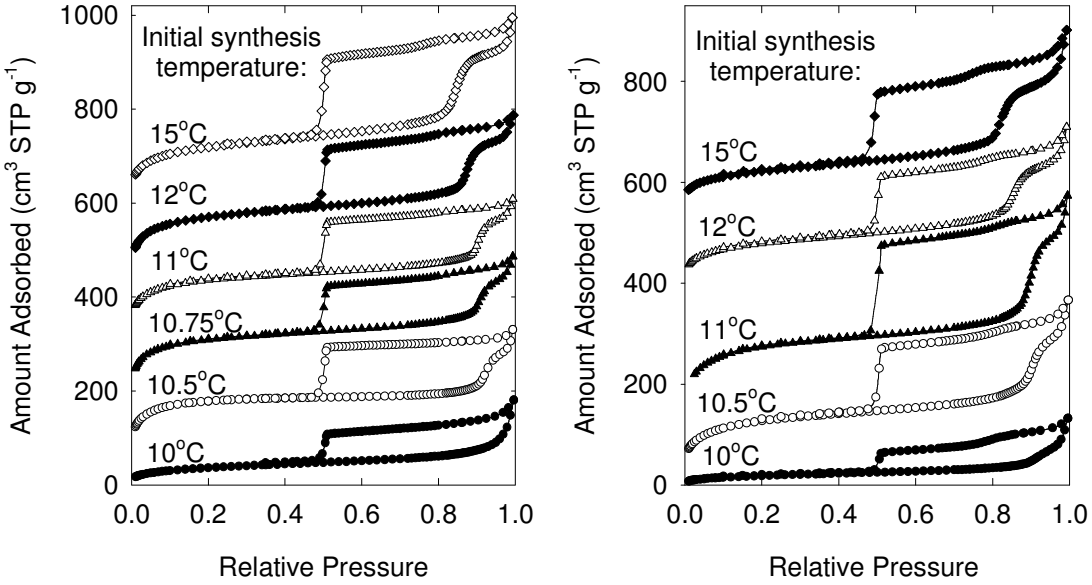

Figure 3.1.15 Nitrogen adsorption isotherm for extracted ethylene-bridged PMOs (left): samples synthesized at different initial synthesis temperature: a) 10, b) 10.5, c) 10.75, d) 11, e) 12 and f) 15 °C (sample synthesized at 12 °C initial synthesis temperature was calcined under nitrogen at 300 °C) and ethenylene-bridged PMOs (right) samples synthesized at different initial synthesis temperature: a) 10, b) 10.5, c) 11, d) 12 and e) 15 °C using cyclohexane as expander. (left) The isotherms were offset vertically by 80, 185, 210, 260, and 480 cm^3 STP g-1 for samples synthesized at initial synthesis temperature of 12, and 15 °C respectively. (right) The isotherms were offset vertically by 80, 390, and 550 cm^3 STP g-1 for samples synthesized at initial synthesis temperature of 11, 12, and 15 °C respectively (figure taken from reference 68).

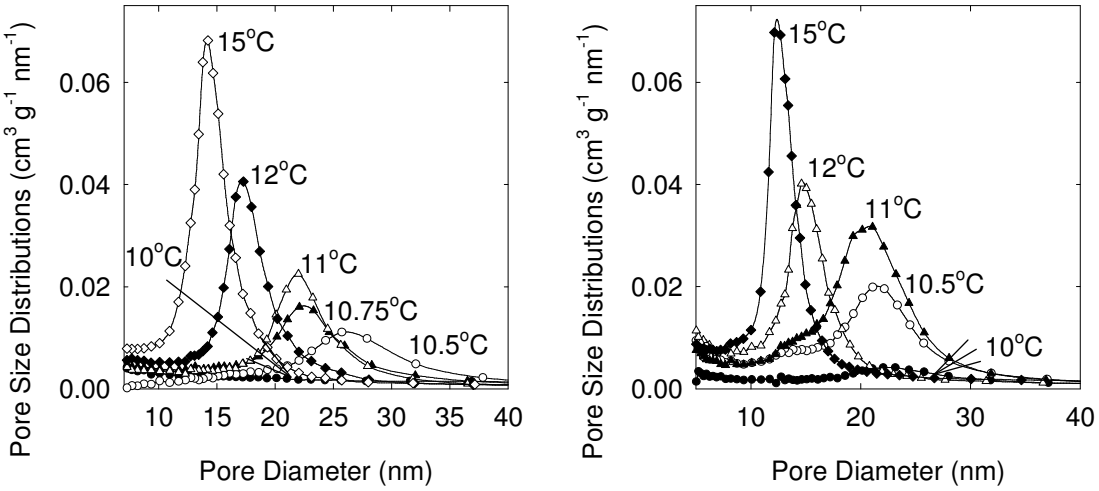

Figure 3.1.16 pore size distribution for extracted ethylene (left) and ethenylene- (right) bridged PMO samples synthesized at different initial synthesis temperature using cyclohexane as expander (figure taken from reference 68).

The nitrogen adsorption isotherm for both ethylene (Figure 3.1.15, left) and ethenylene- (Figure 3.1.15, right) bridged PMO shows steep capillary condensation step

at relative pressure of 0.85 and 0.83 respectively, which indicates that the materials have large pore sizes. The PSDs show maxima at 14.1 and 12.4 nm, respectively (Figure 3.1.16), which are larger than the largest pore diameters reported previously from any 2-D hexagonal PMO.

3.1.2a Effect of initial synthesis temperature. The initial synthesis temperature played a crucial role in determining the unit-cell parameters and pore sizes for the ethylene- and ethenylene-bridged PMOs (Table 3.1.4, Figures 3.1.13, 3.1.15 and 3.1.16). The lowering of the initial temperature from 15 to 10.75 ^{o}C for the ethylene-bridged PMO led to d_{100} increase from 16.8 to 26 nm, the latter being similar to the highest d_{100} reported for SBA-15 silicas.[116] As temperature decreased, the SAXS patterns become less resolved. TEM confirmed a 2-D hexagonal structure for the samples synthesized in the 10.75 – 15.00 ^{o}C range (Figure 3.1.17), although samples prepared at 10.75 – 11.00 ^{o}C also contained characteristic structures seen predominantly for 10.50 ^{o}C sample (see below).

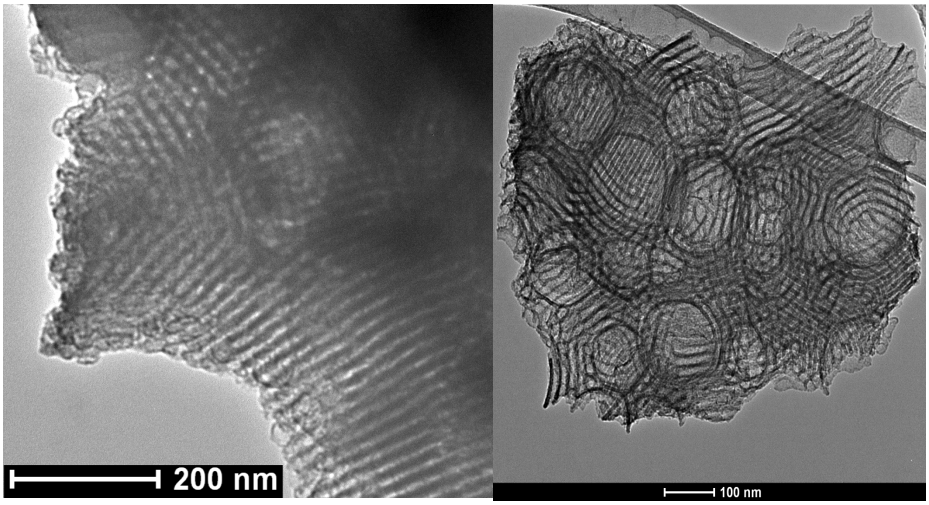

Figure 3.1.17 TEM image of extracted (left) ethylene- and (right) ethenylene-bridged PMO synthesized at initial temperature of 11 °C (figure taken from reference 68).

The SAXS pattern for the sample prepared at 10.5 ^{o}C was somewhat less resolved and TEM no longer provided evidence for 2-D hexagonal structure, although cylindrical mesopores that were embedded in apparently non-mesoporous framework were clearly seen (Figure 3.1.18). These pore channels tended to be parallel to one another and in some cases formed monolayer structures, which allowed us to clearly see the elongated shape of individual mesopores, which were quite uniform in diameter, straight or curved.

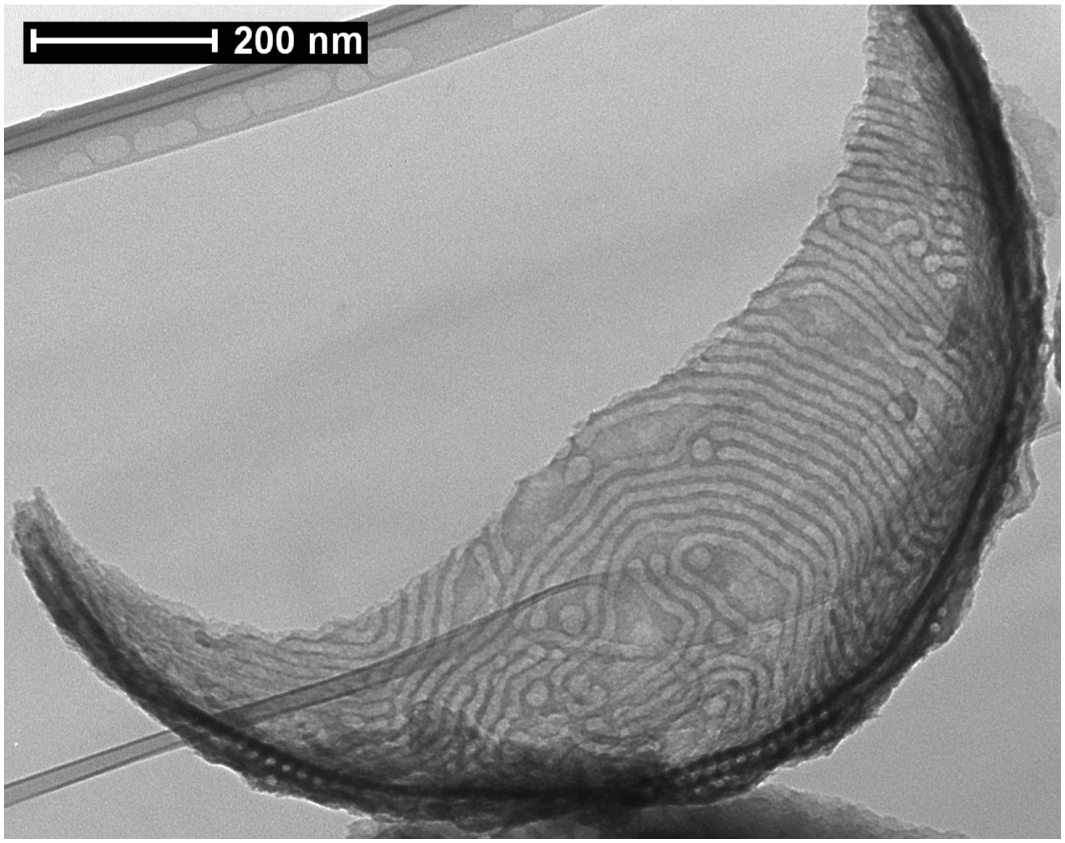

Figure 3.1.18 TEM image of ethylene-bridged PMO synthesized at initial temperature of 10.5 °C (figure taken from reference 68).

Hemispherical ends of the channels were clearly seen, so were circular pore openings at the edge. The observed morphology of the channels is expected to closely reflect the shape of the micelles that originally templated the material, thus providing a unique insight into the miceller structures. It should be noted that the mesopore voids are

expected to reflect primarily the hydrophobic core of the block copolymer micelle (in this case, PPO domains swollen with cyclohexane), whereas the space once occupied by PEO blocks is not expected to be readily visible, because PEO chains or strands of chains are expected to be occluded in the organosilica matrix,[70] as they template disordered (primarily microporous) network of pores in the organosilica walls. The fact that the channels, including their ends, seemed to be embedded in the apparently non-mesoporous framework may be the reason why the large mesopores of this PMO were accessible to N_2 molecules through narrow constrictions, as seen from nitrogen adsorption data (Figure 1.10) that will be discussed below. Namely, the micropores (or small mesopores) in the framework may constitute primary access pathways to the uniform mesopores. As was already discussed for methylene-bridged PMO and will be discussed below for other PMOs, their mesopores exhibited narrow entrances as well, so the capped mesopore ends may provide an explanation alternative to that involving plugged mesopore interiors known for some silica-based materials[74,75] and suggested also for some PMOs.[126]

As discussed above for ethylene-bridged PMO, the 2-D hexagonal structure persisted to 10.75 ^{o}C and the cylindrical pore shape was retained even at 10.50 ^{o}C. The largest nominal (BJH) pore diameter for 2-D hexagonally ordered PMO was 22 nm (10.75-11.00 ^{o}C synthesis), which is about two times larger than the largest pore size of ethylene-bridged PMOs reported earlier. In addition, the largest nominal pore diameter for our material with a confirmed cylindrical pore shape was 26 nm. As in the case of methylene-bridged PMO, the adsorption isotherms for ethylene-bridged PMOs exhibited broad hysteresis loops with capillary evaporation primarily at the lower limit of

adsorption-desorption hysteresis, indicating the existence of constrictions of diameter not larger than 5 nm in the mesopores.[201]

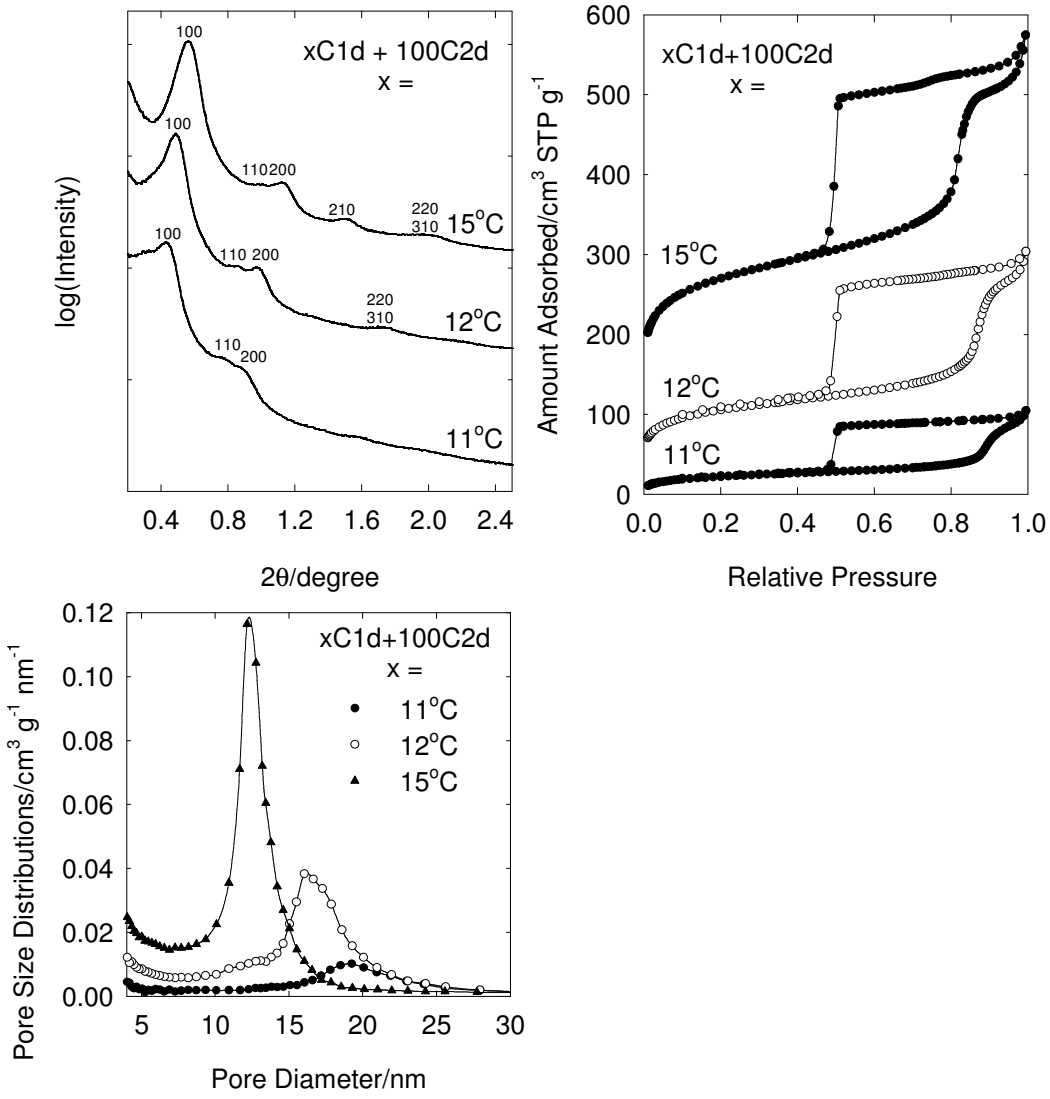

Figure 3.1.19 (top left) SAXS patterns, (top right) nitrogen adsorption isotherm, and (bottom) pore size distribution for extracted ethylene-bridged PMO synthesized at different initial synthesis temperature: 11, 12, and 15 ^{o}C using bis(triethoxysilyl)ethane (BTEE) as precursor and cyclohexane as micelle expander. The isotherms were offset vertically by 35, and 120 cm^3 STP g^{-1} for samples synthesized at initial synthesis temperature of 12, and 15 ^{o}C respectively (figure taken from reference 68).

A similar temperature effect was observed for ethylene-bridged PMOs synthesized using bis(triethoxysilyl)ethane (BTEE) precursor, which is a more cost-

effective and benign alternative to BTME, differing in the presence of ethoxy groups instead of methoxy groups that hydrolyze faster.

BTEE-derived PMOs were highly ordered (Figure 3.1.19), and their pore diameters increased as an initial synthesis temperature decreased from 15.00 to 11.00 ^{o}C (Table 3.1.4), following the trend observed for BTME-derived PMOs, although the later had somewhat larger interplanar spacing. These results point to a minor influence of the kind of the hydrolyzable group in the organosilica precursor on the formation of 2-D hexagonal PMOs templated by P123 swollen by cyclohexane.

The ethenylene-bridged PMOs exhibited a temperature behavior quite similar to that of the ethylene-bridged PMOs. The (100) interplanar spacing increased from 14.6 to 22.1 nm as the initial synthesis temperature was lowered from 15.00 to 10.50 ^{o}C, while the SAXS patterns were quite well resolved for all samples (Figure 3.1.13, right), even for the one prepared at 10.50 ^{o}C. However, there was no significant increase in d_{100} between 11.00 and 10.50 ^{o}C. The sample synthesized at 11.00 ^{o}C still exhibited 2-D hexagonally ordered structures of cylindrical mesopores (Figure 3.1.13), but also featured spectacular maze-like structures (Figure 3.1.20), whose images provide insight into the morphology of the mesopores as well as of the micelles, as discussed above. A further lowering of the initial temperature to 10.00 ^{o}C led to a material with a rather featureless SAXS pattern. The inferences from SAXS were mirrored by nitrogen adsorption data (Figure 3.1.15, right), which revealed uniform mesoporous structures with narrow PSDs (Figure 3.1.16, right) and the increase in the pore diameter for samples synthesized at initial temperatures between 15.00 and 11.00 ^{o}C, with additional minor increase in nominal (BJH) pore diameter (from 20.4 to 21.5 nm) as the temperature decreased to

10.50 ^{o}C. This limiting pore diameter is about two times larger than the largest pore diameters documented for 2-D hexagonal ethenylene-bridged PMOs. The lowering of temperature to 10.00 ^{o}C did not bring any appreciable pore size increase. The presence of constrictions in the mesopore structure was inferred from the shape of the hysteresis loops on nitrogen adsorption isotherms (Figure 3.1.15, right). One can conclude that for both ethylene- and ethenylene-bridged PMOs there is an appreciable temperature range (from 15 down to 10.50-10.75 ^{o}C) in which the temperature decrease brings about the unit-cell size and pore diameter increase, while the periodic nanostructure is no longer a major product in the case where the initial temperature is lowered to 10 ^{o}C.

Figure 3.1.20 TEM image of extracted ethenylene-bridged PMO synthesized an initial temperature of 11.00 °C (figure taken from reference 68).

3.1.2b Effect of amount of precursor. For ethylene-bridged PMO, the unit-cell size and the pore size were found to be largely independent of the BTME/P123 molar ratio. As the relative amount of the organosilica precursor was increased and eventually more than doubled, the 2-D hexagonal structure retained nearly constant d_{100} (16.1-18.0 nm) and similar degree of structural ordering, as seen from the occurrence of five reflections on SAXS patterns (Figure 3.1.21, and Table 3.1.4).

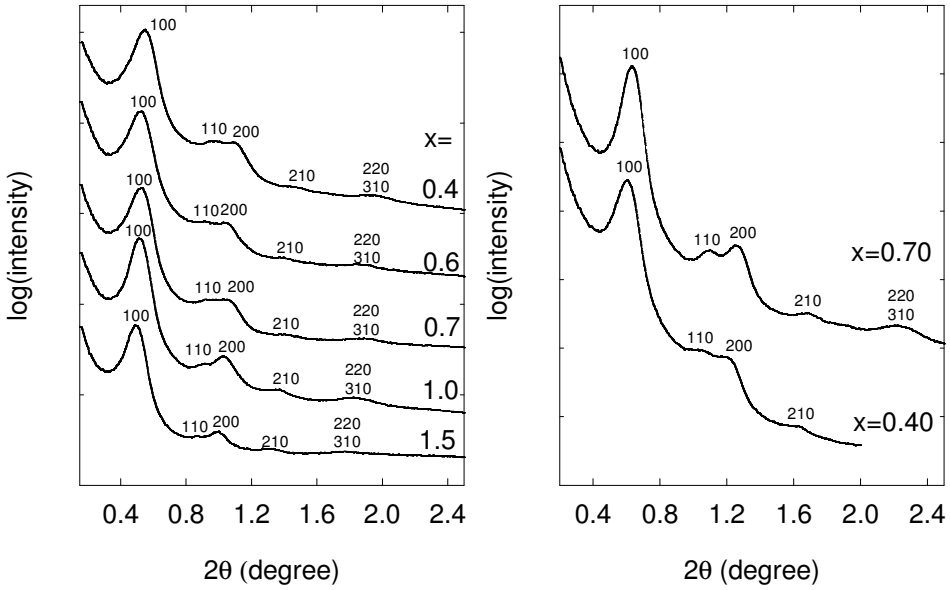

Figure 3.1.21 SAXS patterns of extracted ethylene-bridged (left) and ethenylene-bridged (right) PMOs with different amounts of precursors using cyclohexane as expander at initial synthesis temperature of 15 ^{o}C (figure taken from reference 68).

The lowest BTME/P123 ratio afforded the broadest PSD (Figure 3.1.22). On the other hand, the samples prepared at the two highest BTME/P123 ratios had non-mesoporous domains clearly visible in TEM, while such features were not apparent in the case of the lowest ratio.The intermediate ratios might have afforded a fraction of non-mesoporous organosilica deposited on the outer surface of the ordered nanoporous particles, as dark envelopes around the particles were observed (Figure 3.1.14). In addition, a small amount of worm-like or foam-like regions was seen for the lowest and intermediate BTME/P123

ratios. For the subsequent studies, the second lowest BTME/P123 ratio was chosen. The effect of BTEEn/P123 ratio on the pore size of ethenylene-bridged PMO was also rather minor (Figure 3.1.22, Table 3.1.4).

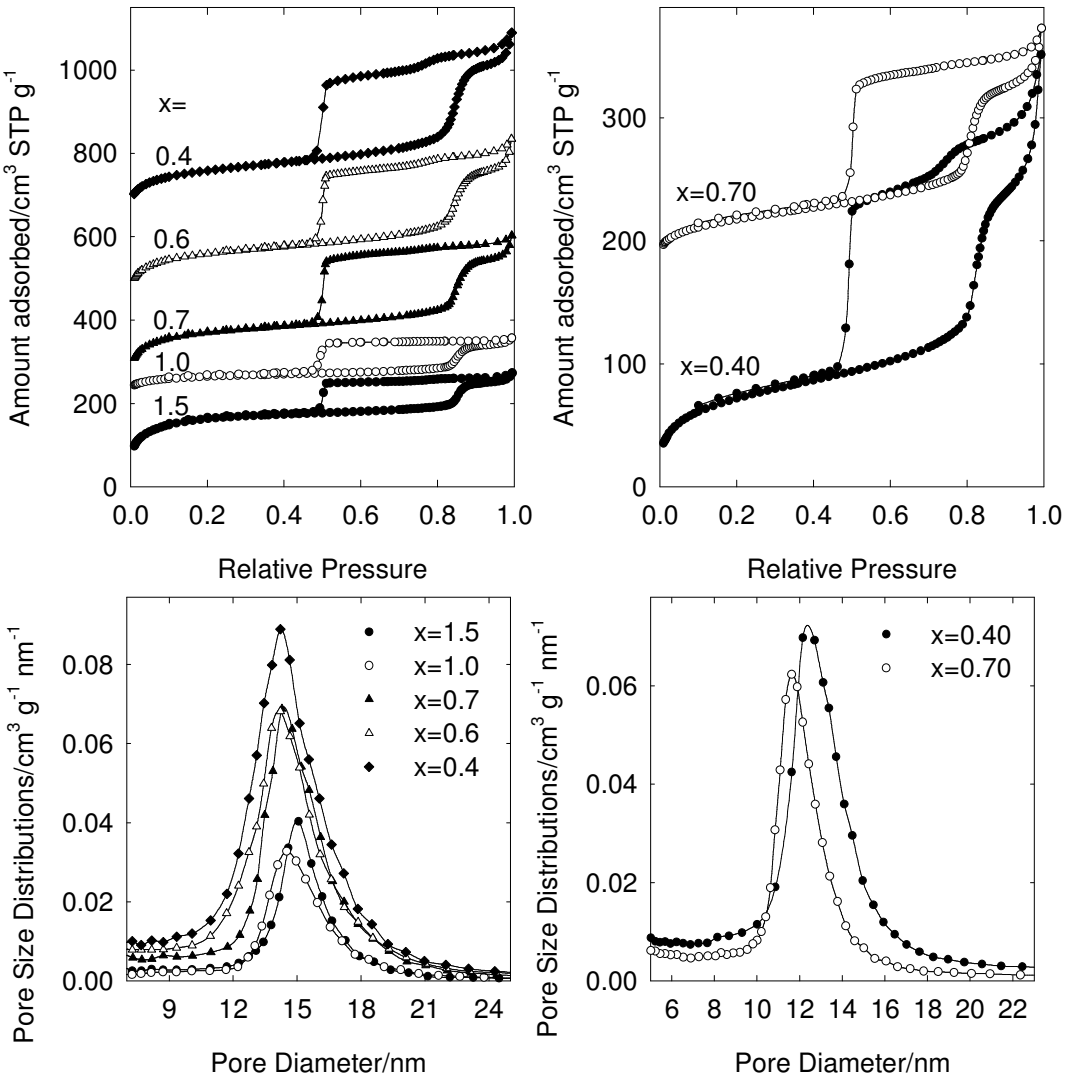

Figure 3.1.22 Nitrogen adsorption isotherms and pore size distributions of extracted (top left and bottom left) ethylene-, and (top right and bottom ight) ethenylene-bridged PMO with different amount of precursor using cyclohexane as expander. The isotherms are offset vertically by 220, 220, 420, and 640 cm^3 STP g^{-1} for samples synthesized with x= 1.0, 0.7, 0.6, and 0.4 respectively. The isotherm was offset vertically by 180 cm^3 STP g^{-1} for x=0.70 (figure taken from reference 68).

Clearly, the synthesis of large-pore PMOs with bridges composed of two carbon atoms proceeded in a similar manner for different proportions of the organosilica precursor to

the surfactant, unlike the synthesis of methylene-bridged PMO that was very sensitive to this factor. The integrity of ethylene and ethenylene bridges after solvent extraction was confirmed by ^{29}Si CP MAS NMR (Figure 3.1.23). ^{29}Si CP MAS NMR shows three peaks at 50, 60, and 64 ppm, corresponding to T sites (Si sites attached to three oxygen atoms T^n, n=1-3): T^1 [*Si*C(OH)$_2$(OSi)], T^2 [*Si*C(OH)(OSi)$_2$], and T^3 [*Si*C(OSi)$_3$], respectively, for extracted material (Figure 3.1.23, left). Extracted ethenylene-bridged PMOs show signals at 67 (shoulder), 75, and 85 ppm, corresponding to T^1, T^2, and T^3 type silicon respectively (Figure 3.1.23, right). After extraction with ethanol, no Q sites (Si sites attached to four oxygen atoms Q^n, n=1-4) (between -90 and -110 ppm) appear indicating the structural integrity of organosilane groups.

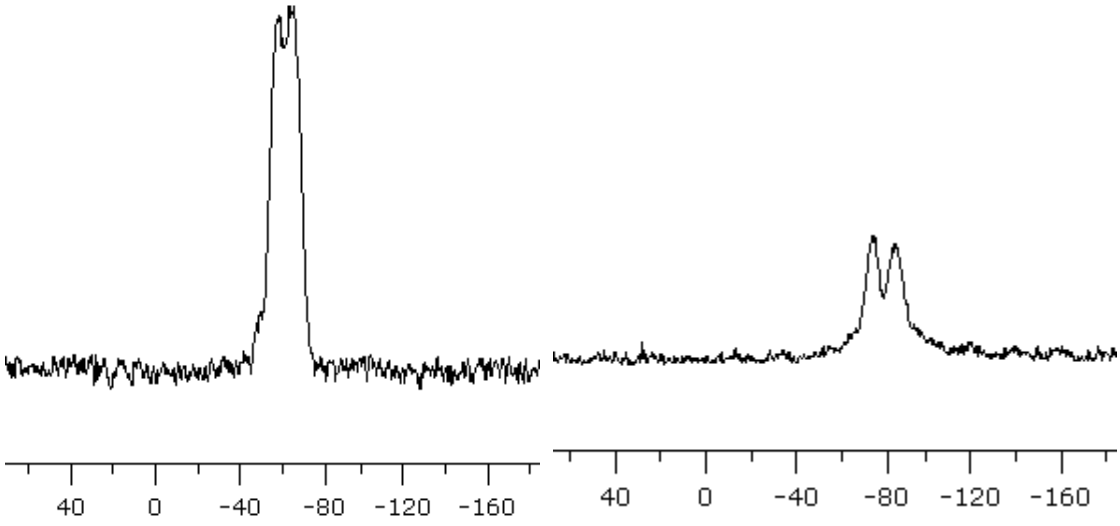

Figure 3.1.23 (left) ^{29}Si CP MAS NMR for extracted (left) ethylene-, and (right) ethenylene-bridged PMOs (figure taken from reference 68).

The results discussed above for methylene, ethylene, and ethenylene-bridged PMO show broad applicability of P123/cyclohexane combination in the synthesis of PMO with aliphatic bridges. Additional evidence pointing to that comes from our work using aliphatic bridging group with a double bond in the middle carbon atom using $(CH_3O)_3$Si-

CH_2-C(=CH_2)-CH_2-Si(OCH_3)$_3$ as a precursor. Under optimized conditions, the material shows a strong peak and a shoulder on SAXS pattern and fairly large pore size (14-15 nm). TEM revealed an ordered, but heterogeneous structure.

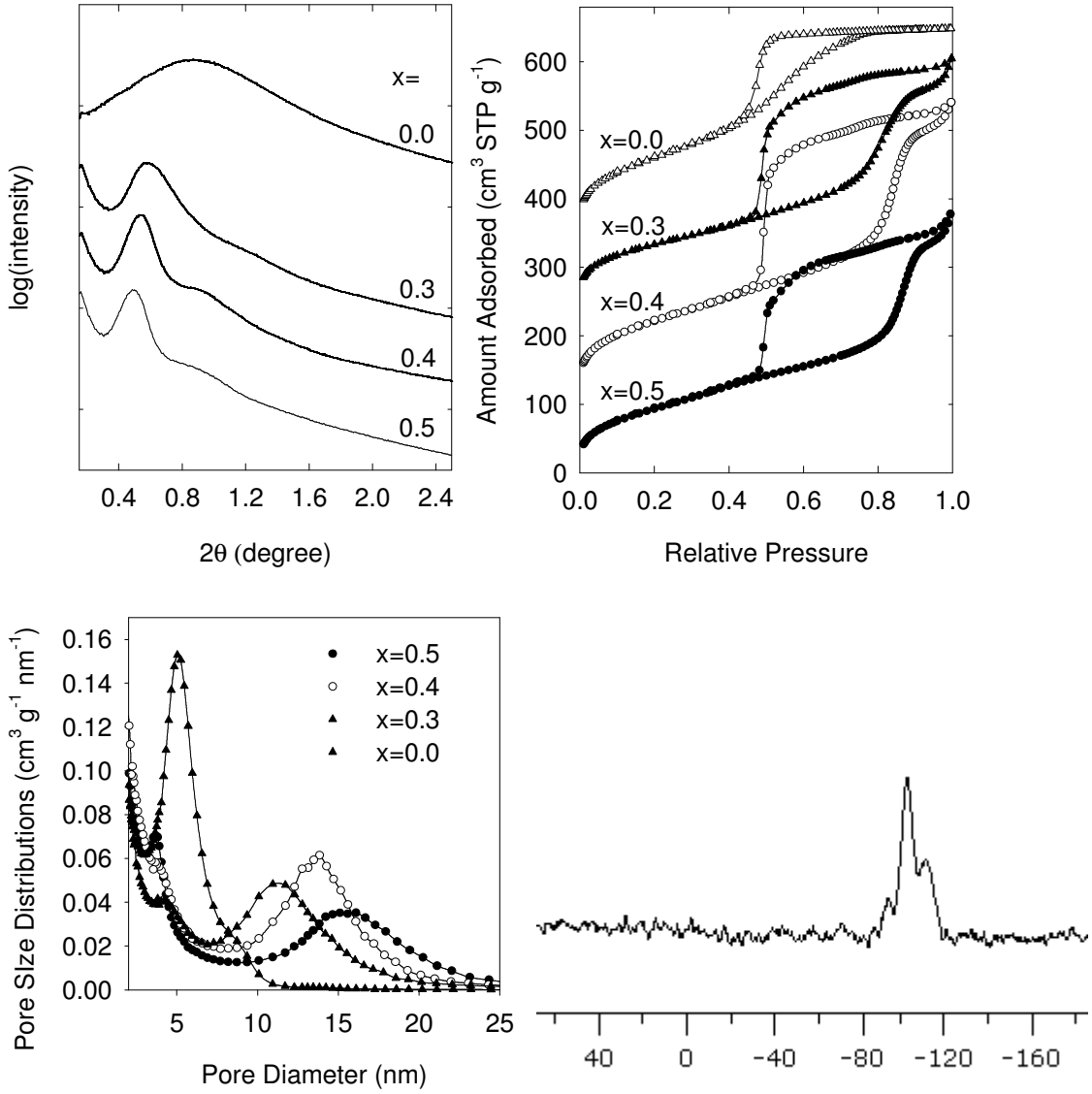

Figure 3.1.24 (top left) SAXS patterns, (top right) nitrogen adsorption isotherms and (bottom left) PSDs of extracted PMOs synthesized using -CH_2(C=CH_2)CH_2-bridging group as precursor with different amount of precursor at 15 ^oC initial synthesis temperature using cyclohexane as expander. (Bottom right) ^{29}Si CP MAS of extracted PMO synthesized using -CH_2(C=CH_2)CH_2-bridging group as precursor (figure taken from reference 68).

Unfortunately, the ^{29}Si CP MAS NMR shows complete cleavage of Si-C bonds and conversion to silica (Figure 3.1.24), which can be related to the similarity of bridging

group to the allyl group that can be used as hydrolyzable group.[205] However, one can speculate that the periodic structure formed before any major cleavage of the bridging groups took place, because in the case of high content of cyclohexane in the synthesis mixture, silica derived from TEOS had a much less ordered, large-pore structure.[116] Therefore, the above results for the new organosilica precursor appear to confirm the general applicability of the P123/cyclohexane pair in the synthesis of large-pore PMOs with aliphatic bridging groups.

3.1.3 Phenylene-bridged PMO. The synthesis of large-pore 2-D hexagonal PMO with phenylene bridging groups using Pluronic P123 surfactant in combination with readily available swelling agents (cyclohexane or hexane) was unsuccessful, affording materials with moderate pore diameters (8-9 nm) and devoid of any significant structural ordering. On the other hand, the use of TIPB, which was demonstrated earlier to be an excellent swelling agent for SBA-15 silica[116] afforded a family of large-pore 2-D hexagonal phenylene-bridged PMOs after identification of a proper temperature range. An initial synthesis temperature of 15 ^{o}C, which was suitable for the synthesis of LP-FDU-12[115] and LP-SBA-15 silicas,[116] as well as large-pore PMOs with aliphatic bridges (see above), was found to be a lower boundary of the range for the formation of 2-D hexagonal phenylene-bridged PMO. The selection of temperatures of 14.5-18 ^{o}C allowed us to obtain PMOs with a wide range of interplanar spacings and pore diameters. The SAXS pattern (Figure 3.1.25) for phenylene-bridged PMO synthesized at an initial synthesis temperature of 18 ^{o}C featured (100), (110), (200), and (210) reflections for 2-D hexagonal structure with d_{100} = 15.0 nm. TEM further supported this structural

assignment (Figure 3.1.26), although the presence of some bulk (non-nanostructured) domains was also likely based on TEM.

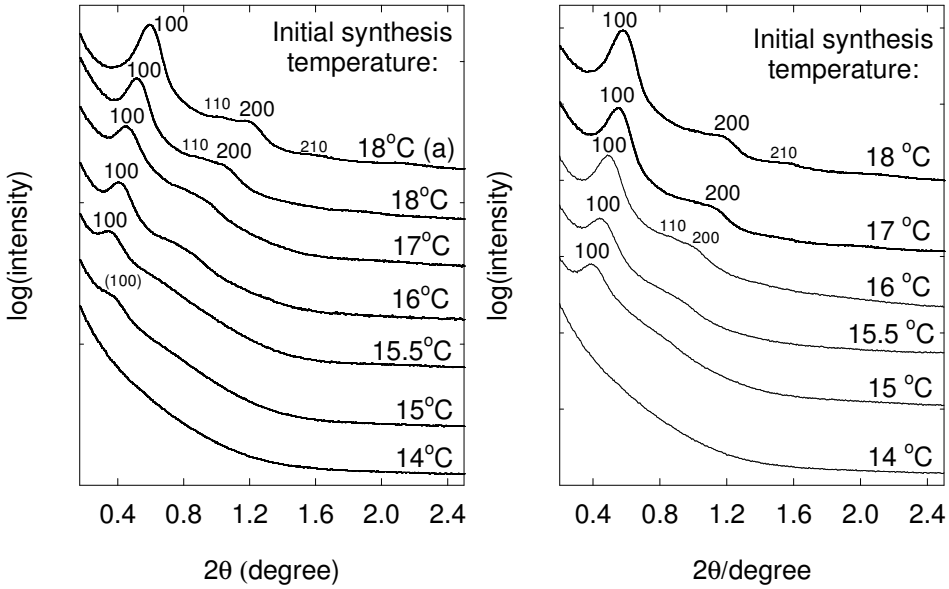

Figure 3.1.25 (left) SAXS patterns of calcined phenylene-bridged PMOs synthesized at different initial temperature using 1.2 ml TIPB expander per 0.6 g P123 except for the sample prepared at 18 °C (see below) and 14 °C which were prepared with 0.6 ml TIPB. (right) SAXS patterns of calcined phenylene-bridged PMOs synthesized at different initial temperature using 0.6 mL TIPB expander per 0.6 g P123. Note that the sample prepared at 18 °C was prepared under the same conditions as the sample denoted 18 °C (a), but it was from a different batch (figure taken from reference 68).

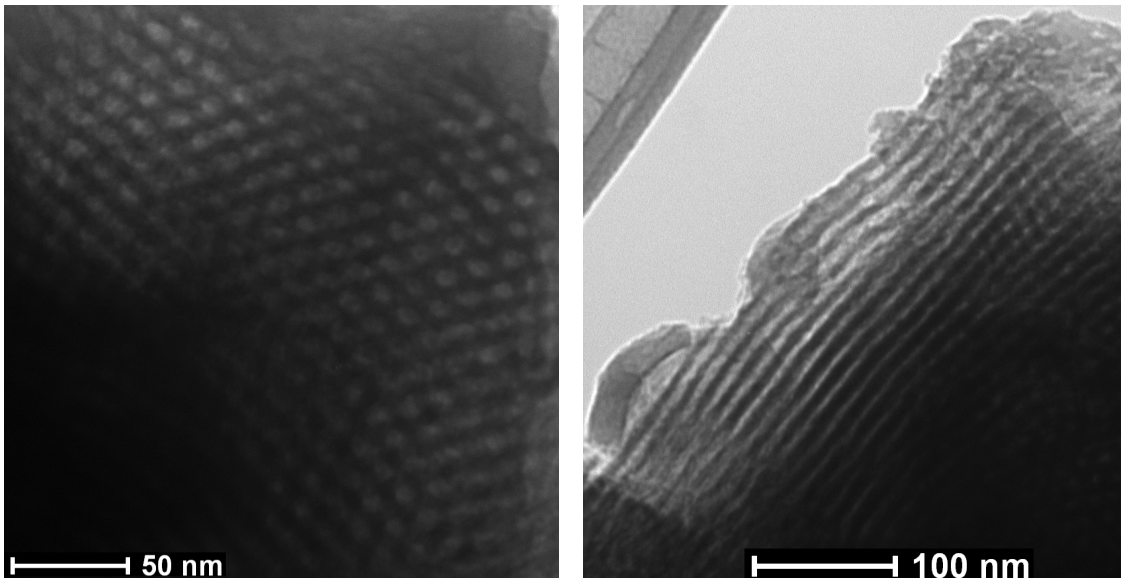

Figure 3.1.26 TEM images of PMO with phenylene bridging groups synthesized at 18 °C (figure taken from reference 68).

^{29}Si CP MAS NMR confirmed that the removal of surfactant by: (i) extraction followed by calcination under air at 250 ^{o}C or (ii) calcination under nitrogen at 300 ^{o}C, did not lead to any appreciably cleavage of Si-C bonds in the PMO framework (Figure 3.1.27).

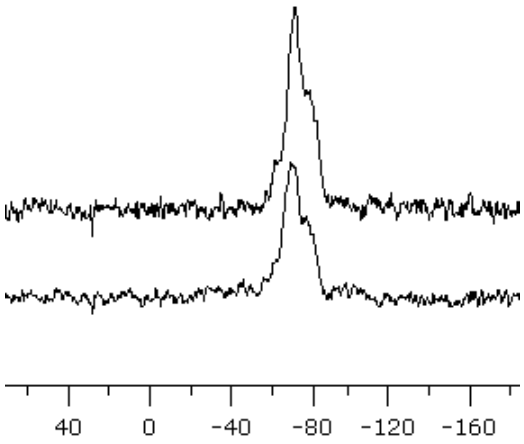

Figure 3.1.27 ^{29}Si CP MAS NMR for phenylene-bridged samples calcined at 300 °C under nitrogen (top spectrum) and calcined at 250 °C under air after extraction with ethanol (bottom spectrum) (figure taken from reference 68).

The PMO synthesized at 18 ^{o}C exhibited an adsorption isotherm (Figure 3.1.28) similar to that discussed above for ethylene- and ethenylene-bridged PMOs, and the nominal (BJH) pore diameter of 12.0 nm (Figure 3.1.28), which is larger than the pore diameter reported earlier for any PMO with 2-D hexagonal structure. The above synthesis was performed with 0.6 ml TIPB per 0.6 g P123, which is similar to the amount used in ULP-SBA-15 synthesis.[116] The nominal pore diameter was increased to 14.4 nm and d_{100} reached 17.3 nm, when the relative amount of TIPB was doubled (this TIPB/P123 ratio was used for most of the samples discussed below, while a lower ratio was used for other samples described in Table 3.1.5. With a decrease of the initial synthesis temperature to 15.5 ^{o}C, the interplanar spacing increased to 26 nm (as seen from SAXS shown in Figure 3.1.25) and the nominal (BJH) pore diameter increased to 27 nm, while the 2-D hexagonal structure was retained (as seen from SAXS and/or TEM,

Table 3.1.5 Structural properties of phenylene-bridged PMOs.[a]

Sample (bridge, initial temp.)	d_{100} (nm)	S_{BET} (m^2/g)	V_t (cm^3/g)	V_{mic} (cm^3/g)	w_{BJH} (nm)
Phenylene, 18 °C, x=0.3 [b]	15.0	609	0.60	0.19	12.0
Phenylene, 18 °C, x=0.3 [c]	17.3	646	0.68	0.21	14.4
Phenylene, 17 °C, x=0.3 [c]	19.6	669	0.89	0.19	17.2
Phenylene, 16 °C, x=0.3 [c]	22.1	722	0.80	0.24	20.3
Phenylene, 15.5 °C, x=0.3 [c]	26.4	646	0.69	0.23	27.5
Phenylene, 15 °C, x=0.3 [c]	~24[d]	664	0.77	0.23	25.1
Phenylene, 14 °C, x=0.3 [b]	-[e]	466	0.40	0.18	-[f]
Phenylene, 17°C, x=0.3 [b]	15.9	642	0.56	0.22	12.7
Phenylene, 16°C, x=0.3 [b]	18.2	514	0.49	0.16	14.8
Phenylene, 15.5°C, x=0.3 [b]	19.6	620	0.50	0.23	16.4
Phenylene, 15°C, x=0.3 [b]	22.7[d]	553	0.52	0.19	21.1
Phenylene, 18°C, x=0.0 [b]	16.4	751	0.97	0.19	14.5
Phenylene, 18°C, x= - 0.1 [b]	16.5	820	1.25	0.17	15.6
Phenylene, 17°C, x= - 0.1 [b]	18.6	820	1.23	0.21	17.5
Phenylene, 17°C, x= - 0.1 [b]	-[e]	792	1.34	0.21	-[f]
Phenylene, 16°C, x= - 0.1 [b]	19.6	785	1.19	0.19	18.3
Phenylene, 15.5°C, x= - 0.1 [b]	20.8	790	1.17	0.21	20.8
Phenylene, 15°C, x= - 0.1 [b]	24.5	820	1.21	0.23	25.8
Phenylene, 14.5°C, x= - 0.1 [b]	25.9[d]	757	1.04	0.22	26.4
Phenylene, 14°C, x= - 0.1 [b]	-[e]	760	1.00	0.22	27.3
Phenylene, 18°C, x= - 0.15 [b]	18.0	896	1.46	0.19	16.9
Phenylene, 18°C, x= - 0.2 [b]	19.2	927	1.65	0.17	18.5
Phenylene, 18°C, x= - 0.3 [b]	-[e]	874	1.78	0.05	-[f]

[a] Notation: d_{100}, (100) interplanar spacing for either calcined or extracted sample. $S_{BET,}$ BET specific surface area; $w_{BJH,}$ BJH pore diameter; $V_{t,}$ total pore volume, $V_{mic,}$ micropore volume; [b] Amount of TIPB used was 0.6 ml per 0.6 g P123; [c] Amount of TIPB used was

1.2 ml per 0.6 g P123; [d] Calculated assuming that the first peak is (100) reflection of 2-D hexagonal structure, which is consistent with TEM observation; [e] Could not be evaluated due to absence of peak on SAXS pattern; [f] No clear peak on mesopore size distribution.

see illustrative image in Figure 3.1.30). As in the case of other PMO families, the mesopores exhibited constrictions, as seen from broad adsorption-desorption hysteresis loops on the isotherms (Figure 3.1.28). One can conclude that 2-D hexagonal phenylene-bridged PMOs with d_{100} and pore diameter up to two times larger than that reported earlier for this PMO composition were successfully synthesized.[68]

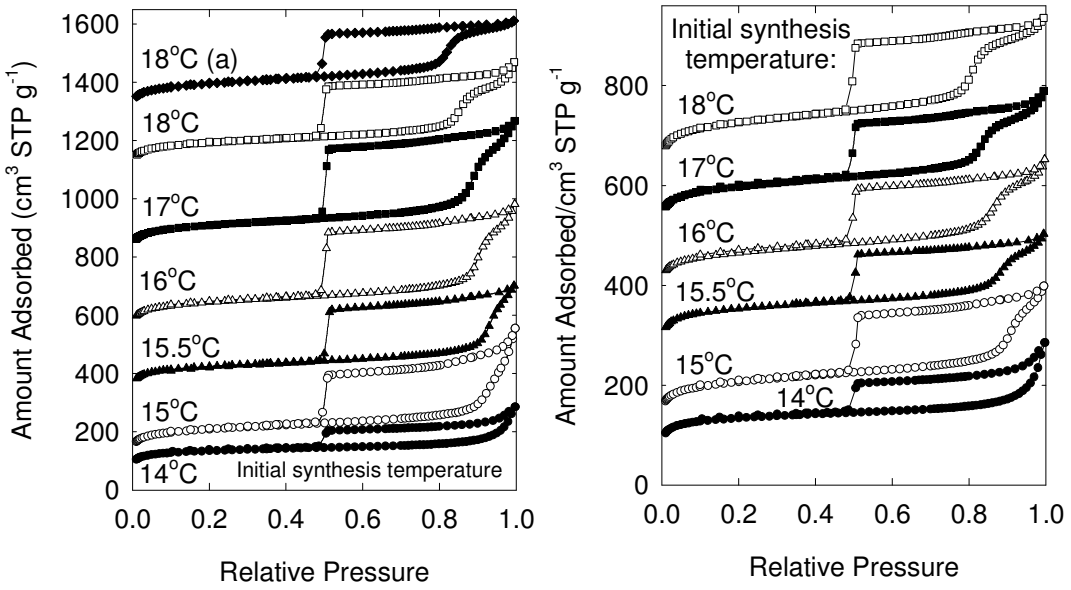

Figure 3.1.28 (left) nitrogen adsorption isotherms of calcined phenylene-bridged PMOs synthesized at different initial temperature using 1.2 ml TIPB expander per 0.6 g P123 (except for 18 °C (a) and 14 °C, for which 0.6 ml TIPB per 0.6 g P123 was used). (left) Isotherms for sample synthesized at initial synthesis temperature of 15, 15.5, 16, 17, and 18 °C are offset vertically by 50, 180, 320, 430, and 530 cm ^{3} STP g^{-1} respectively. (right) nitrogen adsorption isotherms of calcined phenylene-bridged PMOs synthesized at different initial temperature using 0.6 ml TIPB expander per 0.6 g P123. (right) Isotherms for samples synthesized at initial synthesis temperature of 15, 15.5, 16, 17, and 18 °C are offset vertically by 50, 180, 320, 430, and 530 cm^3 STP g^{-1} respectively (figure taken from reference 68).

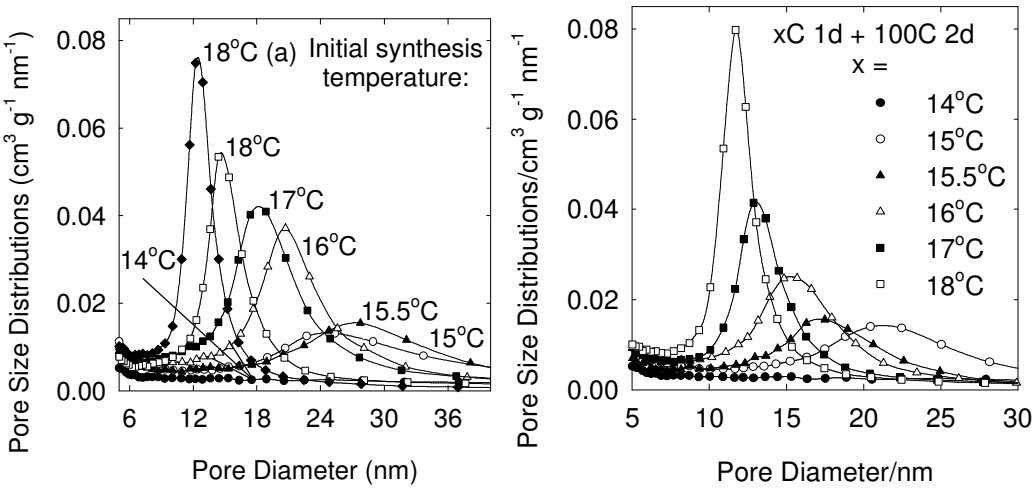

Figure 3.1.29 (left) PSDs of calcined benzene-bridged organosilica synthesized at different initial synthesis temperature using 1.2 ml TIPB as expander per 0.6 g P123 (except for 18 ^{o}C (a) and 14 ^{o}C, for which 0.6 ml TIPB per 0.6 g P123 was used). (right) PSDs of calcined benzene-bridged organosilica synthesized at different initial synthesis temperature using 0.6 ml TIPB as expander per 0.6 g P123 (figure taken from reference 68).

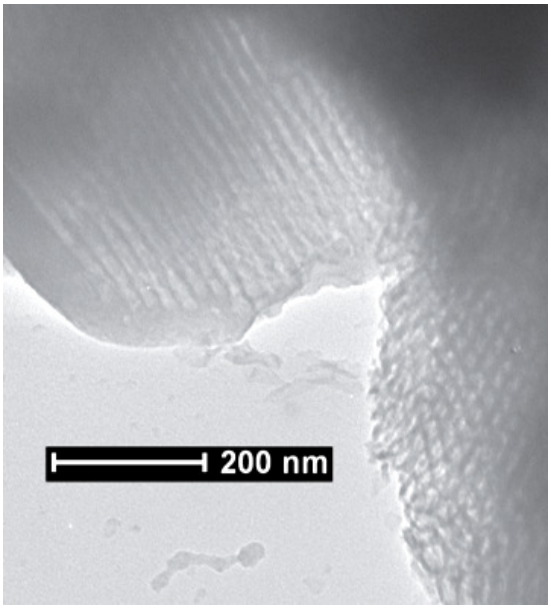

Figure 3.1.30 TEM image of phenylene-bridged PMO synthesized at 15.5 ^{o}C (calcined under nitrogen at 300 ^{o}C) (figure taken from reference 68).

3.1.3a Effect of amount of precursor. For phenylene-bridged PMO, the unit-cell size and the pore size was found to be dependent on BTEB/P123 molar ratio. As the relative amount of organosilica precursor was lowered, the intensity of (110) peak on the SAXS

pattern was found to increase up to organosilica precursor amount of x= -0.1 (20% less Si per P123 in comparison to the conditions for SBA-15 synthesis) and then after further lowering of the precursor amount, the quality of the material decreased and for x= -0.3 there was almost no evidence of formation of a periodic structure (Figure 3.1.32). For the lowest BTEB/P123 molar ratio (i.e., x= -0.3 in this case), there appears to be a second capillary condensation step which indicates the occurrence of secondary mesoporosity. It is clear that there is an optimum amount of precursor necessary for the formation of 2-D hexagonal structure with high pore volume. In this case, x= -0.1 was found to be the optimum amount to get large-pore-volume ordered mesoporous materials.

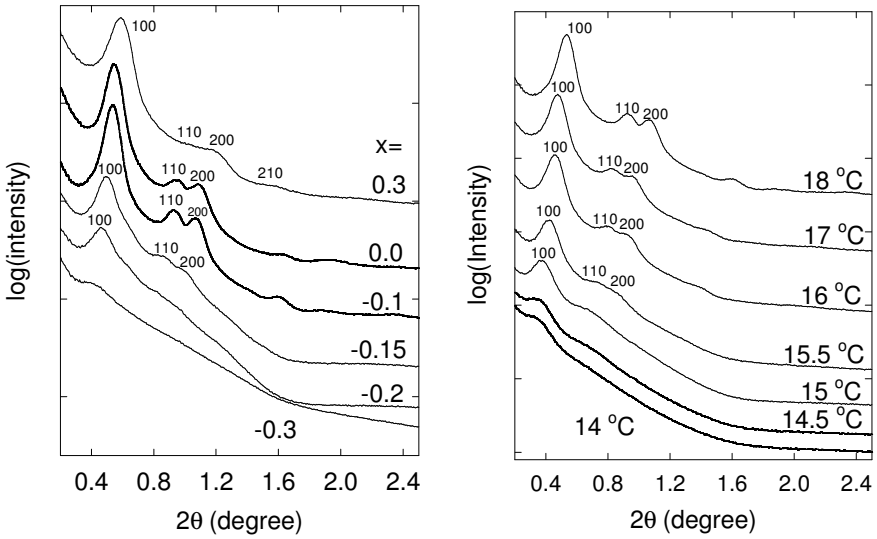

Figure 3.1.31 SAXS patterns of calcined phenylene-bridged PMOs synthesized with (left) different amount of precursor at initial synthesis temperature of 18 ^{o}C and (right) with different initial synthesis temperature at x= -0.1 using TIPB as a micelle expander.

3.1.3b Effect of initial synthesis temperature. After optimization of the amount of precursor, we further studied the influence of initial synthesis temperature in order to enlarge the pore size. We observed that with the decrease in the initial synthesis temperature from 18 ^{o}C down to 14 ^{o}C, results in the (100) peak position shifted toward lower 2θ value, indicating enlargement of the interplanar spacing (Figure 3.1.31).

Materials synthesized in initial temperature range from 18-15.5 ^{o}C, exhibited SAXS patterns with reflections that can clearly be indexed as (100), (110), and (200) peaks, indicating the formation of 2-D hexagonal structure. After further lowering the temperature to 15 ^{o}C, there was a shoulder in addition to (100) peak, and materials synthesized at 14.5 and 14 ^{o}C, exhibited only a shoulder visible on SAXS patterns, indicating the loss of long range structural ordering. However, TEM showed 2-D hexagonal domains even for the sample synthesized at 14.5 ^{o}C. The nitrogen adsorption isotherms and PSDs (Figure 3.1.32 and 3.1.33) are consistent with SAXS patterns. All the materials show broad hysteresis loops with capillary condensation pressure increase with lowering of the initial synthesis temperature. For materials synthesized at 14-15 ^{o}C, the capillary condensation pressure remained almost constant with decreasing the step height indicating decrease in the mesopore volume.

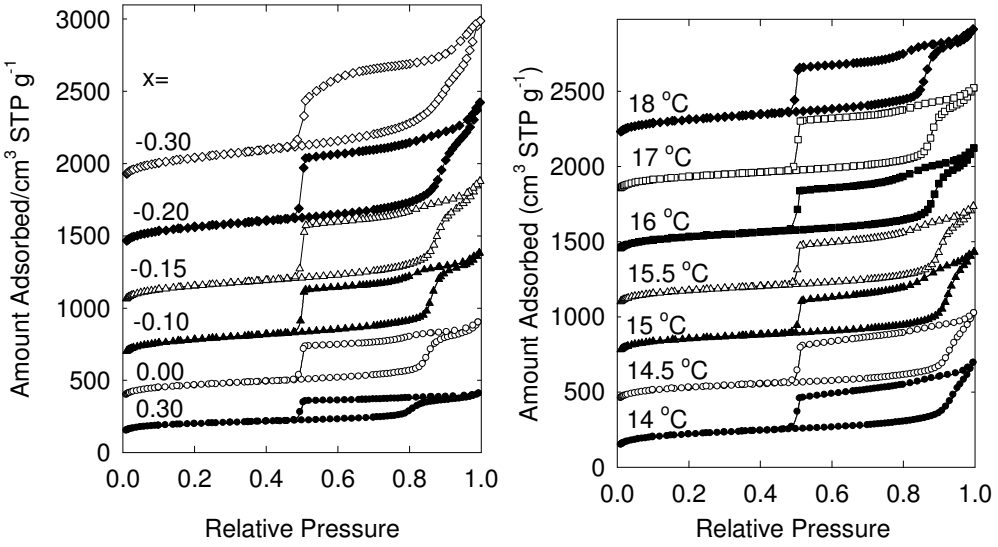

Figure 3.1.32 Nitrogen adsorption isotherms of calcined phenylene-bridged PMOs synthesized with different amount of precursor at initial synthesis temperature of 18 ^{o}C (left) and with different initial synthesis temperature at x= -0.1 (right) using TIPB as a micelle expander. (left) Isotherms were offset vertically by 250, 550, 900, 1300, and 1800 cm^3 STP g^{-1} for samples synthesized with x= 0.00, -0.10, -0.15, -0.20, and -0.30, respectively. (right) Isotherms were offset vertically by 310, 620, 950, 1310, 1700, 2080 cm^3 STP g^{-1} for samples synthesized at 14.5, 15, 15.5, 16, 17, and 18 ^{o}C temperature.

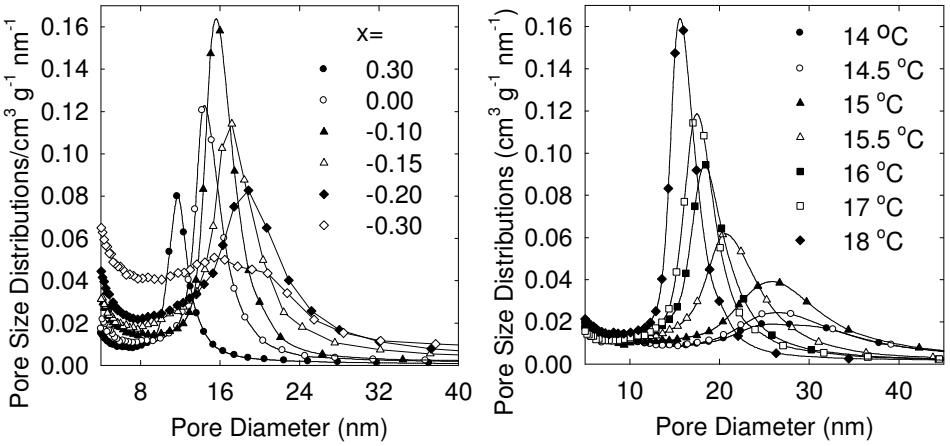

Figure 3.1.33 Pore size distributions of calcined phenylene-bridged PMOs synthesized with different amount of precursor at initial synthesis temperature of 18 ^{o}C (left) and with different initial synthesis temperature at x= -0.1 (right) using TIPB as a micelle expander.

3.1.3c Effect of hydrothermal treatment temperature. The phenylene-bridged PMOs were treated hydrothermally at higher temperature (100-170 ^{o}C for 2 days during the synthesis) to check whether that treatment removes the constrictions present in the main mesopores. The SAXS patterns show that after such treatment all the peaks did not change intensity appreciably. Unlike in the case of methylene-bridged PMO, the accessibility of the mesopores did not seem to improve upon hydrothermal treatment at 130 ^{o}C or 150 ^{o}C for 2 days. At 170 ^{o}C for two days, there appears to be almost complete removal of constrictions present in the mesopores as seen from the desorption branch of adsorption isotherm (Figure 3.1.34). However, ^{29}Si CP MAS NMR for phenylene-bridged PMO hydrothermally treated at 170 ^{o}C for two days shows appearance of peaks at 95, 103, and 110 ppm, corresponding to Q sites indicating cleavage of Si-C bonds (Figure 3.1.34). At the same time, there are still peaks at 65 (shoulder), 72, and 81 ppm corresponding to T sites which indicates that there still exists considerable amount of organic groups.

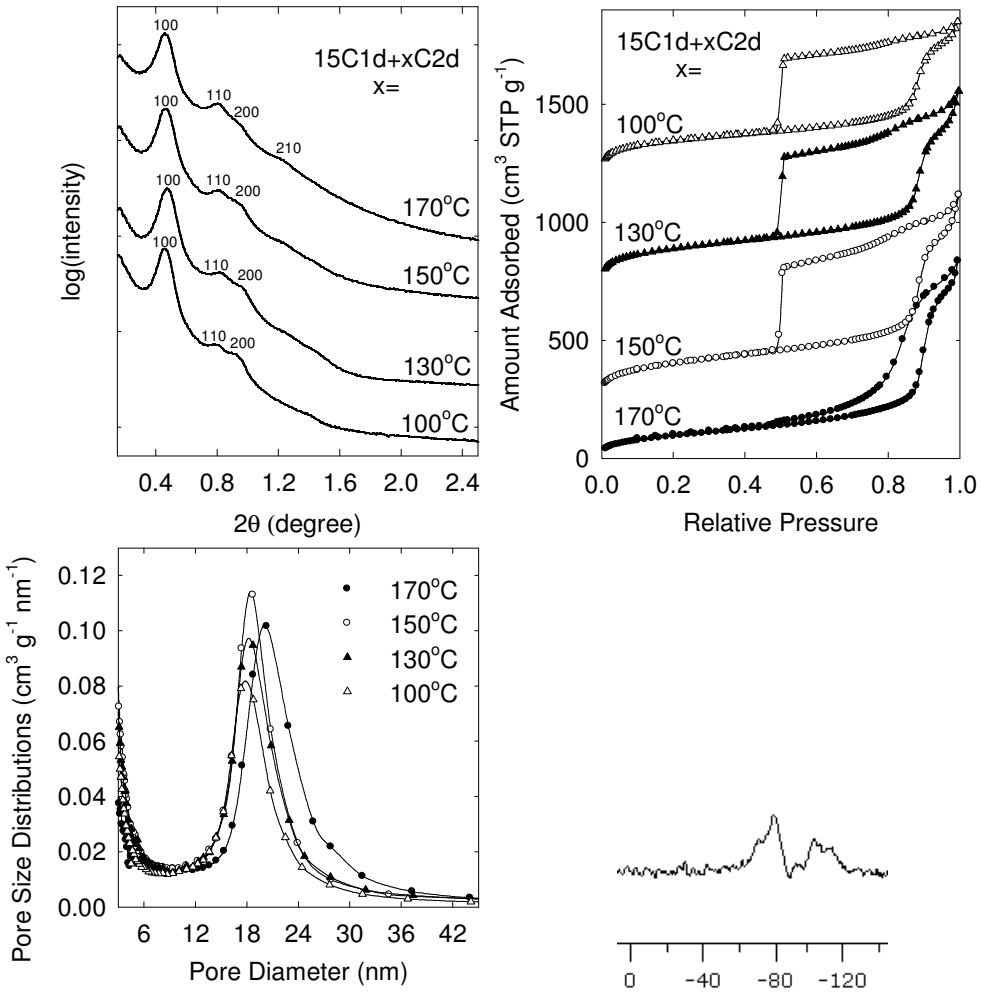

Figure 3.1.34 SAXS patterns, nitrogen adsorption isotherms, and PSDs for materials hydrothermally treated at different temperatures. ^{29}Si CP MAS NMR for phenylene-bridged PMO hydrothermally treated at 170 ^{o}C for 2 days.

3.1.4 Proposed mechanism of synthesis of large-pore-PMOs. The successful formation of 2-D hexagonal large-pore PMOs under sub-ambient conditions using Pluronic P123 as a surfactant and cyclohexane or TIPB as a swelling agent follows the predictions applied in selecting a surfactant/swelling-agent combination for the synthesis of ultra-large-pore SBA-15.[116] It was already demonstrated[116,199] that the identity of the hydrolyzable group (ethoxy or methoxy) of the tetraalkoxysilane silica precursor does not have any dramatic effect on the formation of ULP-SBA-15. Similarly, there was no major difference between the results for two different organosilica precursors (BTME and

BTEE with methoxy or ethoxy groups, respectively) for 2-D hexagonal ethylene-bridged PMO. On the other hand, the presence and identity of the bridging organic group in the precursor and ultimately in the PMO framework has a major effect on the formation of the material and its unit-cell size. Let us consider first the use of a large relative amount of cyclohexane, which is known to afford poorly-defined, large-pore pure-silica product.[116] Under these conditions, methylene-bridged PMOs with very large d_{100} and pore diameter formed at a particular organosilica-precursor/P123 molar ratio, in a quite wide temperature range from 17 down to 14 ^{o}C, and with an interplanar spacing and pore diameter increase paralleled by a significant loss of ordering at 13 ^{o}C. On the other hand, PMOs with slightly larger, two-carbon atom bridging groups (ethylene and ethenylene) were formed at temperatures from 15 to 10.5-10.75 ^{o}C, and only at the lower limit of this range (10.5-11.0 ^{o}C), their unit-cell sizes approached that of the methylene-bridged PMO, which formed a well-ordered nanostructure only at 14 ^{o}C or higher. The formation of the PMOs with two-carbon-atom bridges was largely independent on the organosilica-precursor/surfactant molar ratio, unlike in the case of methylene-bridged PMO. Therefore, for a particular surfactant/swelling-agent combination, the formation of an ordered structure as well as its unit-cell and pore dimensions are not merely governed by the temperature, but also are significantly influenced by the precursor and/or framework composition. This suggests that the organosilica precursor or more likely, the product of its hydrolysis, mediate the formation of the swollen micelles. The interactions of the organosilica component with the hydrophobic core of the micelles are additionally suggested by the occurrence of the constrictions in the cylindrical mesopores, which may indicate some extent of penetration of organosilica framework into the hydrophobic

domain of the templating micelle. The three-component system (surfactant/(swelling agent)/(organosilica precursor and /or framework) that appears to govern the formation of the large-unit-cell organosilica/surfactant composites is likely to have a unique stability domain in the composition/temperature space, and thus it is not surprising that a small change in the initial temperature or composition may in some cases produce a major change in the structural properties (unit-cell size, pore diameter) of the resulting PMO.

The synthesis of phenylene-bridged PMO using Pluronic P123/TIPB pair can be best compared to the synthesis of LP-SBA-15 using the same surfactant/swelling-agent pair.[116,199] At temperatures where the PMO formed, its (100) interplanar spacing was larger than that for SBA-15 prepared at the same temperature. However, PMO did not form below 14.5 ^{o}C, whereas SBA-15 turned into a disordered ultra-large-pore structure at a much lower temperature (~ 12 ^{o}C). This result confirms the notion that the precursor and/or framework composition influences the formation and dimensions of the swollen micelles.

Part 2. Synthesis of Periodic Mesoporous Organosilica with Large Spherical Pore[108]

3.2.1 Choice of swelling agent. The SAXS data of ethylene-bridged organosilicas synthesized using different swelling agents are shown in Figure 3.2.1

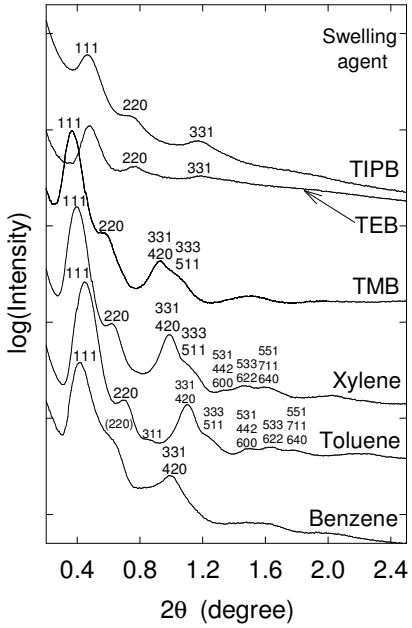

Figure 3.2.1 SAXS patterns of extracted ethylene-bridged PMOs with different swelling agents (figure taken from reference 108).

A series of aromatic swelling agents, namely benzene, toluene, xylene, TMB, 1,3,5-triethylbenzene (TEB), and 1,3,5-triisopropylbezene (TIPB) with increasing number of alkyl substituents or their size and hence with decreasing solubilization in the Pluronics micelles in aqueous media (based on literature data and our reasoning) have been examined.[108] Solubilization of aromatic hydrocarbons in Pluronics decreases with increasing the number and /or size of alkyl substituent on the benzene ring. Based on that, the swelling agents can be arranged in a series of decreasing solubilization in Pluronics: benzene > toluene >xylene> TMB > 1,3,5-triethylbenzene > 1,3,5-triisopropylbezene.[116,151,152] The swelling agents with different substituents on the

benzene ring affect the quality of the products significantly, as seen from SAXS patterns (Figure 3.2.1). In most cases, well-resolved SAXS patterns were obtained, which could be indexed on fcc structure. For TEB and benzene, SAXS patterns were somewhat less resolved, can also be indexed on fcc. The largest unit cell parameter (a = 41.4 nm) was obtained with material synthesized using TMB as swelling agent under the considered conditions of materials synthesis, although the quality of the material obtained using xylene as swelling agent was somewhat higher as seen from SAXS patterns. The unit cell parameter for the material obtained using xylene as swelling agent was 38.3 nm. It is important to note that only the use of TMB as a swelling agent in the synthesis of organosilica with spherical mesopores was reported in the literature.[107] TIPB has been used in alkylammonium –template synthesis of periodic mesoporous organosilicas which were weekly ordered[138] and in our work on phenylene-bridged PMO where ordered 2-D hexagonal structure was obtained.[68] However, the use of benzene, toluene, and xylene as swelling agents were never reported in the literature for their successful use in synthesizing PMOs with spherical pores.

The nitrogen adsorption isotherms and pore size distributions of the materials synthesized using different swelling agents are shown in Figure 3.2.2.

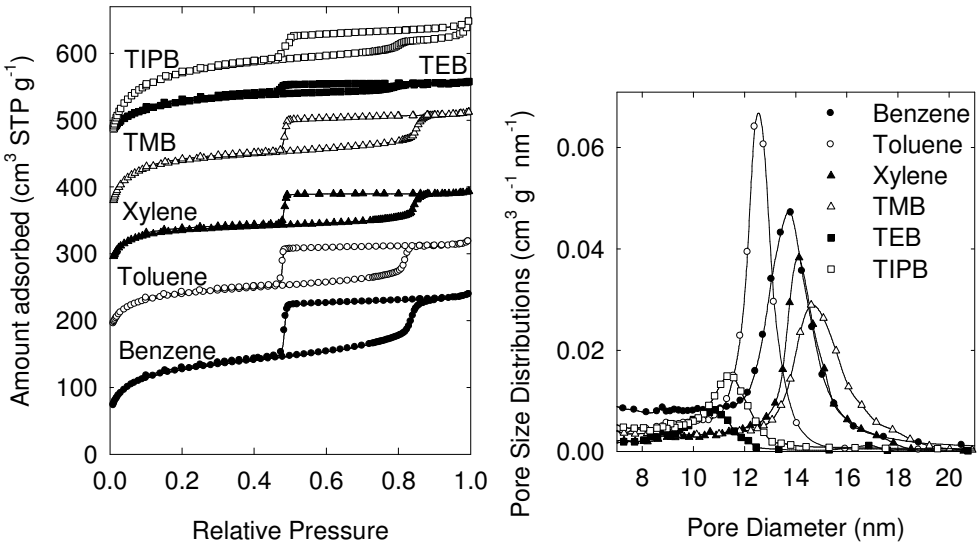

Figure 3.2.2 Nitrogen adsorption isotherms and pore size distributions of extracted ethylene-bridged PMOs with different swelling agents (0.5 g) and KCl salt (2.5 g) (except for synthesis with benzene as swelling agent in which case no salt was used). The isotherms for toluene, xylene, TMB, triethylbenzene and triisopropylbenzene were offset vertically by 120, 220, 260, 440, and 350 cm^3 STP g^{-1} respectively for clarity. The stirring speed was controlled either using mechanical stirring (for TMB, TEB, and TIPB) or magnetic stirring (for benzene, toluene, and xylene). During the synthesis the reaction system was covered (in case of mechanical stirring, a small whole was left for the stirrer shaft) (figure taken from reference 108).

Nitrogen adsorption isotherms for the samples synthesized using benzene, toluene, xylene, and TMB show broad hysteresis loops with steep capillary condensation steps at relative pressures of 0.83 – 0.85. This indicates that the materials have large uniform pores. The height of the capillary condensation step in the case of material synthesized using triethylbenzene was small indicating the smaller volume of uniforms pores. The BJH pore diameter for sample synthesized with TMB as a swelling agent reached 14.6 nm (capillary condensation pressure of 0.85 p/p_o). While PSDs calculated using the BJH method allow one to estimate the size of pores based on the capillary condensation phenomenon, the pore diameter is significantly underestimated in case of spherical mesopores.[113] Here, it is shown that using xylene and toluene as swelling agents, PMOs with even larger pore size could be obtained.

Table 3.2.1 Structural parameters of materials synthesized using BTME precursor under different conditions.[a]

swelling agent (mass in g) and mass of KCl (in g)[b]	a (nm)	S_{BET} (m^2/g)	V_t (cm^3/g)	V_{mic} (cm^3/g)	V_p (cm^3/g)	w_{KJS} (nm)
TMB(0.5), KCl(5.0)	28.5	397	0.26	0.13	0.12	9.5
TMB(0.5), KCl(2.5)	41.3	688	0.39	0.24	0.13	14.6
TMB(0.5), KCl(1.25)	41.9	576	0.30	0.24	0.05	14.4
TMB(0.5), KCl(0)	c	807	0.40	d	d	e
TMB(1.0), KCl(2.5)	41.3	353	0.22	0.14	0.07	14.3
Xylene(0.5), KCl(2.5)	39.3	405	0.27	0.16	0.10	14.1
Xylene(0.5), KCl(1.25)	41.9	632	0.36	0.26	0.09	13.9
Xylene(0.5), KCl(0.94)	44.8	610	0.35	0.24	0.09	15.0
Xylene(0.5), KCl(0.63)	47.7	413	0.25	0.16	0.06	14.9
Xylene(0.5), KCl(0)	51.0[f]	733	0.37	0.32	0.02	18.7
Xylene(1.0), KCl(2.5)	38.8	414	0.29	0.16	0.11	14.4
Xylene(1.0), KCl(1.25)	45.0	361	0.23	0.14	0.08	15.2
Xylene(1.0), KCl(0.94)	45.7	750	0.41	0.31	0.08	15.0
Xylene(1.0), KCl(0.63)	47.8	439	0.24	0.19	0.04	14.8
Xylene(1.0), KCl(0)	49.4	786	0.42	0.33	0.05	17.5
Xylene(0.0), KCl(2.5)	na	794	0.39	na	na	na
Toluene(0.5), KCl(2.5)	34.4	425	0.30	0.15	0.13	13.1
Toluene(0.5), KCl(1.25)	41.9	449	0.34	0.15	0.16	15.7
Toluene(0.5), KCl(0.94)	41.9	305	0.24	0.11	0.11	15.5
Toluene(0.5), KCl(0.63)	39.3	453	0.31	0.15	0.13	13.7
Toluene(0.5), KCl(0.0)	41.9	433	0.28	0.16	0.10	14.6
Toluene(1.0), KCl(2.5)	36.0	400	0.29	0.14	0.13	13.7
Toluene(1.0), KCl(1.25)	42.5 43.1	647 578	0.46 0.43	0.24 0.20	0.19 0.19	16.0 17.1
Toluene(1.0), KCl(0.94)	42.5 41.9	599 378	0.42 0.29	0.23 0.13	0.17 0.14	16.7 15.9

Benzene (0.5), KCl(0.0)	36.8	453	0.37	0.13	0.19	13.7
no swelling agent, KCl (2.5)	c	794	0.39	d	d	e
no F127	c	430	0.65	~0.0	g	e

[a] Notation: a, unit-cell parameter for extracted sample; $S_{BET,}$ BET specific surface area; $V_{t,}$ total pore volume, $V_{mic,}$ micropore volume; $V_{p,}$ volume of ordered (primary) mesopres; $w_{KJS,}$ KJS pore diameter-calculated using a procedure calibrated for cylindrical mesopores; underestimation of the pore diameter by ~3 nm expected; [b] amount of swelling agent and KCl per 0.5 g Pluronic F127; [c] no clear peak on SAXS, so the unit-cell parameter is not defined; [d] no good separation between micropore and mesopore ranges, V_t has a major contribution from the micropore volume; [e] no peak on mesopore size distribution; [f] pattern not well resolved; the main SAXS peak tentative assigned as (111) reflection of Fm3m structure; [g] mesopore volume essentially equal to V_t.

Particularly, for toluene and xylene as swelling agents, PMOs with BJH pore size of 16 nm or more were obtained (capillary condensation pressures 0.85-0.90 p/p_o), which is beyond the range of upper limit of pore size achieved using TMB as swelling agent (capillary condensation pressure up to ~ 0.85 p/p_o).[107]

3.2.2 Effect of amount of salt keeping amount of swelling agent constant. The SAXS patterns of extracted samples synthesized with different swelling agents such as TMB, xylene, and toluene and different amounts of salt (KCl) are shown in Figure 3.2.3. In case of TMB as a micelle expander, the unit-cell parameter increased with decreasing the amount of KCl (Figure 3.2.3, top). The sample prepared with 5.0 g of KCl (twice the amount used in the series of samples considered earlier) shows well-resolved SAXS pattern, but its unit-cell parameter was only 28.6 nm. Note that the samples prepared with 2.5 and 1.25 g KCl had unit-cell parameters of 41-42 nm. However, the lowering of the amount of salt led to less-resolved SAXS patterns. The unit-cell parameters determined from the first peak (considering it as (111) peak) are given in Table 3.2.1. In the case of the absence of salt, the use of TMB as a swelling agent does not produce an ordered material, as seen from featureless SAXS pattern.

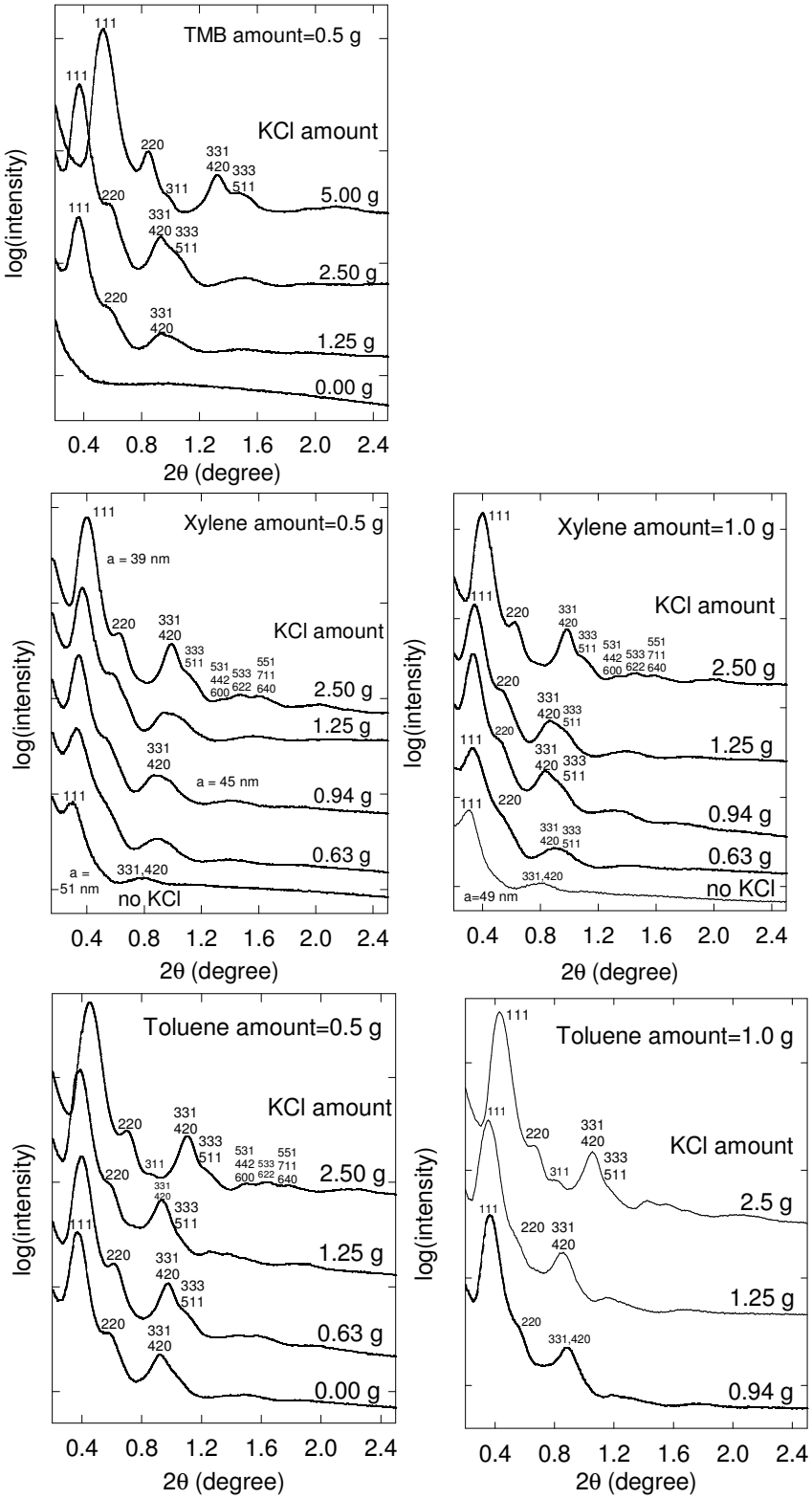

Figure 3.2.3 SAXS patterns of extracted ethylene-bridged PMO prepared in the presence of different amounts of KCl using 0.5 g TMB (top), 0.5 g xylenes (middle left), 1.0 g xylenes (middle right), 0.5 g toluene (bottom left) and 1.0 g toluene (bottom right) as swelling agent (figure taken from reference 108).

In case of material synthesized using xylene as a micelle expander, a similar but even more pronounced trend of the unit-cell size increase with decrease in the amount of salt was observed. As seen from the SAXS patterns, the unit-cell parameter systematically increased with a decrease in the amount of salt. The increase in unit-cell size was paralleled with the decrease in resolution of the SAXS pattern. In absence of salt, no well-resolved SAXS pattern is obtained which could be indexed on fcc structure. However, the first peak still can be hypothesized as the (111) peak of fcc structure based on patterns of other samples from the series. TEM for the selected samples in the series confirmed well-defined periodic structure (Figure 3.2.4). The sample prepared without KCl shows the highest unit-cell parameter which can be estimated as ~ 53 nm (Table 3.2.1), but if one consideres the material as not sufficiently ordered, then the limiting value of the unit-cell parameter would be ~ 48 nm for the PMO with Fm3m structure. This is the highest unit-cell parameter so far obtained in case of PMO structure with spherical mesopores.

More importantly, the sample prepared with 3/8th of the typically used amount of KCl exhibited a SAXS pattern that provides a clear evidence of well-ordered face-centered cubic structure (especially for larger amount of xylene) with the unit-cell parameter of 45-46 nm, which is 8 nm larger than the largest unit-cell size for PMOs with fcc structures reported in the literature.[107] In case of xylene, the unit cell parameter increases slightly with increasing the mass ratio of xylene to F127. In the absence of a swelling agent, the material shows featureless SAXS pattern indicating its disordered nature even though the salt was present (Figure 3.2.19). With toluene as a micelle expander, well-

resolved patterns were obtained, which can be indexed on fcc structure, even for the sample prepared without the addition of salt.

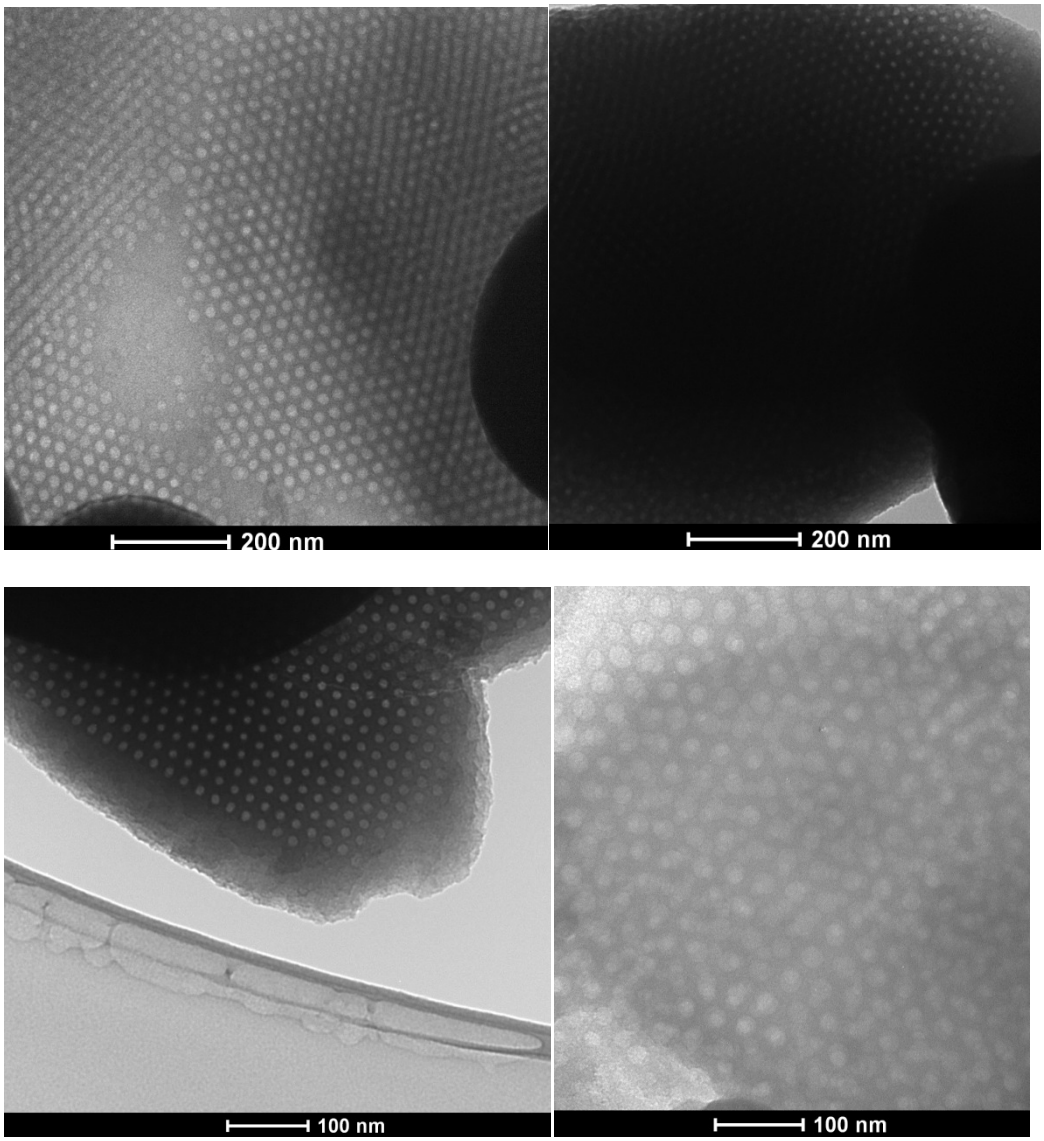

Figure 3.2.4 TEM images of materials synthesized using xylene as swelling agent: top left) 0.5 g xylene and 2.5 g salt, (top right) 0.5 g xylene and 1.25 g salt, (bottom left) 1.0 g xylene and 2.5 g salt, and (bottom right) 1.0 g xylene and 1.25 g salt.

TEM image for the sample prepared in the presence of toluene shows an ordered pore structure (Figure 3.2.5).

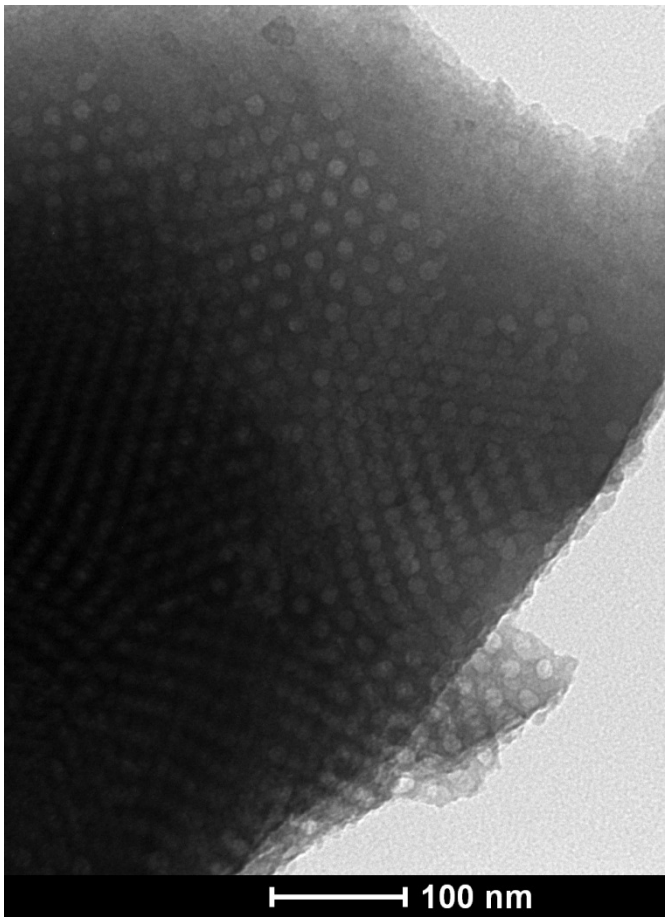

Figure 3.2.5 TEM image of materials synthesized using 0.5 g toluene and standard amount of KCl.

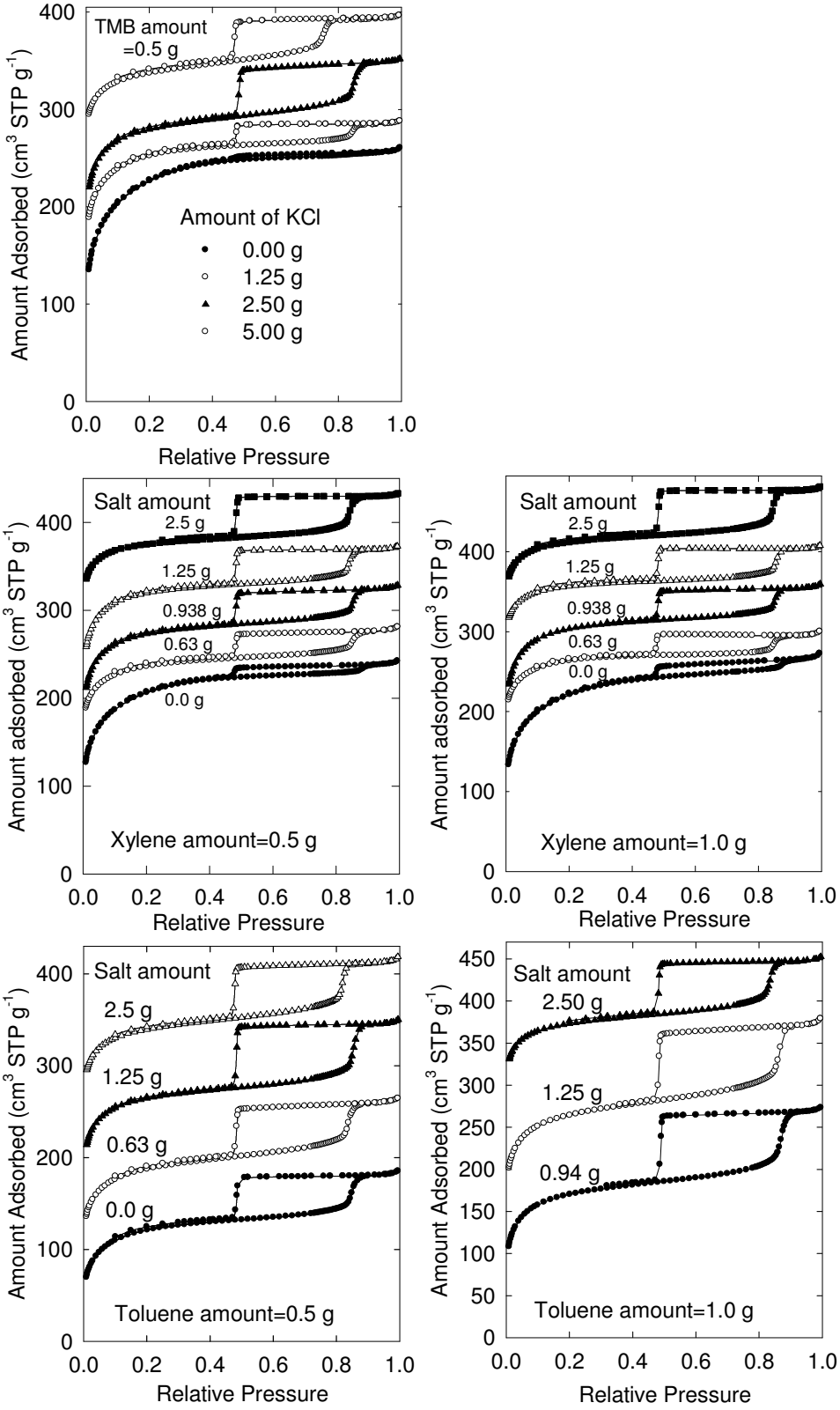

Figure 3.2.6 Nitrogen adsorption isotherms for organosilicas prepared using different amounts of KCl and 0.5 g TMB (top),0.5 g xylenes (middle left), 1.0 g xylenes (middle right), 0.5 g toluene (bottom left), and 1.0 g toluene (bottom right) as swelling agent. For

clarity, (top) isotherms were offset vertically by 90, 100, and 225 cm^3 STP g^{-1} for samples synthesized with 1.25, 2.50, and 5.00 g KCl. (middle left) isotherms were offset vertically by 120, 100, 140, and 260 cm^3 STP g^{-1} for samples synthesized with 0.63, 0.938, 1.25, and 2.5 g KCl. (middle right) isotherms were offset vertically by 90, 30, 190, 225 cm^3 STP g^{-1} for samples synthesized with 0.63, 0.938, 1.25, and 2.5 g KCl. (bottom left) isotherms were offset vertically by 60, 130, and 220 cm^3 STP g^{-1} for samples synthesized with 0.63, 1.25, and 2.5 g KCl. (bottom right) isotherms were offset vertically by 100, and 320 cm^3 STP g^{-1} for samples synthesized with 1.25, and 2.5 g KCl respectively (figure taken from reference 108).

The nitrogen adsorption isotherms are shown in Figure 3.2.6. For TMB and xylene, the height of the capillary condensation step decreases with decreasing the amount of salt, (except for 5 g KCl) indicating that the volume of ordered mesopores decreases with decreasing the amount of salt. It is known that the presence of salt in solution leads to decreased hydration of micelles of Pluronic block copolymers in aqueous solution,[206] wherein water interacts with PEO blocks and may also be present to some extent in the micelle core.[65] Apparently, the depletion of already low amount of water in hydrophobic PPO domains and dehydration of PEO domains increases “contrast” between PEO and PPO domains and enhances the mesopore volume (which is primarily related to the volume of PPO domains).[79,124] However, the overly large amount of salt may somehow hinder the incorporation of the swelling agent in the micelles, resulting in the decrease in the unit-cell parameter and even in a decrease in the mesopore volume. In case of toluene micelle expander, the nitrogen adsorption isotherm shows steep capillary condensation at relative pressure of 0.82-0.86 p/p_o, indicating the presence of large uniform mesopores.

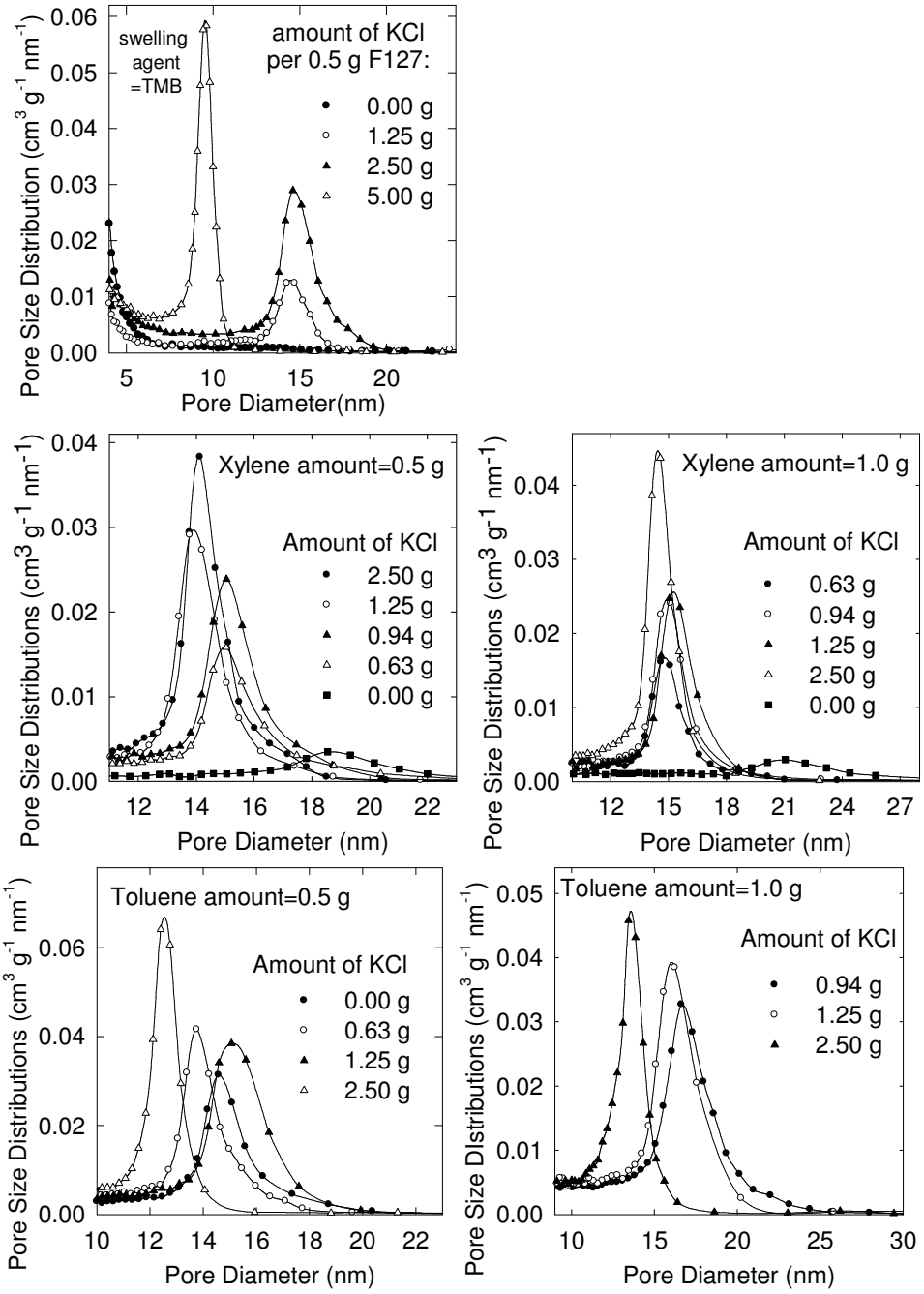

Figure 3.2.7 KJS pore size distributions of materials synthesized using different amount of KCl and 0.5 g TMB (top), 1.0 g xylenes (middle left), 0.5 g xylenes (middle right), 0.5 g toluene (bottom left), and 1.0 g toluene (bottom right) as swelling agent per 0.5 g of F127 block copolymer (figure taken from reference 108).

Pore size distributions (Figure 3.2.7) show that the pore diameter does not change fully systematically with decreasing the amount of salt. In absence of swelling agent, no uniform mesopores are obtained. With double amount of KCl, although the pore size

distributions become significantly narrow, but the pore size decreased (9.5 nm). The regular amount of salt or half of this amount afforded pore diameters about 14.5 nm. In the absence of KCl, no uniform mesopores formed in the case of TMB as a swelling agent. For xylene, pore diameters were 14-15 nm in the presence of the salt. Without addition of the salt, the largest pore diameter of 18-21 nm (capillary condensation pressure 0.88-0.90 p/p_o) was obtained, which is significantly larger than that of the similar material reported earlier from TMB-based synthesis, that had pore diameter of ~15 nm (capillary condensation at 0.85 p/p_o).[107] The use of toluene afforded pore diameters of 15-17 nm for about half of the amount of salt used in the standard synthesis. These are the largest pore diameters that were achieved in our study while maintaining an appreciable degree of structural ordering. With toluene as a swelling agent, in the absence of salt, ordered porous material with pore size ~ 15 nm was obtained, which is the largest pore diameter obtained in case of PMO with spherical mesopores prepared without addition of a salt.

3.2.3a Effect of amount of micelle expander. Use of TMB as swelling agent. The SAXS patterns of extracted samples synthesized with different amounts of TMB swelling agent are shown in Figure 3.2.8. For TMB as micelle expander, the unit-cell parameter remained constant (a = 41.4 nm) with increasing the amount of swelling agent from 0.5 g to 1 g per 0.5 g F127 block copolymer (Figure 3.2.8). The height of capillary condensation step almost remains constant with either 0.5 g or 1.0 g of TMB per 0.5 g F127 block copolymer indicating that the initial amount used (i.e. 0.5 g) is already present in excess amount compared to the solubilization capacity of the block copolymer.

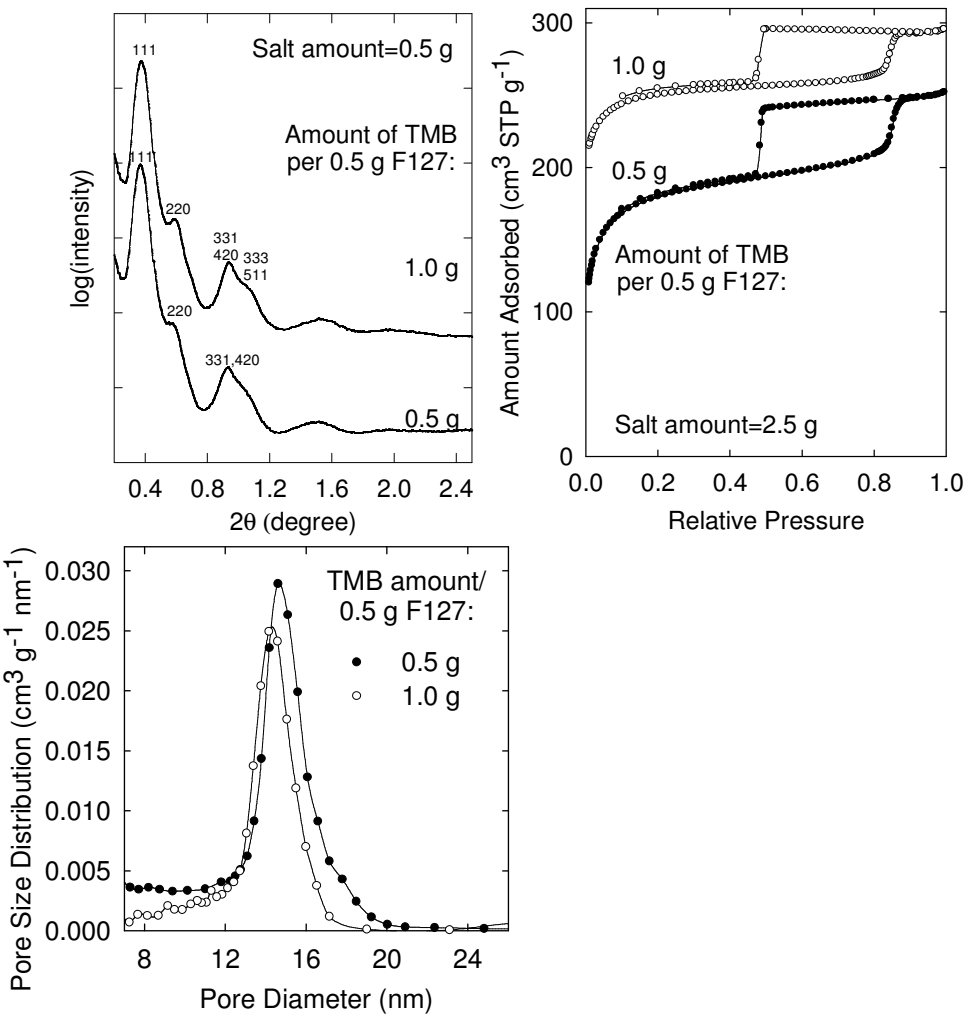

Figure 3.2.8 SAXS patterns (top left), nitrogen adsorption isotherms (top right), and pore size distribution (bottom) of extracted ethylene-bridged PMO prepared in the presence of different amount of trimethylbenzene as expander using standard amount (2.5 g) of KCl. Isotherm was offset vertically by 150 cm^3 STP g^{-1} for sample synthesized with 1.0 g of TMB. Stirring speed used was 2.5 using mechanical stirrer.

3.2.3b Effect of amount of micelle expander. Use of xylene as swelling agent. The SAXS patterns for the samples prepared using different amounts of xylene while keeping the amount of salt constant are shown in Figure 3.2.9. The resolution of SAXS patterns appeared to slightly improve as a larger amount of the swelling agent was added.

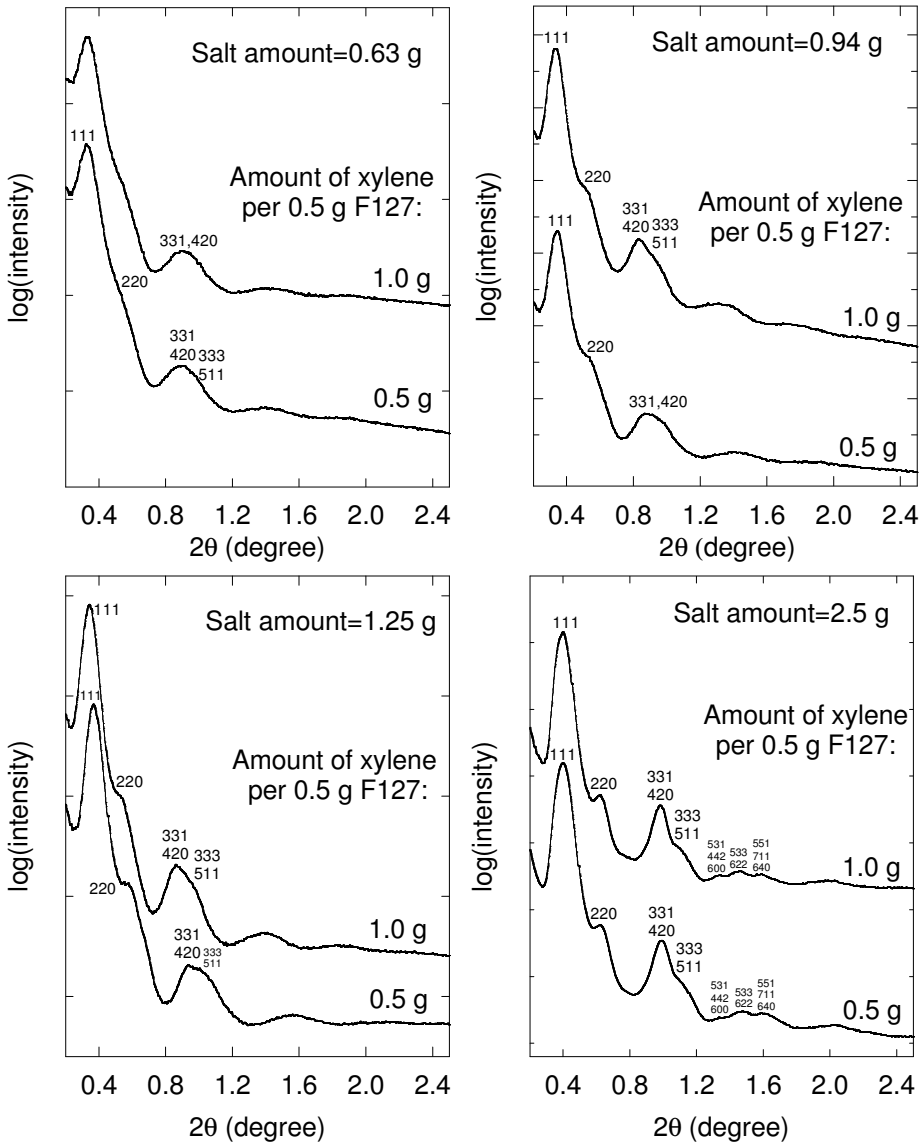

Figure 3.2.9 SAXS patterns of extracted ethylene-bridged PMO prepared in the presence of different amount of xylenes swelling agent keeping the amount of salt constant. Stirring speed used 300 rpm using magnetic stirrer and the reaction container was covered.

The nitrogen adsorption isotherms are shown in Figure 3.2.10. The height of capillary condensation step remains almost constant on increasing the amount of xylene from 0.5 g to 1.0 g per 0.5 g F127 block copolymer. All the materials show broad adsorption-desorption hysteresis loops indicating the presence of mesopores with narrow entrances (diameter below 5 nm).[201]

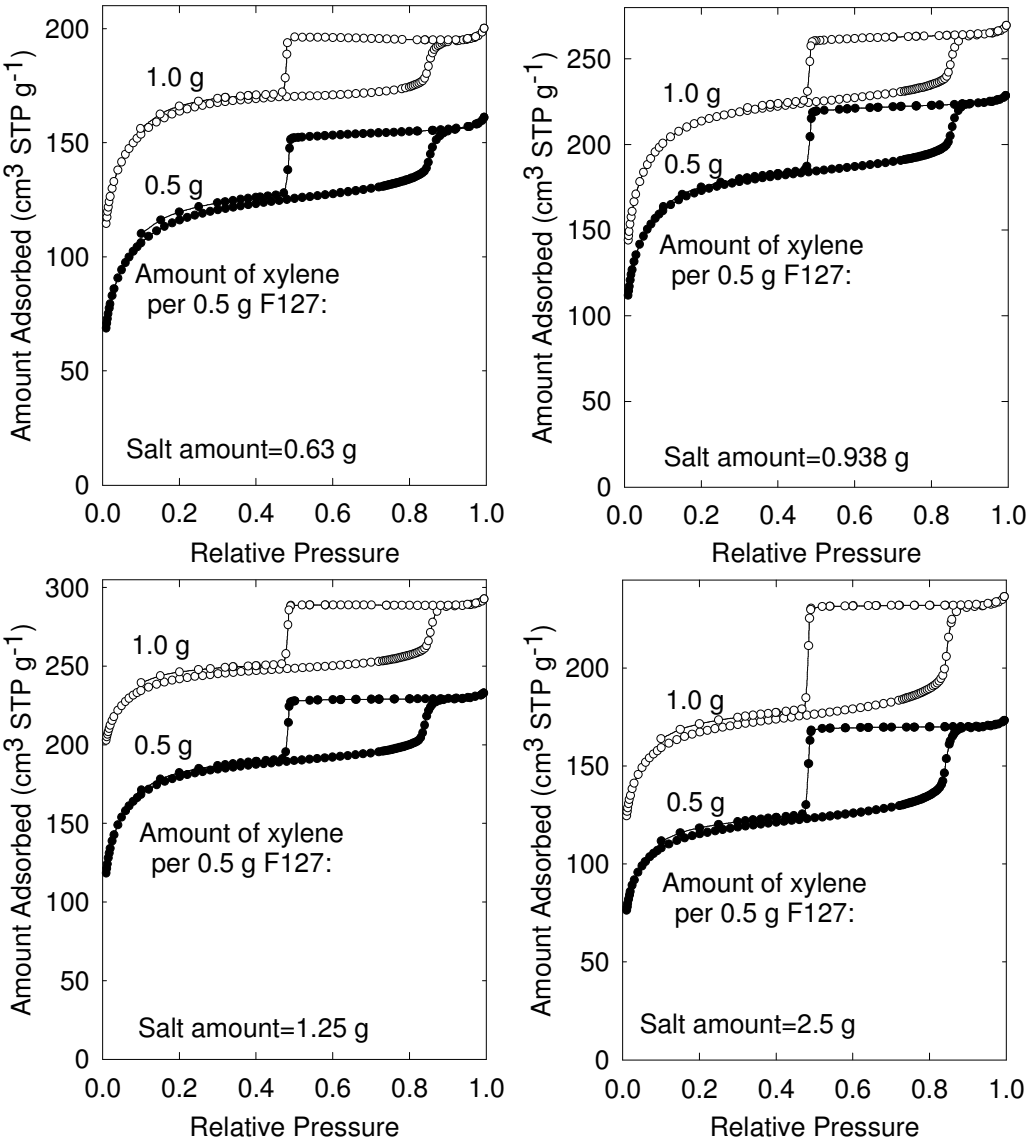

Figure 3.2.10 Nitrogen adsorption isotherms of extracted ethylene-bridged PMO prepared in the presence of different amount of xylenes swelling agent keeping the amount of salt constant. Isotherm was offset vertically by 40, 140, and 50 cm^3 STP g^{-1} for sample synthesized with 1.0 g xylene (salt amount=0.63 g), 1.0 g xylene (salt amount=1.25 g), and 1.0 g xylene (salt amount 2.5 g) respectively. Stirring speed used 300 rpm using magnetic stirrer and the reaction system was covered.

The pore size distributions (Figure 3.2.11) show that with the increase in the amount of the xylene swelling agent, the size of ordered mesopores remains quite constant. When salt amount used was higher, the pore diameter slightly increased with the increase in the amount of xylene from 0.5 g to 1.0 g per 0.5 g of block copolymer, but for lower

concentrations of salt, the pore diameter slightly decreased. It can be concluded that there is no major effect of the amount of the swelling agent in the considered range, probably because the micelles that template the PMO solubilized much less xylene than there was available in the reaction mixture in both cases.

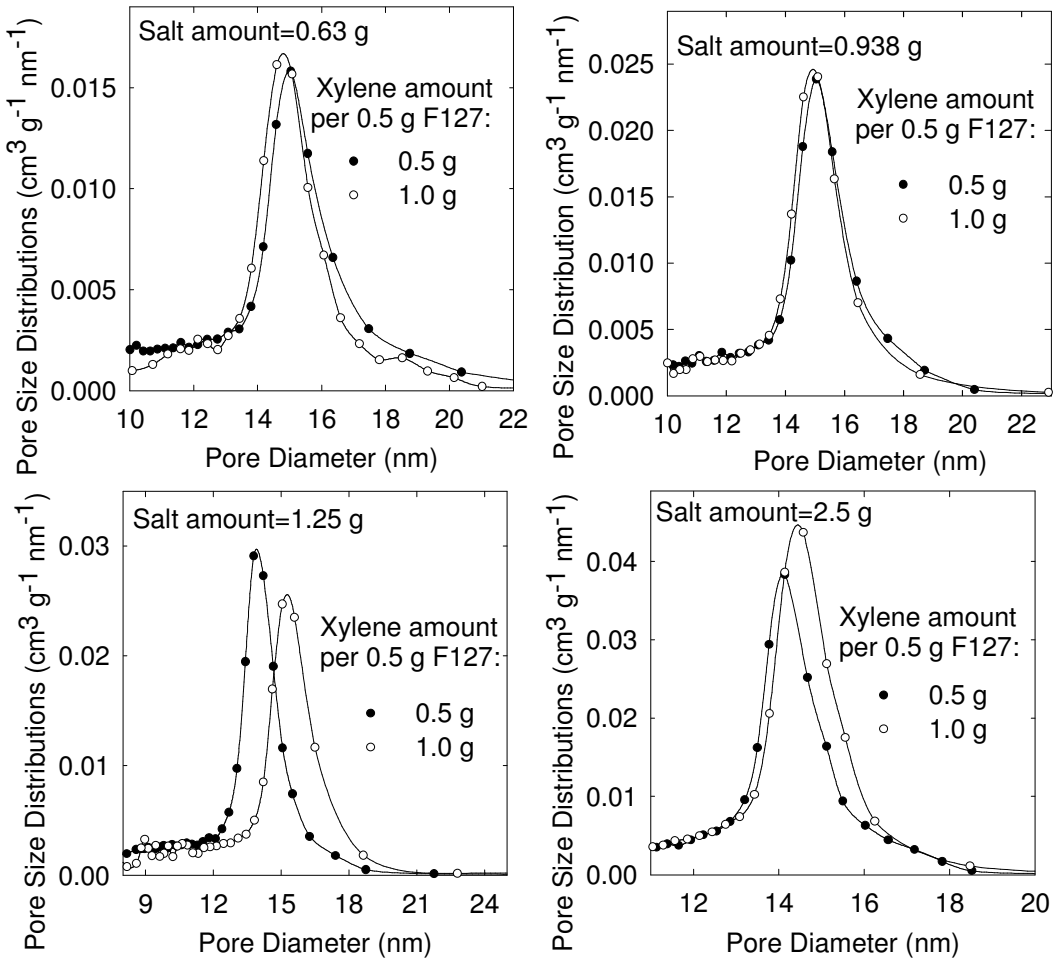

Figure 3.2.11 Pore size distributions of extracted ethylene-bridged PMO prepared in the presence of different amount of xylenes swelling agent keeping the amount of salt constant. Stirring speed used 300 rpm using magnetic stirrer and the reaction system was covered.

3.2.3c Effect of amount of micelle expander. Use of toluene swelling agent. The SAXS patterns for the samples prepared using different amounts of toluene keeping the amount of salt constant are shown below (Figure 3.2.12). In case of a regular amount of KCl, the unit-cell parameter increases from 34.4 nm to 36 nm with increasing the amount

of toluene from 0.5 g to 1.0 g (Figure 3.2.12). With toluene micelle expander, the pore diameter increases from 12.6 nm to 13.7 nm for the standard amount of KCl. In the case of lower amounts of salt (0.94 g or 1.25 g per 0.5 g F127), the pore diameter increases slightly with increased amount of toluene, while the SAXS pattern became somewhat less resolved.

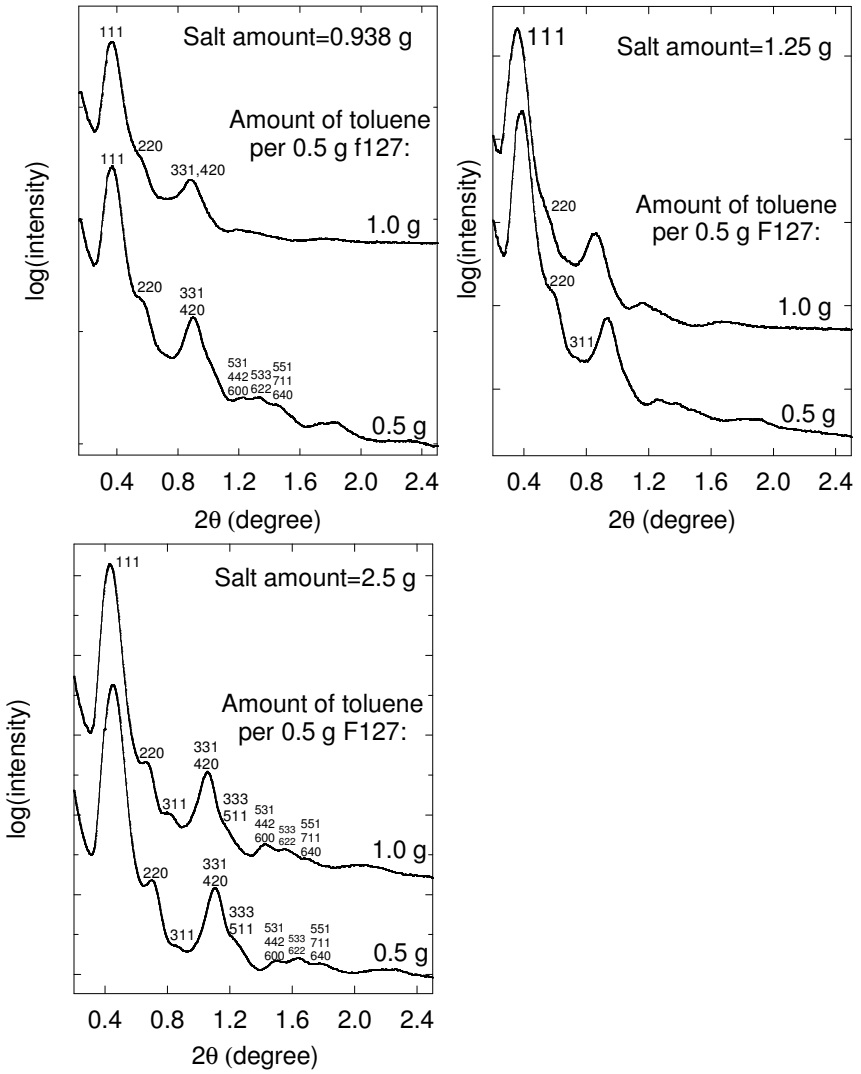

Figure 3.2.12 SAXS patterns of extracted ethylene-bridged PMO prepared in the presence of different amount of toluene (0.5 or 1.0 g per 0.5 g F127) swelling agent keeping the amount of salt constant. Stirring speed used 300 rpm using magnetic stirrer and the reaction container was covered.

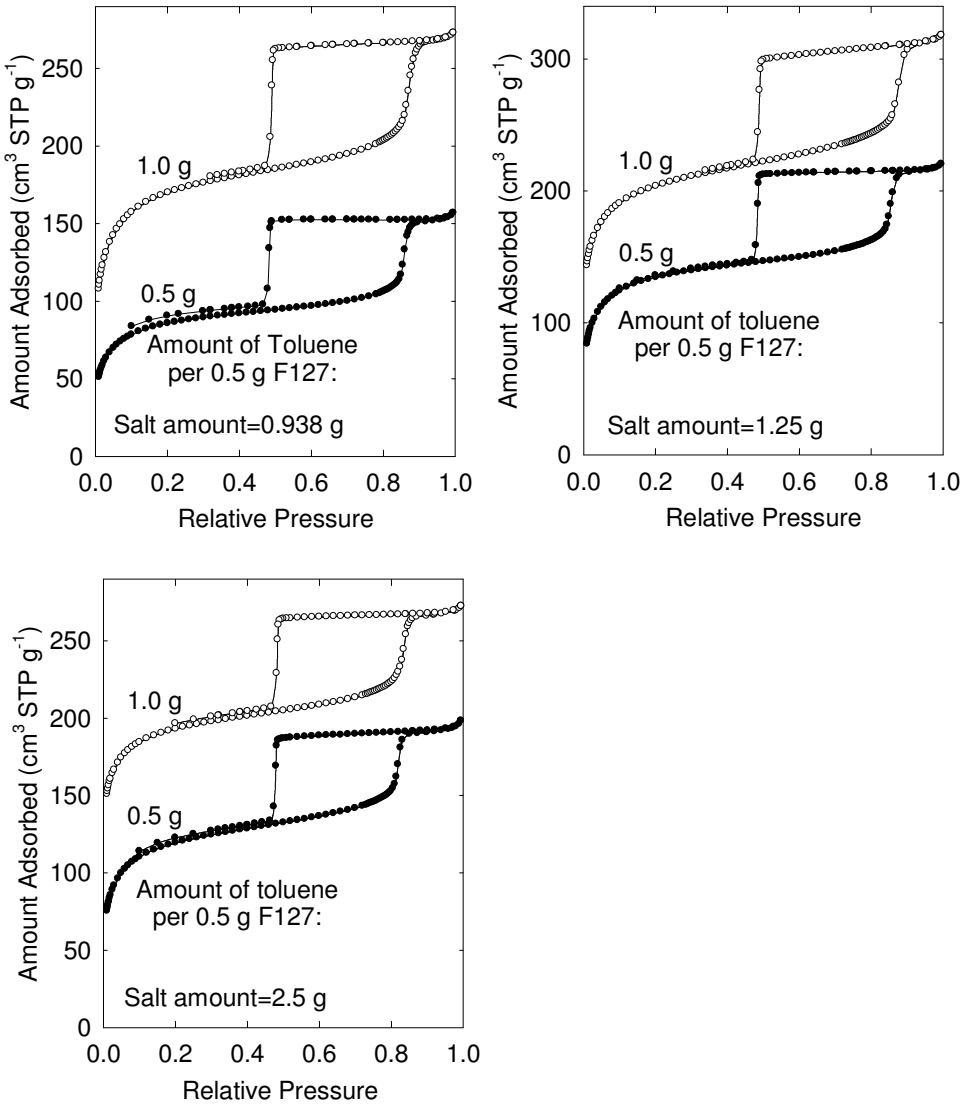

Figure 3.2.13 Nitrogen adsorption isotherms of extracted ethylene-bridged PMO prepared in the presence of different amount of toluene (0.5 or 1.0 g per 0.5 g F127) swelling agent keeping the amount of salt constant. Isotherms were offset vertically by 40, and 80 cm^3 STP g^{-1} for samples synthesized with 1.0 g toluene (salt amount=1.25 g), and 1.0 g toluene (salt amount=2.5 g) respectively. Stirring speed used 300 rpm using magnetic stirrer and the reaction container was covered.

The adsorption isotherms were not changed much as the amount of swelling agent was increased (Figure 3.2.13). The pore size distributions (Figure 3.2.14) show that with increasing the amount of toluene micelle expander keeping the salt amount constant, the pore size increases, but not to a large extent.

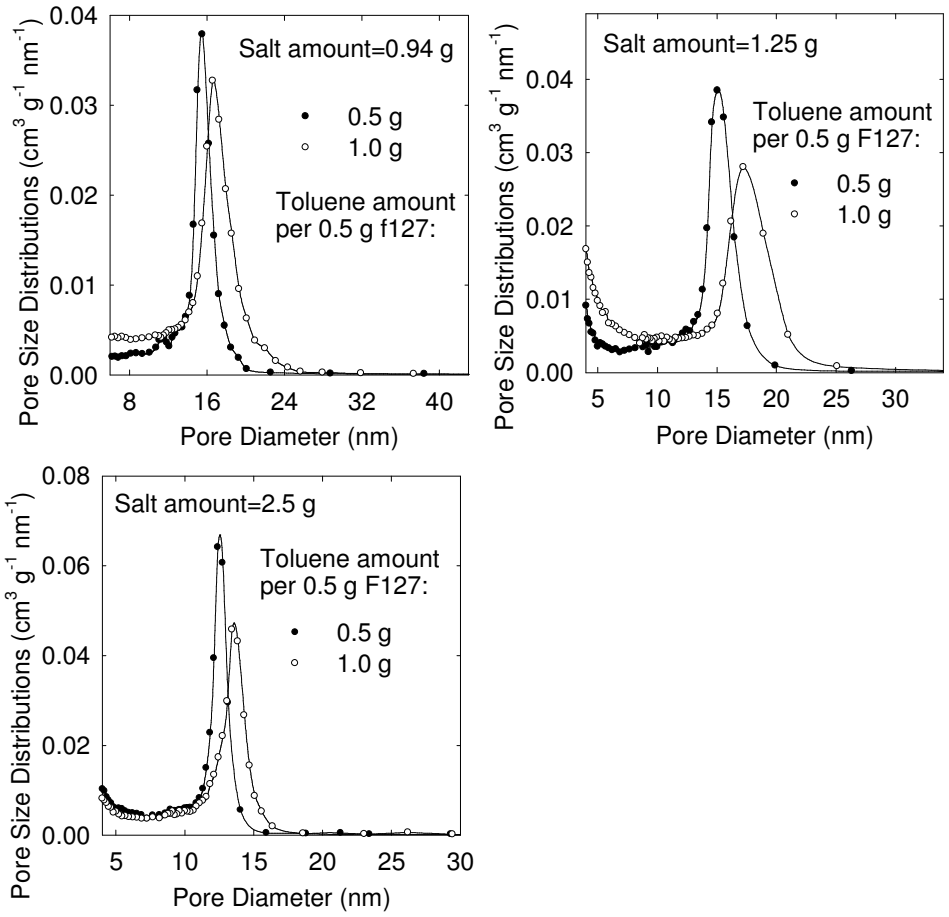

Figure 3.2.14 Pore size distributions of extracted ethylene-bridged PMO prepared in the presence of different amount of toluene swelling agent keeping the amount of salt constant. Stirring speed used 300 rpm using magnetic stirrer and the reaction system was covered.

3.2.4 Formation of closed-pore material. In case of materials synthesized with xylene as a swelling agent, we calcined the material at different temperatures under argon atomosphere starting from 400 ^{o}C onwards to check whether the material forms closed pores with retention of structural ordering. For this purpose, two different materials were chosen: one prepared at initial synthesis temperature of 15 ^{o}C (denoted as LT) and the other sample that was further hydrothermally treated at 100 ^{o}C in the original synthesis mixture (denoted as HT) for 1 day. The SAXS pattern for as-synthesized materials and samples prepared by heating at different temperatures under argon atmosphere show clearly well-resolved patterns indicating the presence of the face-centered-cubic structure

(Figure 3.2.15). After heating at 500 ^{o}C, the LT and HT materials shrank 20 and 18 %, respectively. This high shrinkage caused the closure or significant narrowing of pore entrances connecting the main mesopores, which is inferred from negligible uptake of nitrogen gas (Figure 3.2.16). This thermal treatment leads to significant cleavage of Si-C bonds and conversion to siloxane (Si-O-Si) linkages (based on appearance of Q peaks between -90 to -110 ppm), as seen from ^{29}Si CP MAS NMR spectrum (Figure 3.2.15).

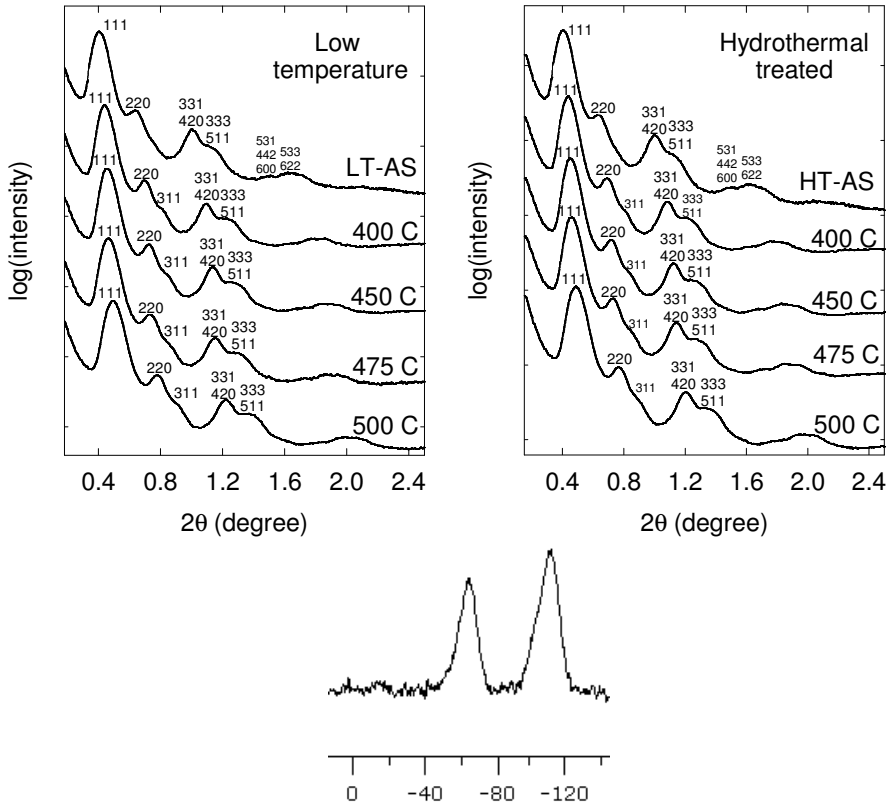

Figure 3.2.15 SAXS patterns for ethylene-bridged PMOs synthesized at low temperature (LT-AS, top left), and further hydrothermal treatment at 100 ^{o}C for 1 day (HT-AS, top right) calcined at different temperatures under argon atmosphere. ^{29}Si CP MAS for ethylene-bridged organosilica (LT) with spherical pores heated at 500 ^{o}C under argon atmosphere.

However, the intensity of T sites is still appreciable indicating the presence of significant amount of Si-C-Si bonds. This is a unique case of closed-pore material with

Fm3m structure and organic bridging (or pendant) groups. A further study will be needed to fully understand the composition of this material.

All the materials were further characterized by gas adsorption technique in order to get further insight about the pore closure. The adsorption isotherms show broad hysteresis loops for the materials calcined under argon from 400 to 475 ^{o}C.

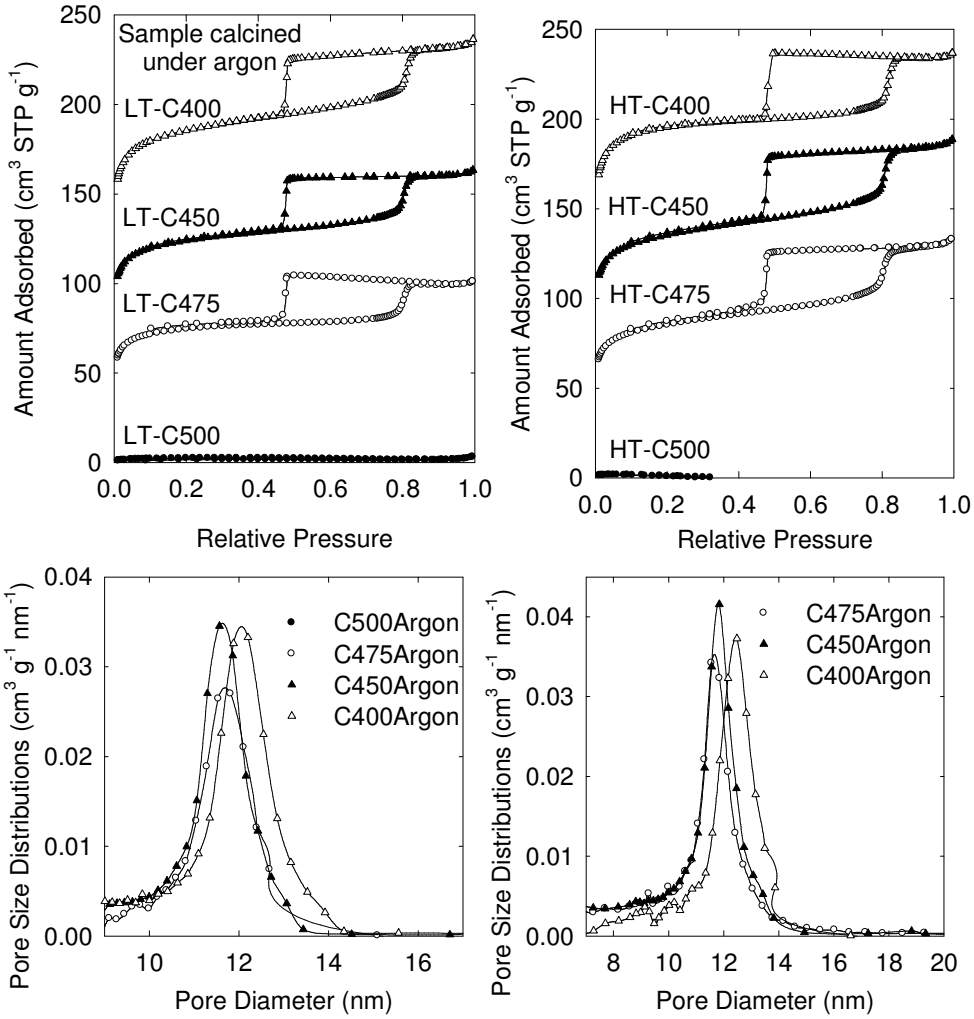

Figure 3.2.16 Nitrogen adsorption isotherms and pore size distributions for ethylene-bridged organosilica with spherical pores heated at different temperatures under argon atmospheres. Isotherms were offset vertically by 40, and 70 cm^3 STP g^{-1} for samples calcined at 450, and 400 ^{o}C prepared at low temperature. Isotherms were offset vertically by 40, and 70 cm^3 STP g^{-1} for samples calcined at 450, and 400 ^{o}C prepared after hydrothermal treatment.

These materials show steep capillary condensation steps indicating that the material has uniform mesopores. The capillary evaporation step ends at the lower limit of adsorption-desorption indicating that the entrance size is below 5 nm.[201] Further heating at 500 ^{o}C, the materials show virtually zero adsorption of nitrogen gas (Figure 3.2.16) indicating that the mesopores are not accessible (they are closed).[162] These closed-pore materials were found promising as low-dielectric-constant materials.[207-209]

3.2.5 Effect of stirring speed. As seen from SAXS patterns, the stirring speed has influence on the quality of the materials. For materials synthesized using TMB as a swelling agent, the mechanical stirring was used while for materials synthesized using other swelling agents, the magnetic stirring was used. Different stirring speeds (in this case mechanical stirring was used), that is very slow (2.0), slow (2.5), moderate (3.0), and high (3.5) were used to optimize the synthesis condition in case of materials synthesized using TMB as a swelling agent. As seen from SAXS patterns (Figure 3.2.18), the quality of the materials decreases as the stirring speed decreases and at the same time the unit-cell parameter increases as seen from shifting of the position of first peak (111) toward lower 2θ value. With TMB as a swelling agent, the relatively slower stirring speed (2.5), afforded the largest unit-cell parameter (a = 41.4 nm). However, with high stirring speed (3.5), the periodicity of the materials obtained was better, as seen from SAXS pattern, although the material shows smaller unit-cell parameter (36.0 nm). So for studies described above, stirring speed of 2.5 was used for materials synthesized using TMB as a swelling agent. For materials synthesized using xylene as a swelling agent, the magnetic stirring was used. Different stirring speeds were used, such as 250, 300, 350, and 400 rpm. All the materials obtained using different stirring speeds are well ordered,

as seen from SAXS patterns (Figure 3.2.17). TEM image for materials synthesized using stirring speed of 350 rpm shows nice ordering of the mesopores (Figure 3.2.17 below).

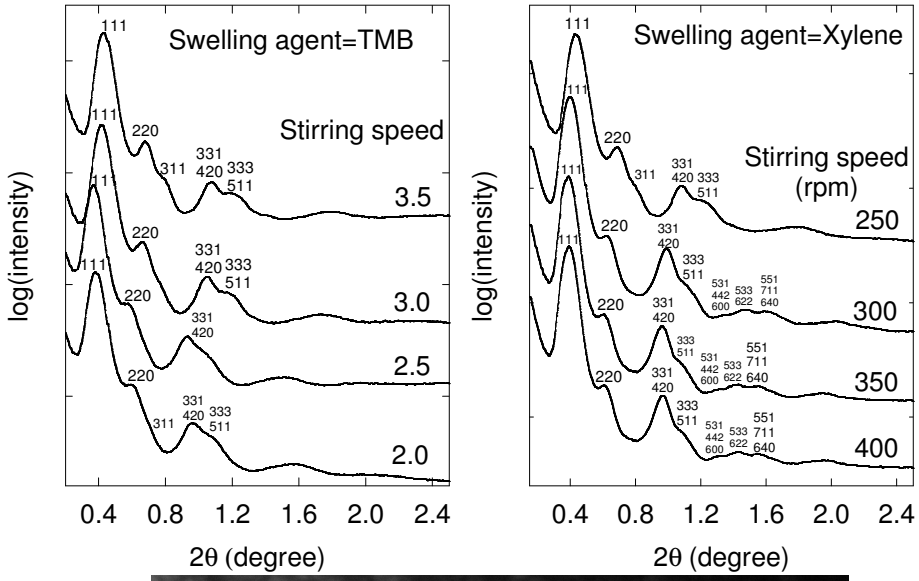

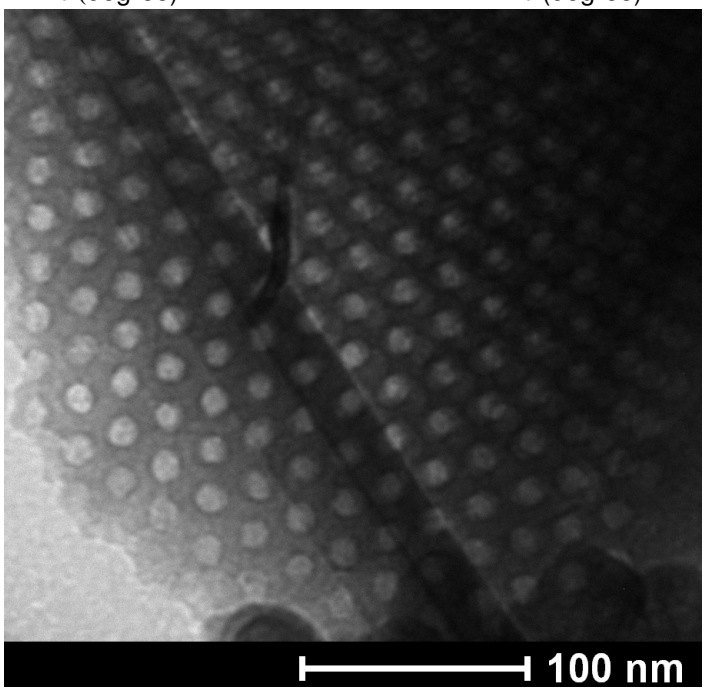

Figure 3.2.17 SAXS patterns of samples synthesized with different stirring speeds and 2.5 g of KCl and 0.5 g of TMB as swelling agent. The stirring speed was controlled using mechanical stirring (for TMB) or magnetic stirring (for xylene). (below) TEM image (110 projection) for the sample synthesized using xylene as a swelling agent with stirring speed of 350 rpm.

The nitrogen adsorption isotherms and pore size distributions for the above mentioned materials show broad adsorption-desorption hysteresis loops (Figure 3.2.18).

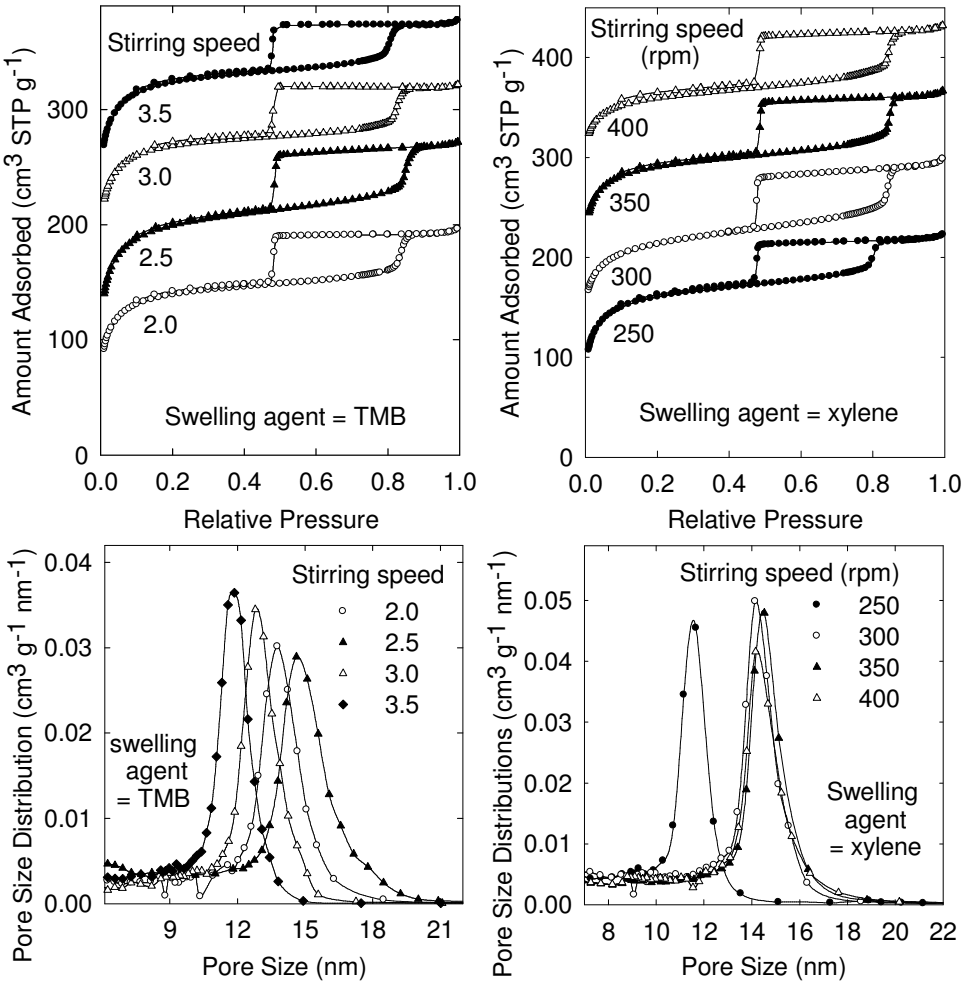

Figure 3.2.18 Nitrogen adsorption isotherms of samples synthesized with different stirring speeds and 2.5 g of KCl and 0.5 g of TMB (left) and xylene (right) as swelling agent. (left) Isotherms were offset vertically by 20, 130, and 150 cm^3 STP g^{-1} for samples synthesized with stirring speed of 2.5, 3.0, and 3.5 respectively. (right) isotherms were offset vertically by 90, 160, and 270 cm^3 STP g^{-1} for samples synthesized with stirring speed of 300, 350, and 400 rpm respectively. The stirring speed was controlled either using mechanical stirring (for TMB) or magnetic stirring (for xylene).

Large pore size was obtained in case of materials synthesized using TMB as a swelling agent and stirring speed of 2.5. Higher or lower stirring speed reduces the pore size. So for further optimization of reaction conditions, the stirring speed of 2.5 was used

for the materials synthesis using TMB as a swelling agent. In case of xylene as a swelling agent, stirring speed of 300 rpm was used.

3.2.6 Control experiment. To understand further the formation of PMOs, control experiments were performed. For this purpose, experiments were designed as follows: 1) experiment without block copolymer, but in the presence of salt (KCl) and swelling agent (TMB), 2) experiment without salt, but in the presence of the block copolymer (F127) and TMB swelling agent, and 3) experiment without swelling agent, but in the presence of salt and block copolymer.

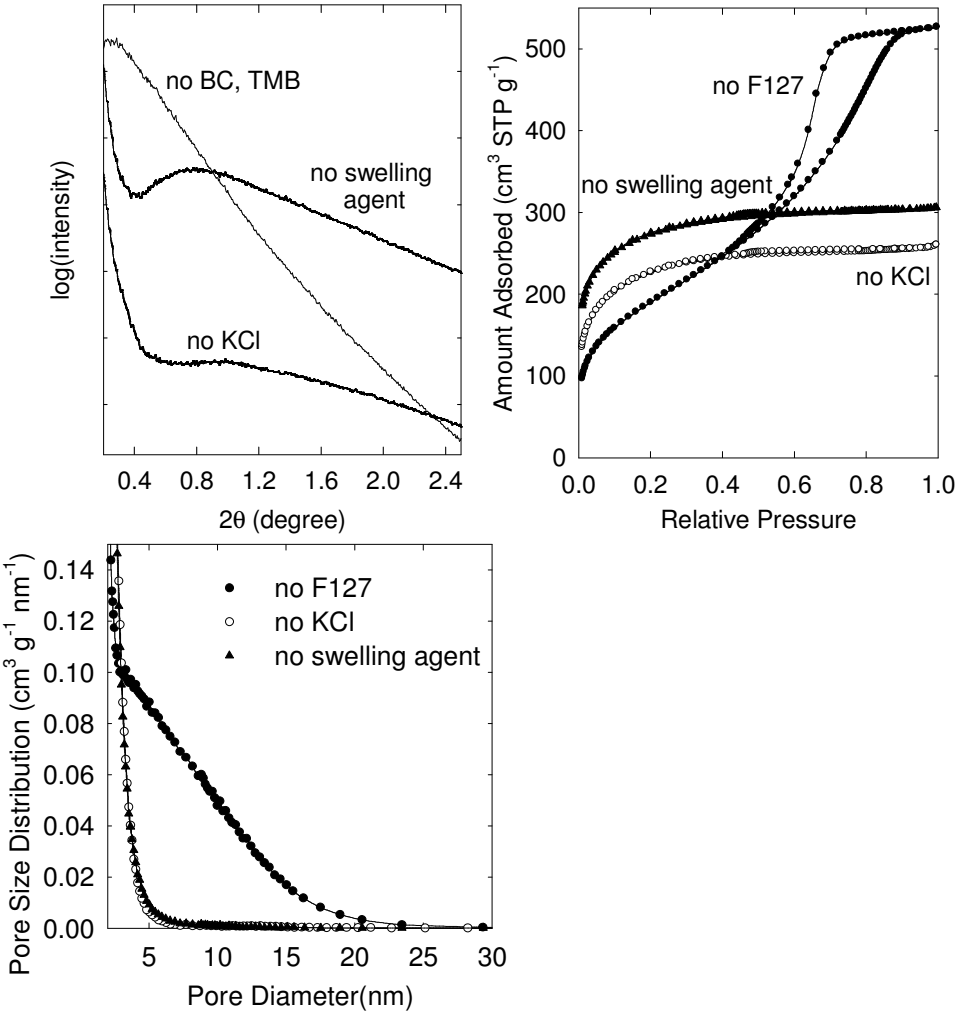

Figure 3.2.19 SAXS patterns (top left), nitrogen adsorption isotherms (top right), and pore size distributions (bottom, left) of samples synthesized at initial temperature of 15 ^{o}C with 2.5 g of KCl and 0.5 g TMB, but without block copolymers.

Unlike reaction 1) the other two show similar gas adsorption behavior and hence are likely to exhibit similar pore size distributions. These materials are primarily microporous and without any ordered mesopores. Reaction 1) produces material with mesopores of a broad distribution of sizes (Figure 3.2.19).

The block-copolymer in most cases was removed by solvent extraction using ethanol, but it is possible to remove the template block copolymer by calcination. The sample was heated under nitrogen at 300 ^{o}C and higher temperature and analyzed by solid state ^{29}Si NMR technique to see whether there appears any cleavage of Si-C bonds. ^{29}Si CP MAS spectra show some degree of cleavage of organic groups under heating at both 300 and 350 ^{o}C under nitrogen as seen from appearances of Q site (between -90 to -110 ppm) (Figure 3.2.20). Other peaks (T sites, ~ 50 ppm) indicate that most of the Si-C bonds integrity remain intact. It is also clear that increasing the calcination temperature, the degree of cleavage of Si-C bonds increases, as seen from higher intensity of Q sites at higher temperature (350 ^{o}C).

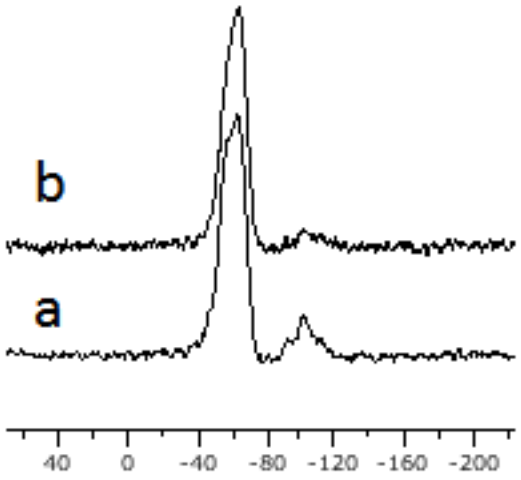

Figure 3.2.20 ^{29}Si CP-MAS of ethylene-bridged organosilica calcined at a) 350 ^{o}C and b) 300 ^{o}C under nitrogen atmosphere. The sample was prepared using toluene as a swelling agent and without salt.

3.2.7 Change in properties for ethylene-bridged PMO synthesized at lower temperature and further hydrothermal treatment. After synthesizing large-pore ordered materials with ethylene-bridges in the framework, we were interested to understand the evolution of mesopores and the effect of hydrothermal treatment of the material after initial synthesis at sub ambient temperature (15 ^{o}C). For this purpose, we analyzed materials after synthesis at lower temperature (15 ^{o}C) and further heating at higher temperature (100 ^{o}C for 1 day). The materials were prepared under standard conditions that we developed using TMB as a swelling agent.[108] The obtained materials were characterized by SAXS technique. The materials synthesized at lower temperature (LT) and further heated at higher temperatures (HT) show well-resolved patterns (Figure 3.2.21), indicating all the materials are well-ordered with face-centered-cubic (Fm3m) structure.

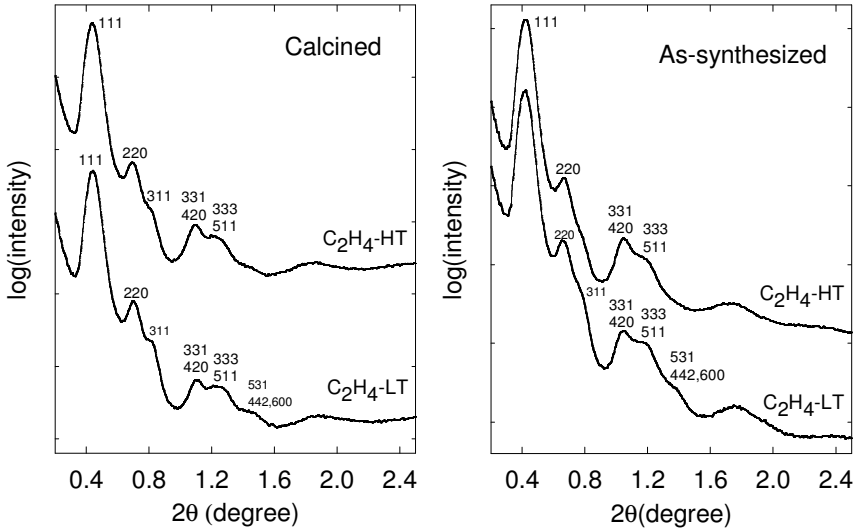

Figure 3.2.21 SAXS patterns for extracted and as-synthesized ethylene-bridged PMOs synthesized at initial synthesis temperature of 15 ^{o}C and further hydrothermally heated at 100 ^{o}C for 1 day.

Although in both cases there is a difference between the intensity of some of the peaks for materials synthesized at lower temperature and those further heated at higher

temperature. For example, (311), (531)/ (442)/ (600) peaks are prominent for material synthesized at low temperature, while those peaks are not visible for the same material after the heating of the synthesis mixture at 100 ^{o}C for 1 day. The reason behind this difference in peak intensities is not fully clear. But it could be related to the difference in relative arrangement of the organosilica framework and block-copolymer template that may change to some extent upon hydrothermal treatment at 100 ^{o}C for 1 day. It is known that the relative intensity of peaks depends on the relation between the pore size and unit-cell size for a particular structure.[210] The difference may be due to the fact that at higher temperature, both PPO and PEO become more hydrophobic and they may redistribute with respect to organosilica framework.

Table 3.2.2 Unit-cell Parameters and physicochemical properties of the organosilicas.

Sample	a (nm)	a_{uc} (nm)	a/ a_{uc}	S_{BET} (m^2/g)	w_{KJS} (nm)	V_t (cm^3/g)
PMO-C_2H_4-LT	34.8	36.4	0.96	437	11.2	0.24
PMO-C_2H_4-HT	35.2	36.9	0.95	573	11.6	0.35

Notation: a, unit-cell parameter for calcined or extracted sample; a_{uc}, unit-cell parameter for as-synthesized sample.

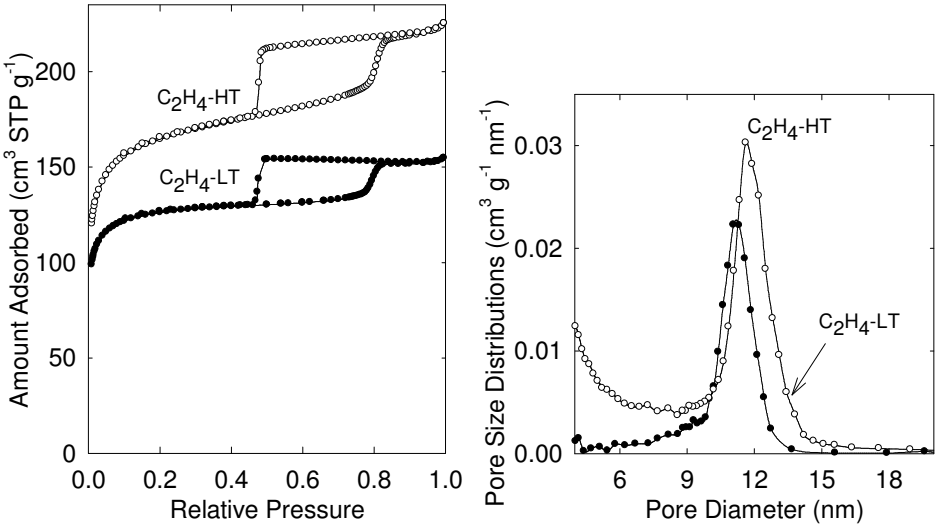

Figure 3.2.22 N_2 adsorption isotherms and pore size distribution of ethylene-bridged PMO synthesized at initial synthesis temperature of 15 ^{o}C (LT) and further hydrothermally heated at 100 ^{o}C for 1 day (HT).

We further analyzed the materials by gas adsorption technique to get insight about the physicochemical properties. As seen from gas adsorption isotherms (Figure 3.2.22, Table 3.2.2), two materials show different characteristics unlike their SAXS patterns. The SAXS patterns for materials synthesized at low temperature (15 ^{o}C) and further heating at 100 ^{o}C for 1 day show well-resolved patterns both of which can be indexed on fcc structure.

3.2.8 Proposed mechanism of formation of large-pore PMOs with spherical mesopores. Based on literature data and our own observation, we proposed the following mechanism. Swelling agents, such as TMB, xylene, toluene, or benzene swell the hydrophobic core of Pluronic block copolymers, which is poly(propylene oxide) (PPO). Upon addition of organosilica precursor, which interacts primarily with hydrophilic corona of the block copolymer micelles (poly(ethylene oxide) (PEO)), the precursor hydrolyzes under the reaction conditions. Here, the swelling agent plays vital role to obtain large-pore materials presumably by helping to induce a distribution of the organosilica precursor/framework between the PEO and PPO domains. Recently, we have used a similar strategy to synthesize ordered mesoporous silicas with 2-D hexagonal structure with ultra-large-pore with nominal (BJH) pore size up to ~ 26 nm.

Part 3. A Versatile Synthesis of Mesoporous Organosilica Hollow Nanospheres and its Implications for Synthesis of Hollow Organosilica Nanotubules

3.3.1 Transition from consolidated PMO structures to hollow individual particles.

In some cases, we observed formation of hollow individual particles in the surfactant-templated synthesis of organosilicas. We hypothesized that the formation of single micelle/organosilica nano-composites in the presence of a limited amount of the precursor, and thus its inability to form consolidated structures, is responsible for the formation of the hollow nanostructures. To verify our hypothesis, we gradually increased the amount of the precursor from low amount for which single micelle/organosilica nano-composites form to higher amount for which it is possible to obtain consolidated structures,[108] whereas other reaction conditions remained constant.

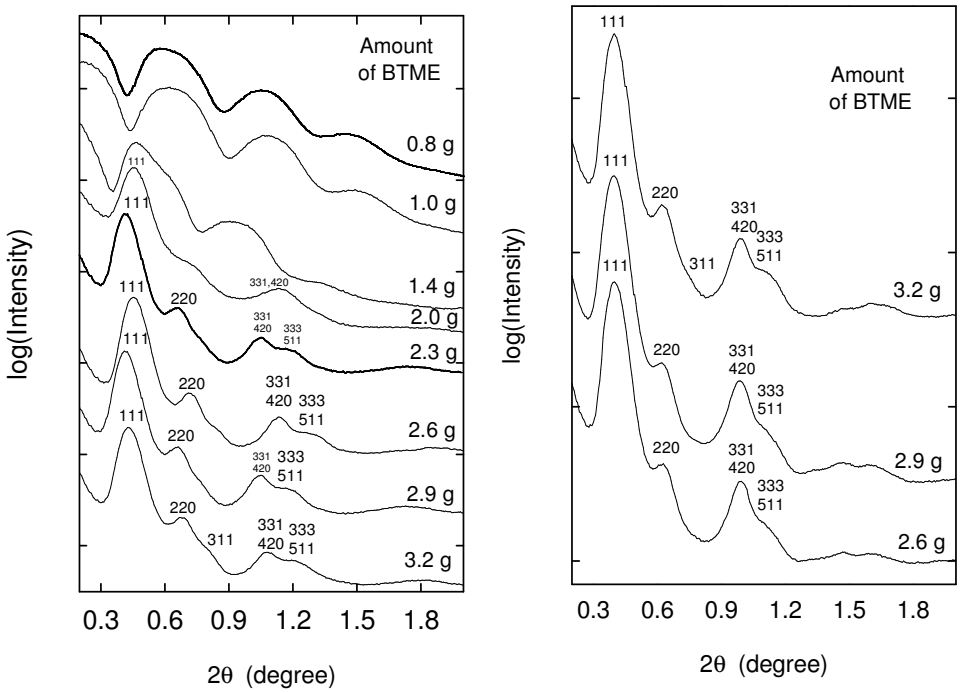

Figure 3.3.1 SAXS patterns of extracted ethylene-bridged PMOs with different amounts of precursor prepared in presence of trimethylbenzene (left) and xylene (right) as swelling agent. Amount of BTME used per 0.5 g F127 block copolymer. In case of xylene as swelling agent only higher amount of precursor was used.

We did SAXS study for each sample to understand the evolution between ordered consolidated structures and individual nanoobjects. As seen from SAXS patterns (Figure 3.3.1), on increasing the amount of organosiloxane precursor bis(trimethoxysilyl)ethane (BTME) from 0.8 g to 3.2 g per 0.5 g of F127 block copolymer, the SAXS pattern becomes gradually well-resolved and eventually the resolution remains almost constant on further increasing the amount of organosiloxane precursor. While the SAXS pattern obtained with low amount of precursor could not be indexed on any particular structure type, the materials obtained with higher amount of precursor exhibited the SAXS patterns clearly indexable on face-centered-cubic (Fm3m) structure. In fact, the SAXS patterns (Figure 3.3.1) for the whole series of samples prepared with different amount of organosiloxanes precursor could be divided into three groups. Samples prepared using higher amount of precursor for example 2.3 g to 3.2 g per 0.5 g of block copolymer, show well-resolved patterns characteristic of face centered cubic (Fm3m) structure. These materials are highly ordered as seen from well-resolved SAXS patterns (Figure 3.3.1). When the precursor amount was low, for example 0.8 g to 1.4 g per 0.5 g of F127 block copolymer, the patterns were not resolved and could not be indexed on any particular structure. The sample synthesized using 2.0 g of organosiloxane precursor (intermediate amount of precursor between isolated nanoobjects and fully consolidated structure, as will be discussed below), shows less resolved SAXS pattern, although it resembles a pattern for the other samples prepared with higher amount of precursor where the SAXS patterns are well-resolved and can be indexed on face-centered-cubic structure. Actually, this SAXS pattern resolution is in between that for the two other series of samples. So from a SAXS pattern, it is clearly visible that there is a transition from highly ordered

consolidated structures to some other structures (isolated nanoobjects, see below) on decreasing the amount of organosiloxane precursor. This phenomenon gives insight about the formation of single micelles in solution instead of forming aggregated micelles of certain shapes. It is possible that single micelles then aggregate (perhaps also rearrange and reshape) if the organosiloxane precursor amount is sufficient and thus form certain ordered structures (for instance, face-centered-cubic, Fm3m, structure). It is also clear that there is a certain range of amount of the precursor at which the ordered structure forms. For example, materials synthesized with organosiloxane precursor in the amount from 2.3 to 3.2 g per 0.5 g of F127 block copolymer have almost the same quality as seen from similar resolution of the SAXS patterns (Figure 3.3.1). To this end, studied the higher amount of precursor with another swelling agent, namely xylene, to see whether a similar behavior is observed. In case of xylene as a swelling agent, only relatively higher amounts of precursor (where it is expected to form fully consolidated structure) were selected for the initial study. All these materials showed well-resolved SAXS patterns (Figure 3.3.1, right) consistent with face-centered cubic structure. The transition from isolated nanoobject to consolidated ordered structure is observed by TEM (Figure 3.3.2). The TEM images clearly show the gradual consolidation of individual nanoobjects to form ordered materials. TEM image (Figure 3.3.2) shows that the material prepared at low precursor/polymer ratio consists of small, uniform spherical particles that can be either separate or aggregated. Aggregates of particles are particularly clear for samples prepared with 1.4 g of BTME. The spherical particles appear to be hollow inside. TEM clearly shows nicely ordered structure for the samples prepared with higher amount of precursor (i.e. 2.3 to 3.2 g of precursor).

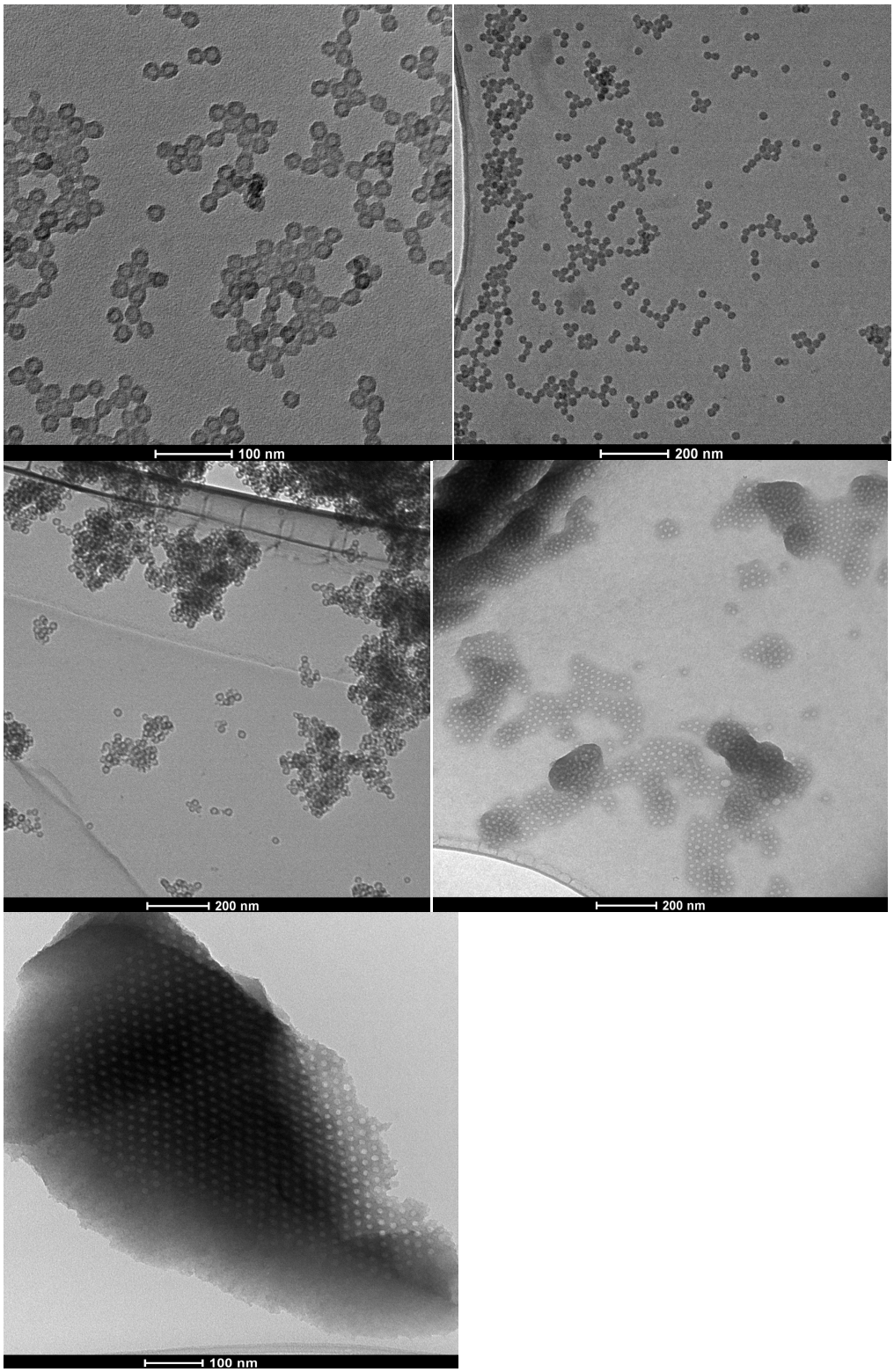

Figure 3.3.2 TEM images for the ethylene-bridged organosilica samples prepared with different amount of bis(trimethoxysilyl)ethane, BTME precursor using TMB as swelling agent: 0.8 g (top left), 1.0 g (top right), 1.4 g (middle left), and 2.0 g (middle right), and 3.2 g (bottom) of BTME. Amount of BTME used per 0.5 g F127 block copolymer.

The whole series of materials were further characterized by nitrogen adsorption technique in order to better understand the transition from isolated nanoobjects to fully consolidated structures.

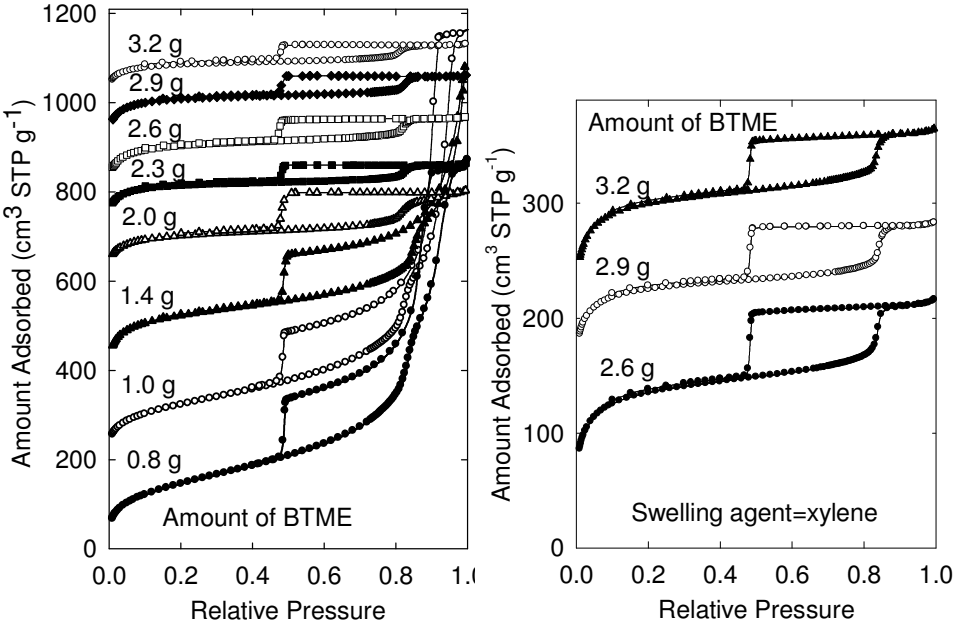

Figure 3.3.3 Nitrogen adsorption isotherms of extracted ethylene-bridged PMOs with different amounts of precursor prepared in presence of trimethylbenzene (left) and xylene (right) as swelling agent. Amount of BTME used per 0.5 g F127 block copolymer.

The nitrogen adsorption isotherms (Figure 3.3.3) for the sample synthesized using the precursor amount of 2.3 to 3.2 g show broad adsorption-desorption hysteresis loops. The loops featured steep capillary condensation steps at a relative pressure of 0.8-0.85 and steep capillary evaporation steps at the lower limit of adsorption-desorption hysteresis (0.48 p/p_o). The steep capillary condensation step indicates that the pores are uniform, whereas the sharp capillary evaporation step at the lower limit of hysteresis indicates that the entrances to the main pores are below 5 nm.[201] The broad hysteresis loops are typical for large cage-like pores. In all these cases, the adsorption isotherm levels off after the capillary condensation in the ordered mesopores was completed (in cases where relatively higher amount of precursor (2.3 to 3.2 g) was used). This indicates that these

materials are consolidated. Nitrogen adsorption isotherm for the sample synthesized using 2.0 g of precursor shows similar isotherm to the above-mentioned samples. Although, after capillary condensation step, the adsorption isotherm does not completely levels off indicating that the obtained materials are loosely aggregated to some extent or have defects. For the samples synthesized using even lower amount of the precursor, the shape of the adsorption isotherms shows a different behavior. In these cases, the isotherms did not level off at pressures above the capillary condensation pressures in uniform mesopores and a significant increase in amount adsorbed (p/p_o ~0.80 – 0.85) was observed at relative pressures above ~ 0.85. This increase can be attributed to adsorption in secondary (interparticle) mesopores as confirmed from TEM (Figure 3.3.2). Thus the capillary condensation step seen on the isotherms at p/p_o of 0.8 – 0.85 arises from filling of the interiors of these hollow objects, while the subsequent increase in adsorbed amount corresponds to the capillary condensation in a space between the particles. For materials synthesized with higher BTME content, the particles are larger and smoother, indicating that the structure is better consolidated in this case. Pore size distributions (PSDs) are shown in Figure 3.3.4, which shows biomodal distributions in pore sizes when lower amount of precursor was used. The bimodality in the pore size distribution appears due to the adsorption in the main mesopores and in the spaces between the nanoobjects. PSDs in case of materials obtained when relatively higher amount of precursor was used, only one peak is present indicating that the material is consolidated.

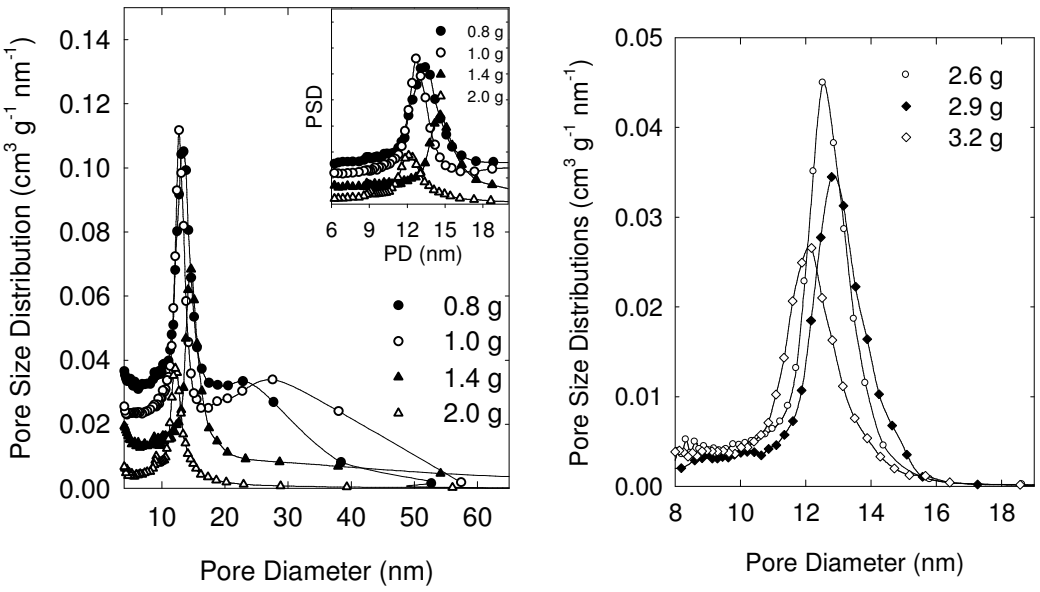

Figure 3.3.4 Pore size distribution of extracted ethylene-bridged PMOs with different amount of precursor.

3.3.2 Understanding the mechanism of formation of hollow nanospheres. The transition from the consolidated structure to individual nanospheres (or nanotubules, as will be shown later) was triggered by the decrease in the amount of the organosilica precursor relative to the amount of the triblock copolymer template. In this regard, based on SAXS patterns, TEM images and nitrogen adsorption and thermogravimetry analysis data, the proposed mechanism of formation of nanospheres is as follows. The block-copolymers PEO-PPO-PEO forms single micelles, which could be spherical (or tubular) in shape, depending upon the Pluronic copolymer used. For example, while Pluronics P123 forms cylindrical micelles, Pluronic F127 forms spherical micelles. Upon addition of the precursor in the amount that is sufficiently lower than that required for formation of consolidated structures, the precursor interacts with the hydrophilic PEO corona of the micelle and on the interface of PEO corona and PPO core.[69] The organosilica precursor interacts more favorably with PPO than silica framework does in silica /Pluronic composites. If the relative amount of the organosilica precursor with respect to the PEO-

PPO-PEO micelles is limited, the concentration of the precursor on the surface of the micelle is likely to be small and the cross-linking between the organosilica/micelle nanoparticles is likely to be retarded, thus preventing the consolidation of the organosilica-micelle composites.

3.3.3 Hollow nanospheres with different organic bridging groups. Transmission electron microscopy (TEM) shows the formation of hollow nanospheres in cases of organosilicas with methylene, ethylene, ethenylene, and phenylene bridges (Figure 3.3.5).

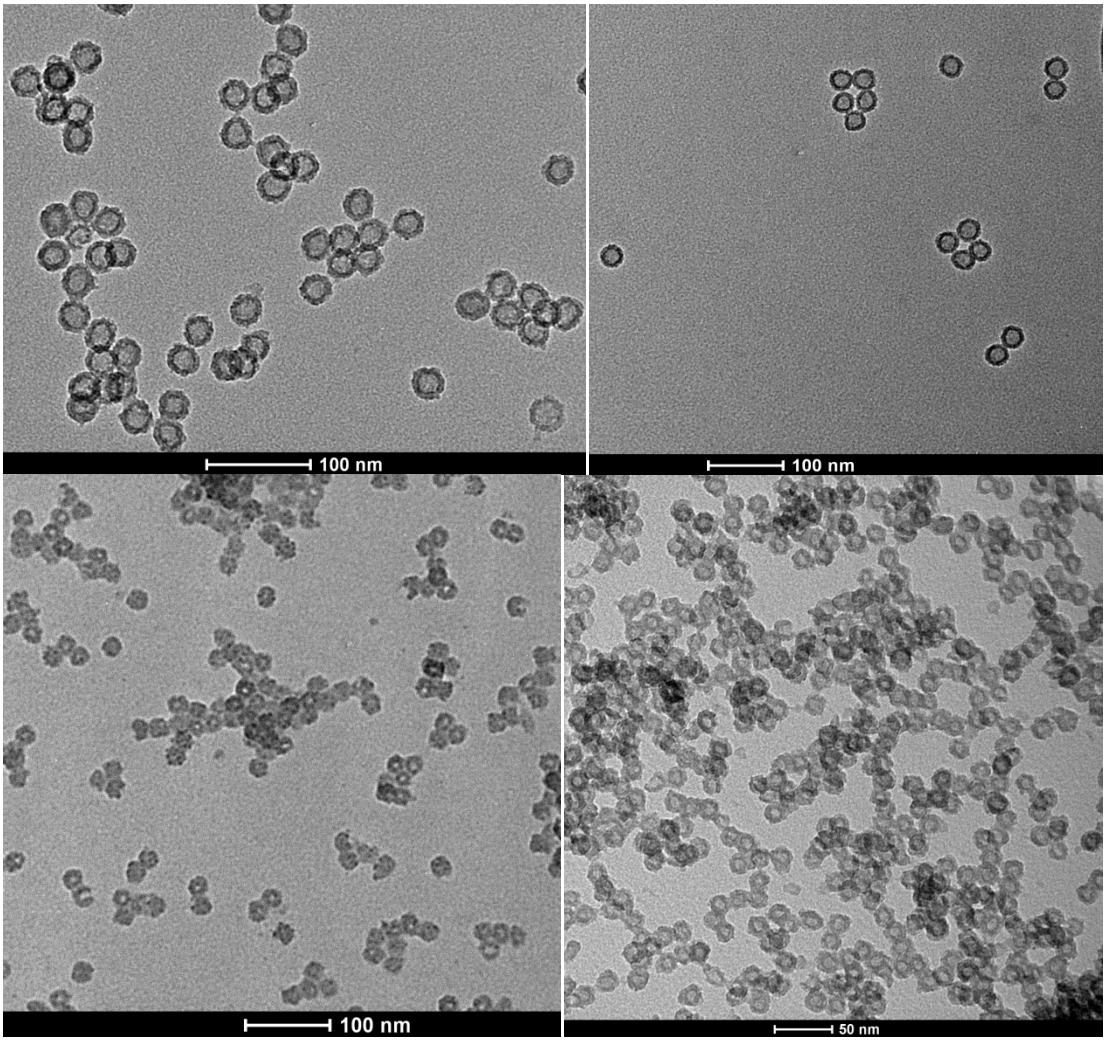

Figure 3.3.5 TEM images of organo-silica hollow nano-spheres with different organic bridging groups: (top left) methylene (-CH_2-), (top right), ethylene (-CH_2CH_2-), (bottom left), ethenylene (-CH=CH-), and (bottom right) phenylene (–C_6H_4-).

In case of methylene, ethenylene, and phenylene-bridged hollow nanospheres, xylene was used as a swelling agent, while in case of ethylene-bridged hollow nanospheres toluene was used as a swelling agent. In the case of methylene-bridged hollow nanospheres, the cavity size of ~ 18 nm was obtained. This cavity size was further confirmed by nitrogen adsorption technique (Figure 3.3.6), which shows the pore size of 18.3 nm. In case of ethylene-, ethenylene-, and phenylene-bridged hollow nanospheres, the pore size of 21.2, 10.8, and 7.9 nm were obtained, respectively.

The TEM images clearly show the void space and the shell. The wall thickness can be estimated by subtracting the inner diameter from the outer diameter from TEM images, due to the sufficient contrast between empty core and the shell. From high-resolution TEM images, it seems that the walls are porous, which is further confirmed by accessibility of nitrogen gas to the interior during gas adsorption measurements. The porous nature of the walls could be related to the occlusion of hydrophilic poly(ethylene oxide) block of the block copolymer in the organosilica framework as is known for other materials, such as mesoporous pure-silica materials.[70,71] The materials were characterized by nitrogen adsorption technique and in all cases, the materials show two-step adsorption behavior (Figure 3.3.6). The first step of capillary condensation appears due to the adsorption in the inner space of uniform hollow nanospheres, and the second capillary condensation step (close to saturation vapor pressure) can be attributed to the condensation of nitrogen gas in the interstitial space between the particles. This two-step behavior further suggests that the materials are not consolidated structures. The pore size distributions (PSDs) show narrow peaks related to uniform mesopores (Figure 3.3.6, right). The broad hysteresis loop indicates that the hollow nanospheres have narrow gaps

in the walls. The effect of the low ratio of the framework precursor to the surfactant is expected to lead to the thinning of the pore walls.[72]

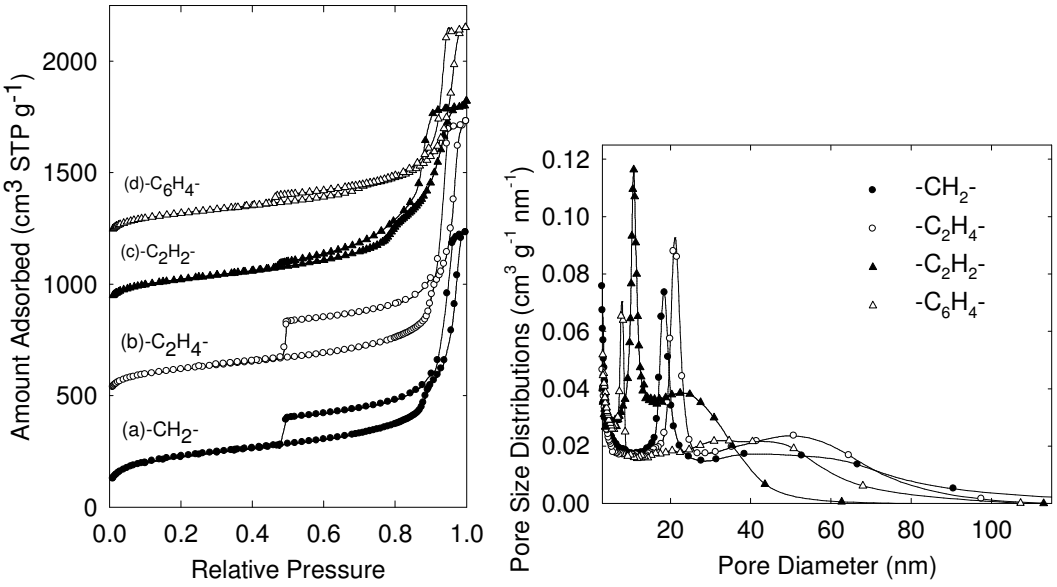

Figure 3.3.6 Nitrogen adsorption isotherms (left) and pore size distributions (right) of hollow nanospheres with different organic bridging groups, such as a) methylene (-CH_2-), b) ethylene (-CH_2CH_2-), ethenylene (-CH=CH-), and phenylene (–C_6H_4-) bridging groups. The adsorption isotherms were offset vertically by 445, 880, and 1140 cm^3 STP g^{-1} for ethylene, ethenylene and phenylene-bridged hollow nanospheres.

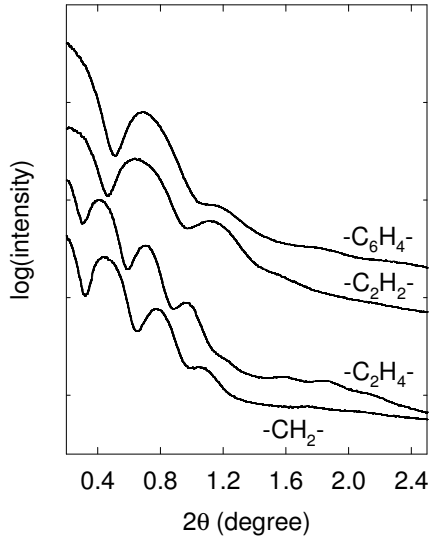

Figure 3.3.7 SAXS patterns of hollow nanospheres with different organic bridging groups: a) methylene (-CH_2-), b) ethylene (-CH_2CH_2-), ethenylene (-CH=CH-), and phenylene (–C_6H_4-) bridging groups.

The materials were further characterized by small-angle X-ray scattering (SAXS). The SAXS patterns in all cases are similar (Figure 3.3.7). The patterns cannot be indexed on any particular structure. Similar SAXS patterns were observed before in case of hollow nanosphere materials.[178-180]

Table 3.3.1 Textural properties of organosilica hollow nanoobjects and nanotubules.

Sample, swelling agent, (calcination temp. under air)	S_{BET} (m^2/g)	w_{BJH} (nm)	V_t (cm^3/g)
-CH_2-NS, xylene	820	18.3, 52.1	1.87[d]
-CH_2-NT, cyclohexane	1184	12.0	1.54
-C_2H_4-HS, benzene	378	18.6	1.52
-C_2H_4-HS, toluene	622	21.2	1.96
-C_2H_4-HS, toluene, (350)	565	17.5	1.58
-C_2H_4-HS,toluene, (500)	423	16.6	1.28
-C_2H_4-HS, xylene	452	17.1	0.77
-C_2H_4-HS, TMB	455	12.7, 26.5	1.49
-C_2H_4-NT, cyclohexane	376	15.3, 44.9	1.72
-C_2H_2-HS, xylene	519	10.8, 23.7	1.42
-C_2H_2-NT, cyclohexane	266	12.4	1.56
-C_6H_4-HS, xylene	635	7.8, 36.9	0.44
-Silica-HS (BTSME), xylene	444	16.8	0.96
-Silica-HS, xylene	210	22.8	1.09

Samples were noted as X-NT/HS, where X is methylene, ethylene, ethenylene, and phenylene and NS, and NT indicate nanospheres and nanotubules respectively. Notation: $S_{BET,}$ BET specific surface area; $w_{BJH,}$ BJH pore diameter; $V_{t,}$ total pore volume. NA, not available.

The above results show that Pluronic F127 block copolymer could be used to successfully synthesize nanospheres comprising of organosilica framework with various organic bridging groups, such as methylene, ethylene, ethenylene and phenylene. The

evidence of versatility of this method comes from the fact that more complicated organosilane precursor, such as $(MeO)_3Si\text{-}CH_2\text{-}C(=CH_2)\text{-}CH_2\text{-}Si(OMe)_3$, when used under similar conditions, still produces hollow nanospheres (Figure 3.3.8). The material showed the pore size of ~17 nm (Table 3.3.1). Unfortunately, the ^{29}Si NMR data (for a related material) show the complete cleavage of the Si-C bonds producing entirely pure silica materials. This can be correlated to similar behavior of producing silica materials when organosilane with allyl functionality was used.[205] However, based on the formation of nanospheres templated by block copolymer F127, one can speculate that the nanospheres form before the cleavage of Si-C bonds, because our attempt to synthesize hollow silica spheres using silica precursor (TEOS) and F127 was unsuccessful. The SAXS pattern for the resulting material (Figure 3.3.8) is somewhat similar to that for other hollow nanosphere materials with different organic bridging groups. The nitrogen adsorption isotherm (Figure 3.3.8) shows two capillary condensation steps which is typical for the material composed of hollow nanospheres.

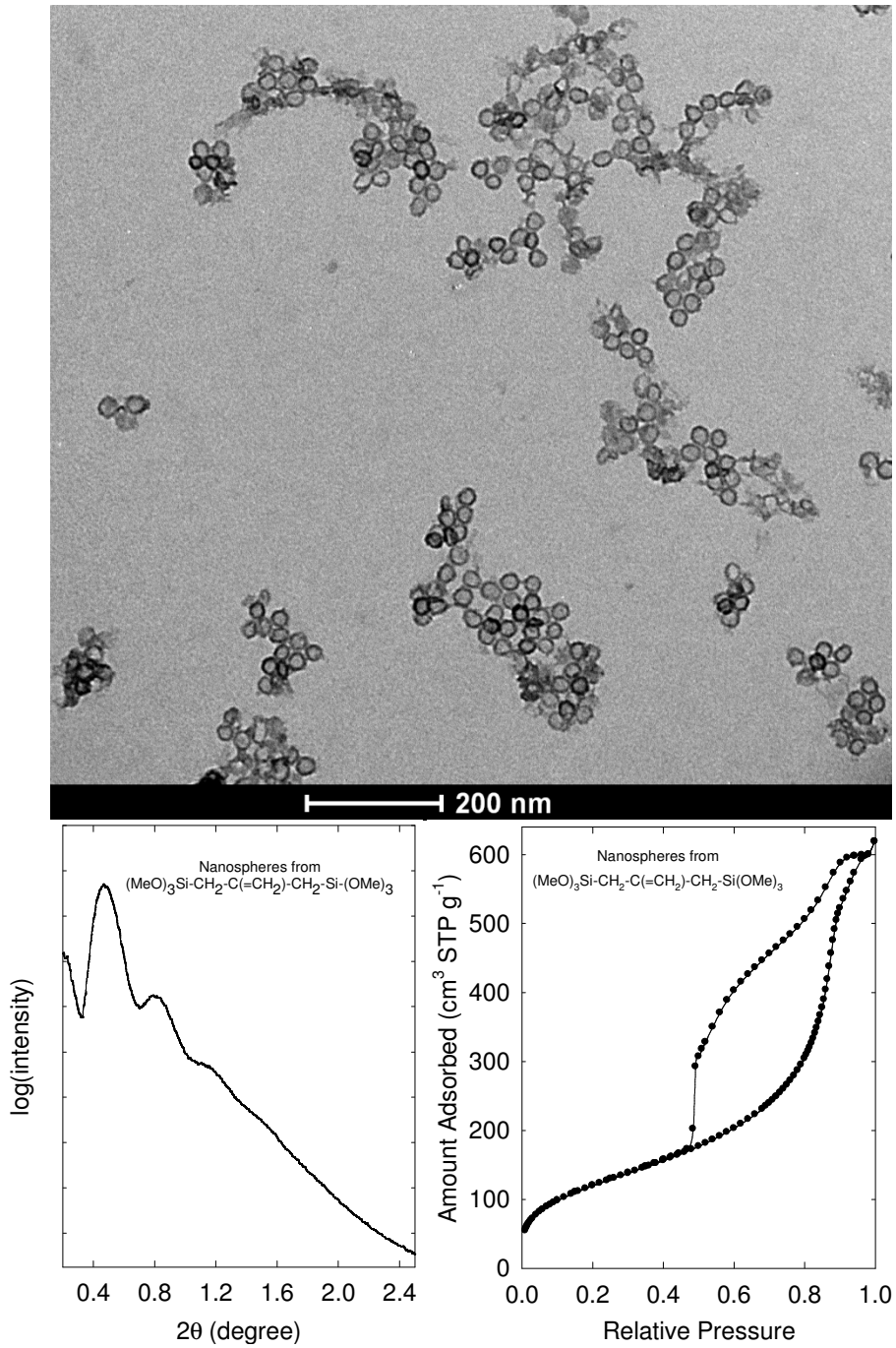

Figure 3.3.8 TEM image (left) and SAXS pattern of hollow silica nanospheres synthesized using $(MeO)_3Si\text{-}CH_2\text{-}C(=CH_2)\text{-}CH_2\text{-}Si(OMe)_3$ as precursor. Nitrogen adsorption isotherm of the material.

The PSD (Figure 3.3.9) is quite narrow and the peak is centered at 16.8 nm. The narrow PSD is consistent with the TEM image (Figure 3.3.8), which shows that the nanospheres are monodisperse.

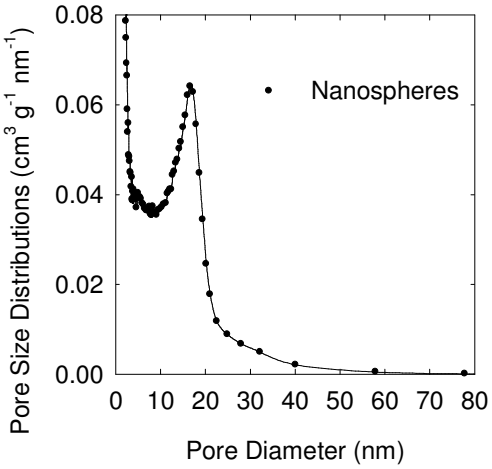

Figure 3.3.9 Pore size distribution of hollow silica nanospheres synthesized using $(MeO)_3Si\text{-}CH_2\text{-}C(=CH_2)\text{-}CH_2\text{-}Si(OMe)_3$ as organosiloxane precursor.

3.3.4 Thermal stability. The thermal stability of the organosilica hollow nanospheres was studied by thermogravimetric analysis. Methylene-bridged hollow nanospheres show some weight loss up to 130 ^oC which is due to the desorption of water. Weight loss at 200 ^oC and at higher temperature can be attributed primarily to the oxidation of block-copolymer and oxidation of swelling agent, because the weight loss associated with conversion of $–CH_2-$ bridges with –O- bridges is very small (Figure 3.3.10). The material calcined at 300 ^oC under air does not show any appreciable weight loss between 200 and 500 ^oC, indicating the complete removal of the template. The TGA for other hollow nanospheres composed of other organic bridging groups are shown in Figure 3.3.11 to 3.3.13. The weight loss after surfactant removal is significantly reduced, although the data for ethylene-bridged sample suggests the retention of some of the template (the weight loss corresponding to conversion of $–CH_2\text{-}CH_2-$ to –O- linkage is about 15 %).

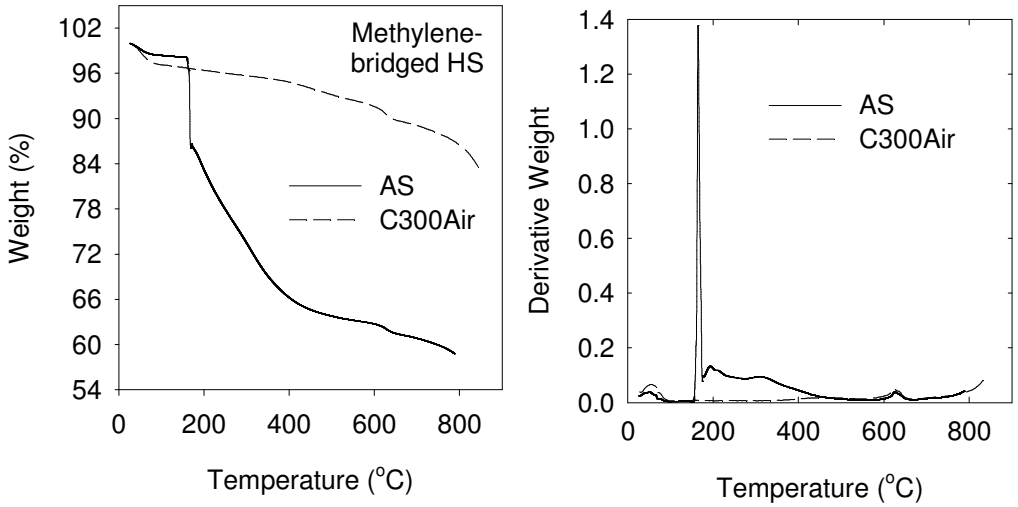

Figure 3.3.10 TGA and differential TGA of a) as-synthesized and b) calcined under air at 300 °C samples for methylene-bridged nanospheres (synthesized using xylene as a swelling agent and salt). The measurement was performed under air atmosphere.

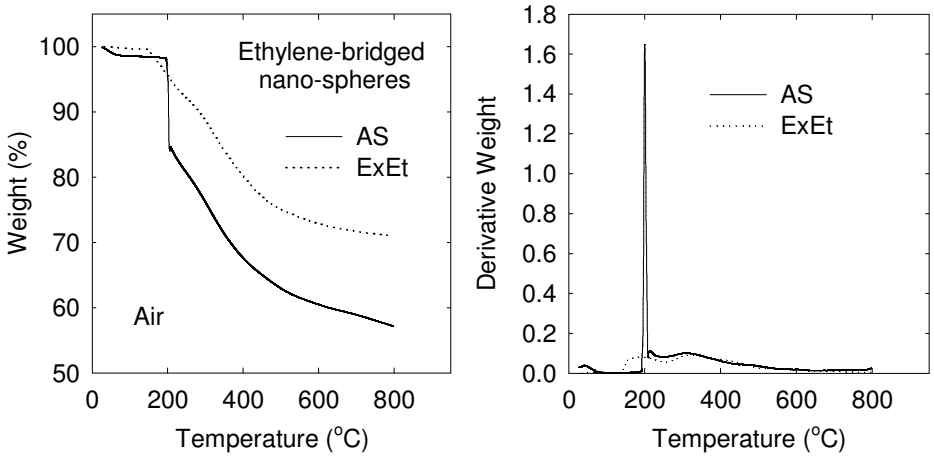

Figure 3.3.11 TGA and differential TGA of a) as-synthesized and b) ethanol-extracted ethylene-bridged nano-spheres (synthesized using TMB as a swelling agent and salt). The measurement was performed under air atmosphere.

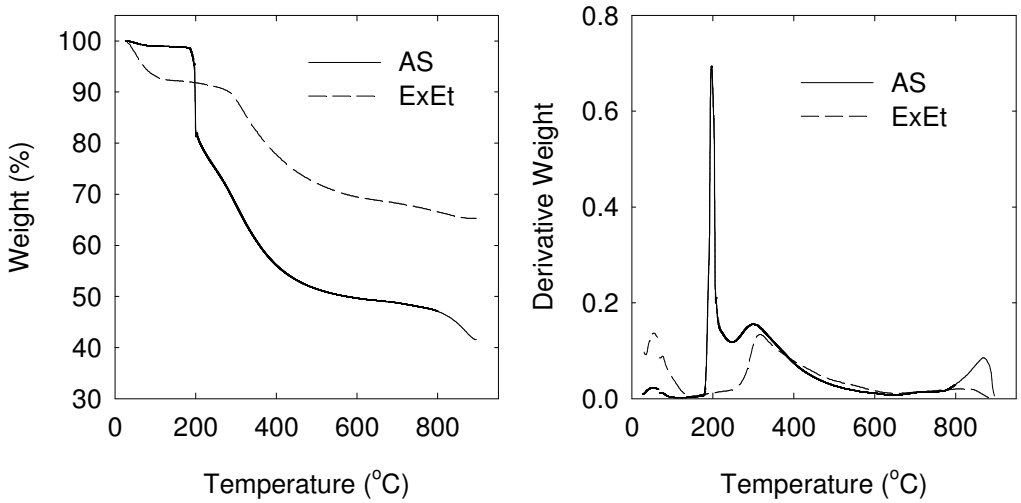

Figure 3.3.12 TGA and differential TGA of a) as-synthesized and b) ethanol-extracted ethenylene-bridged nanospheres (synthesized using xylene as a swelling agent and salt). The measurement was performed under air atmosphere.

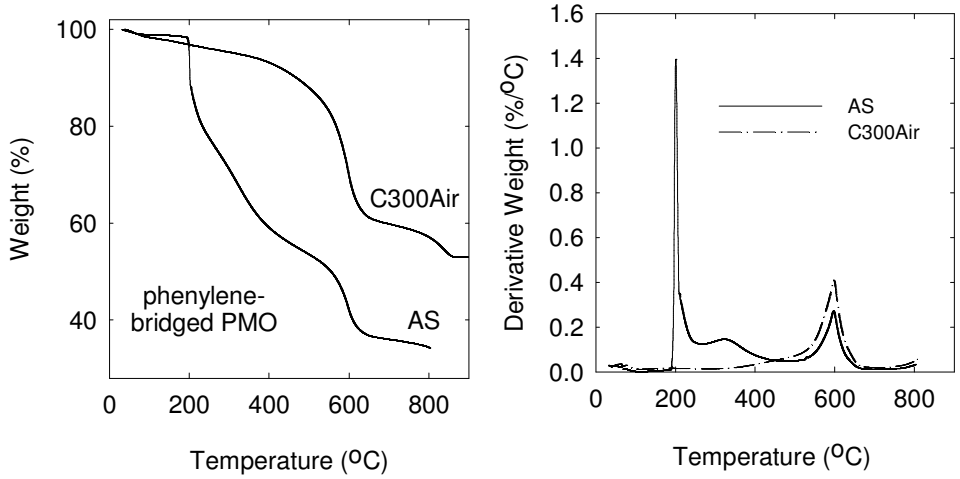

Figure 3.3.13 TGA and differential TGA of phenylene-bridged nanospheres (synthesized using xylene as a swelling agent and salt) a) as-synthesized and b) calcined at 300 °C under air. The measurement was carried out under air.

The as-synthesized phenylene-bridged material shows weight loss at ~ 200 and ~ 600 °C, the first weight loss is due to the decomposition/oxidation of the block copolymer (and possibly swelling agent) and the second weight loss is due to the oxidation of the phenylene-bridging groups indicating that the nanospheres are composed of block-copolymer and organosiloxane framework. The origin of weight losses at ~ 800 °C for

same samples is unclear, but may be related to the silica framework consolidation through the condensation of silanols with release of water.

3.3.5 Conversion to hollow silica spheres. The pure-silica hollow nanospheres were obtained from organosilica hollow nanospheres by heating under air. Ethylene-bridged hollow nanospheres were found stable even upon heating at 500 ^{o}C for 5 hr under air, but the organic groups are certainly removed during this process. This resulting material shows decreasing pore size in comparison to the extracted organosilica material (Figure 3.3.14).

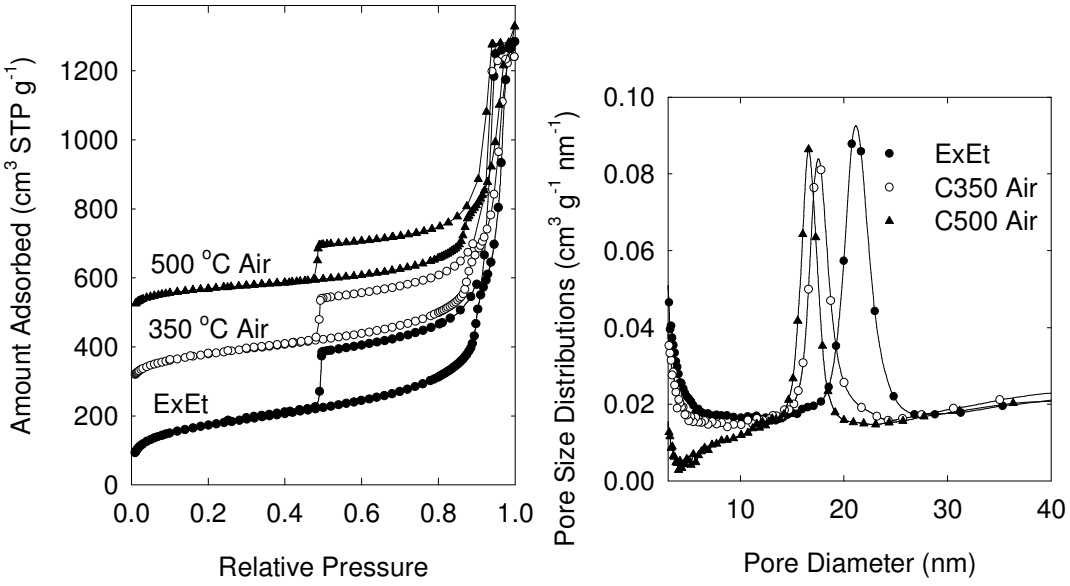

Figure 3.3.14 TEM image (top), nitrogen adsorption isotherm (bottom left) and pore size distributions (bottom right) of ethylene-bridged PMOs either extracted or calcined at 350 ^{o}C or 500 ^{o}C under air to convert it into silica hollow sphere. The adsorption isotherms were offset vertically by 220, and 450 cm^3 STP g^{-1} for hollow nanospheres calcined at 350 and 500 ^{o}C, respectively.

After calcination, the material shows substantially less uptake of gas molecules indicating the shrinkage of the hollow nanospheres. This shrinkage was further confirmed by TEM. After heating at 350 ^{o}C under air, the pore size decreased from 21.2 nm to 17.5 nm (based on gas adsorption data). After further increasing the temperature, that is by

heating the ethylene-bridged hollow nanospheres under air at 500 ^{o}C, we still obtained pure silica hollow nanospheres (Figure 3.3.15). At this temperature, the organic bridging group (Si-R-Si, where R is organic group) converts completely into siloxane linkage (Si-O-Si). During this process, although the void space inside the spheres becomes smaller, the structure still remains intact as seen from TEM image (Figure 3.3.15).

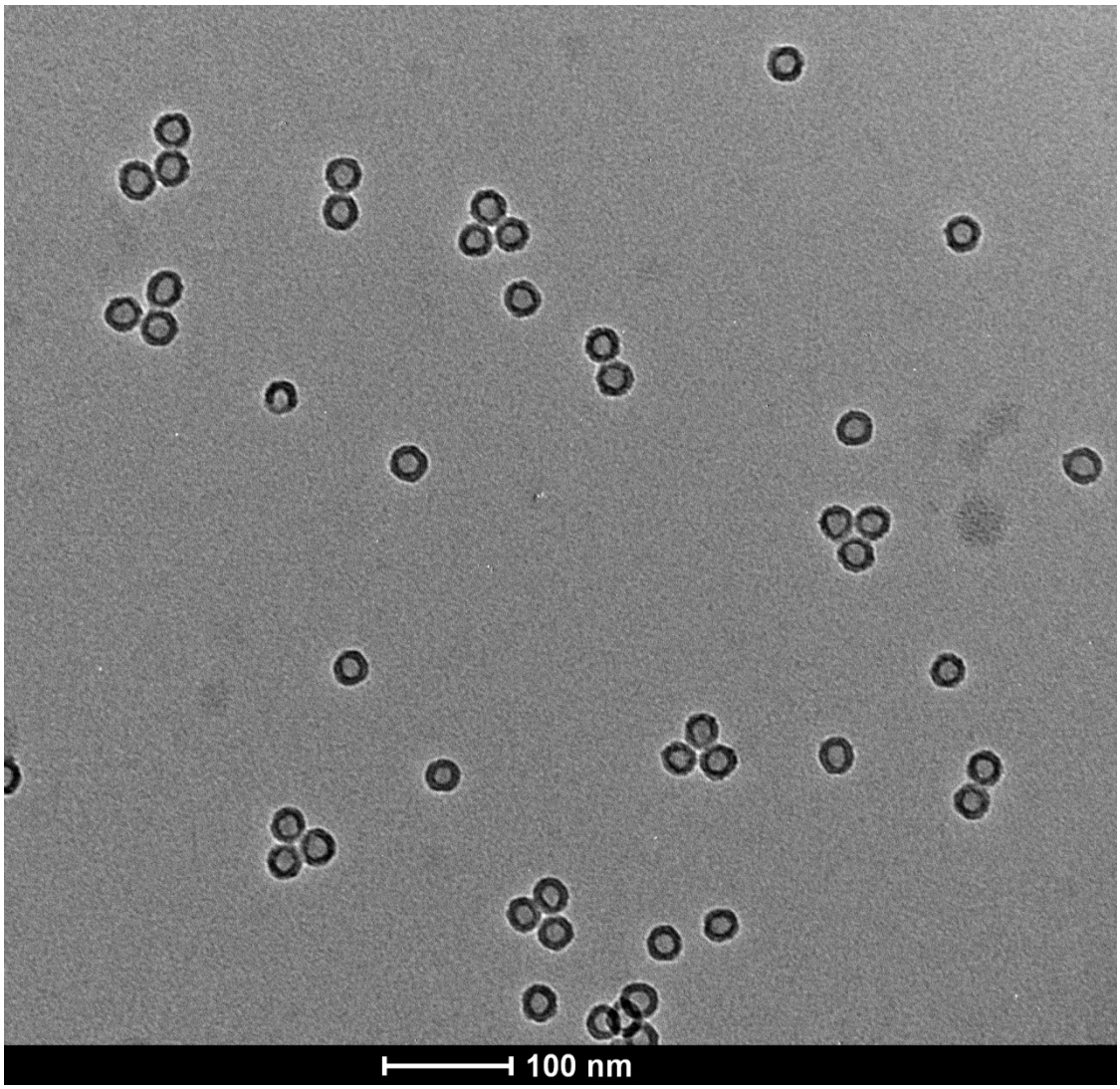

Figure 3.3.15 TEM image of hollow nanosphere obtained by heating ethylene-bridged organosilica hollow nanospheres under air at 500 ^{o}C. At this temperature the organosilica nanospheres are expected to convert into silica hollow nanospheres.

The smaller void space is due to the shrinkage of the sphere. So the calcination under air is another way of tuning the pore size of the hollow nanospheres. Also, this approach could be applied to hollow nanospheres with other organic bridging groups to tune the pore size, if the retention of organic ridging groups is not essential.

3.3.6 Direct synthesis of hollow silica spheres. Our attempt to synthesize hollow silica nanospheres using tetraethylorthosilicate (TEOS) as a silica precursor and using F127 block copolymer as template under similar conditions was not successful. The reason might be that the silica precursor interacts primarily with PEO block, while the organosilica precursor interacts with PEO, but may also interact with PPO domain. Consequently, the interface between the framework-free and framework-containing space is likely to be shifted more towards the center of PPO core in the case of organosilica than it is in the case of pure silica. It was hypothesized that for the individual hollow structures to form, the framework precursor (whether that for organosilica or that for silica) needs to be occluded in the micelles while leaving a negligible amount of it outside the micelles (that is outside PEO domains). Since the silica precursor is expected to have less tendency to penetrate the hydrophobic (PPO) domain, it was inferred that the increase in the relative proportion of PEO domain in the surfactant will be beneficial for the formation of hollow silica spheres. Therefore, Pluronic F108 was employed for pure-silica materials and indeed it led to the formation of hollow silica spheres. TEM image shows the formation of almost monodisperse hollow nanospheres (Figure 3.3.16, top). In some cases, the spheres are broken. The nitrogen adsorption isotherm shows two capillary condensation steps indicating the existence of two kinds of mesopores, as in other hollow nanospheres (Figure 3.3.16, below).

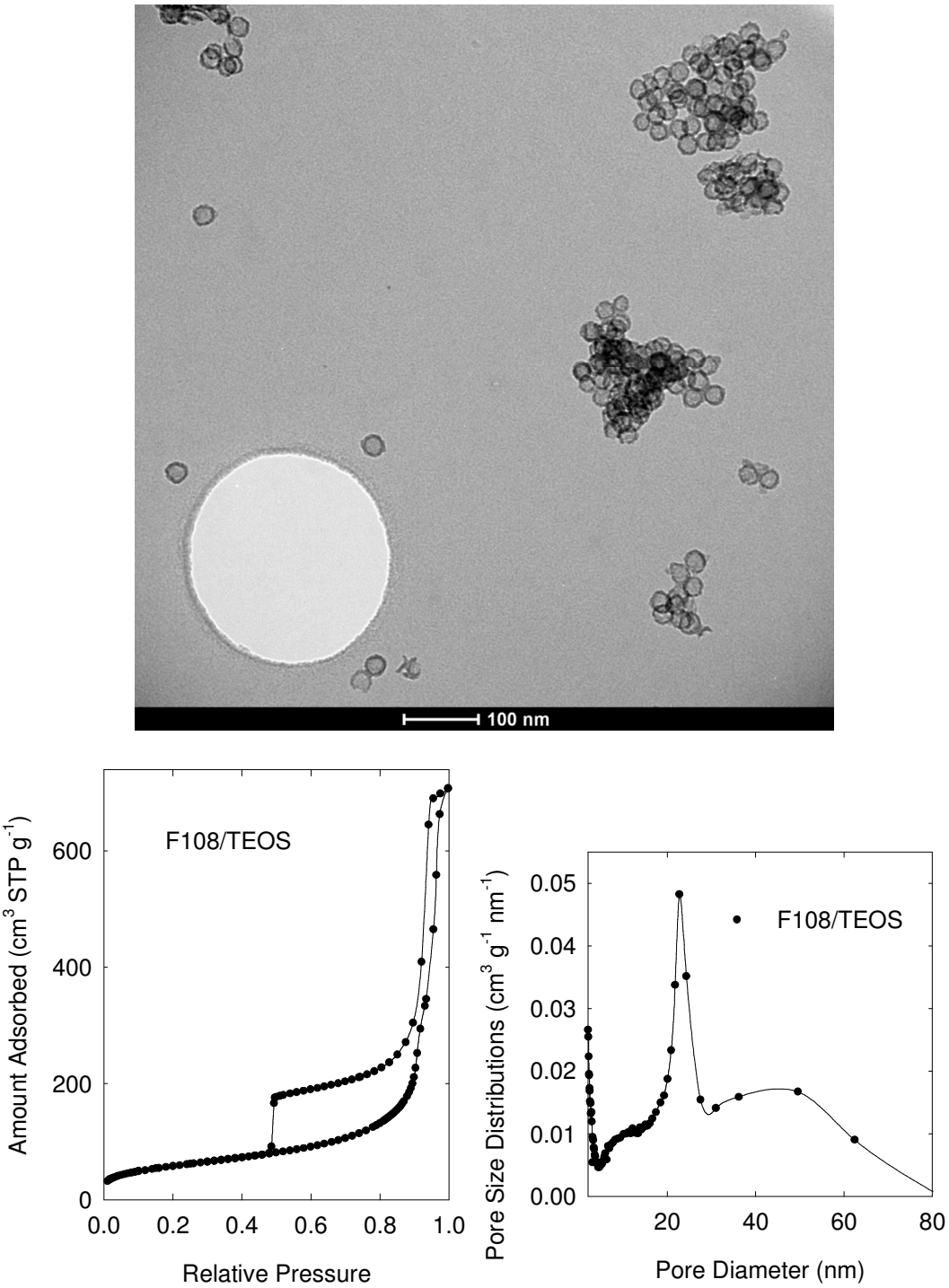

Figure 3.3.16 TEM image (top), nitrogen adsorption isotherm (bottom left) and PSD (bottom right) of hollow silica nanospheres templated by Pluronic F108 block copolymer (calcined at 550 ^{o}C under air).

PSD of the silica hollow nanospheres is quite narrow confirming the TEM image, showing hollow interiors of spheres that are uniform in size. Previously, F108 was used in the synthesis of hollow or partially consolidated silica nanoobjects.[182]

3.3.7 Arresting aggregation. To reduce the interaction between separate micelles, a functionalized silane precursor was added in conjunction with the pure organosilica precursor.[175] For this purpose, organosilane of general formula $R_nSi(OR^1)_{4-n}$ (where, n= 1 to 3 and R, R^1 are methyl or ethyl group) was used. The added organosilane has at least one hydrolysable group, i.e., methoxy, or ethoxy group. We observed the hydrolysis rate in presence of these silanes as follows:

$$Me_3SiOEt > Me_2Si(OEt)_2 > MeSi(OEt)_3$$

After functionalization, the nanospheres seem to preserve the monodispersity as is evidenced from TEM image (Figure 3.3.17).

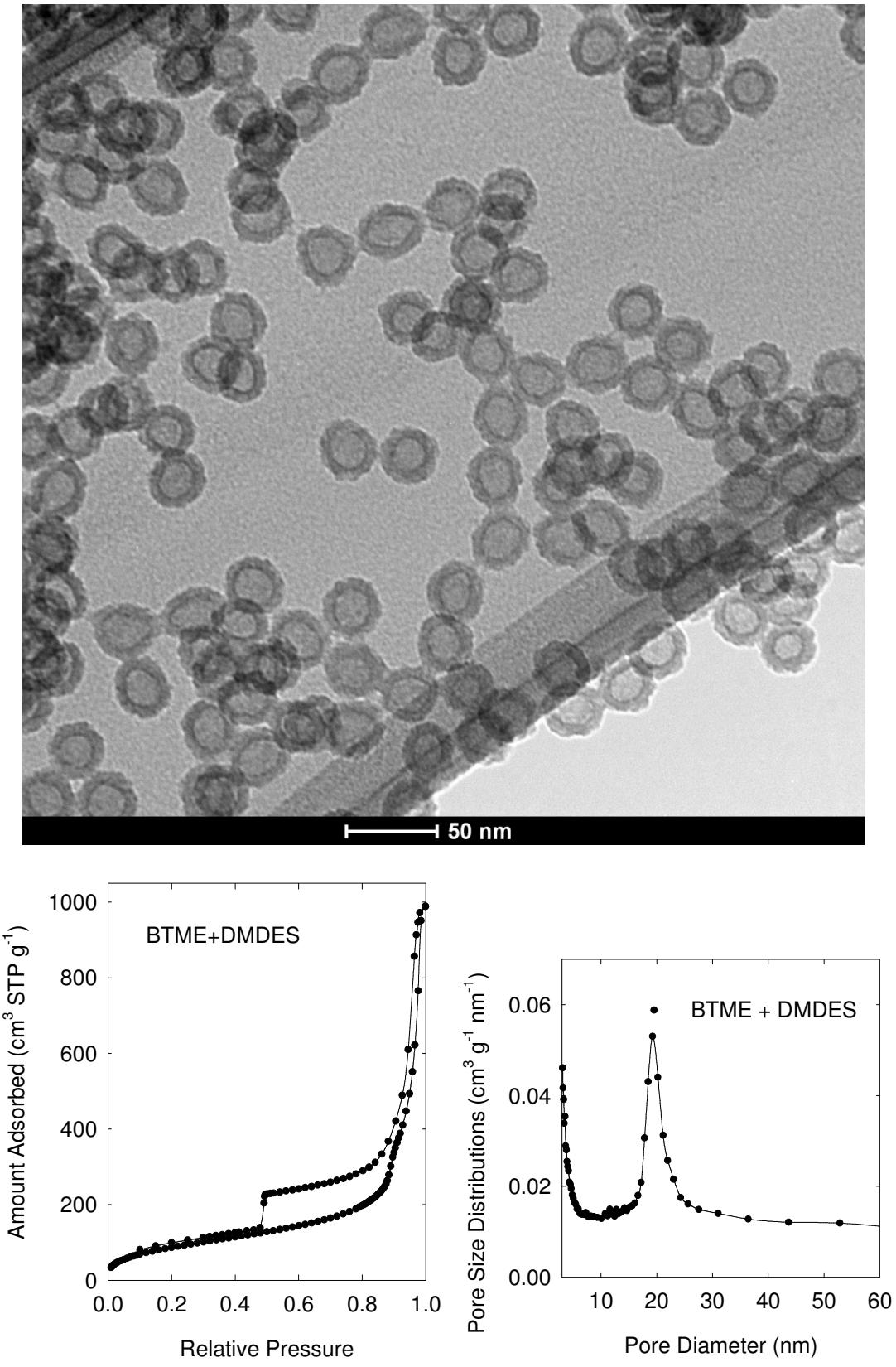

Figure 3.3.17 TEM image of ethylene-bridged hollow nanospheres in presence of dimethyldiethoxysilane (DMDES).

3.3.8 Implications for the synthesis of hollow nanotubules. The formation of hollow nanospheres was found to be triggered by the low amount of precursor (significantly lower than the amount needed for the formation of consolidated structures) for a wide varieties of organosilane precursors (as mentioned above). Based on this understanding of the synthesis of hollow nanospheres, we applied the concept for the synthesis of nanotubules. For this purpose, another block copolymer, namely Pluronic P123, which is known to form cylindrical micelles, was used under similar conditions of a lower amount of precursor (compared to the amount required for synthesis of consolidated structures) for the synthesis of hollow nanotubules. The organosilane precursors with different organic bridging groups, such as methylene, ethylene, ethenylene, and phenylene, were used. The synthesized materials were first analyzed by TEM. The TEM images show indeed that under these conditions the organosilica precursor with methylene, ethylene, and ethenylene bridging groups form hollow nanotubules (Figure 3.3.18). As seen from the TEM images, the nanotubules are cylindrical in nature, which is consistent with the fact that the Pluronic P123 block copolymer are known to form cylindrical micelle, which for instance, template SBA-15 and organosilicas with 2-D hexagonal structures. The formation of single hollow nanotubules further corroborates the formation of single-micelle-templated materials (cylindrical shapes in this case) in solution. The formation of single micelles is triggered by the low organosiloxane/block copolymer ratio (sufficiently lower than that necessary for the formation of ordered consolidated structure). This hypothesis is further proven by the fact that under similar conditions, sufficiently high organosiloxane/block copolymer ratio give rise to ordered 2-D hexagonal structure.[68]

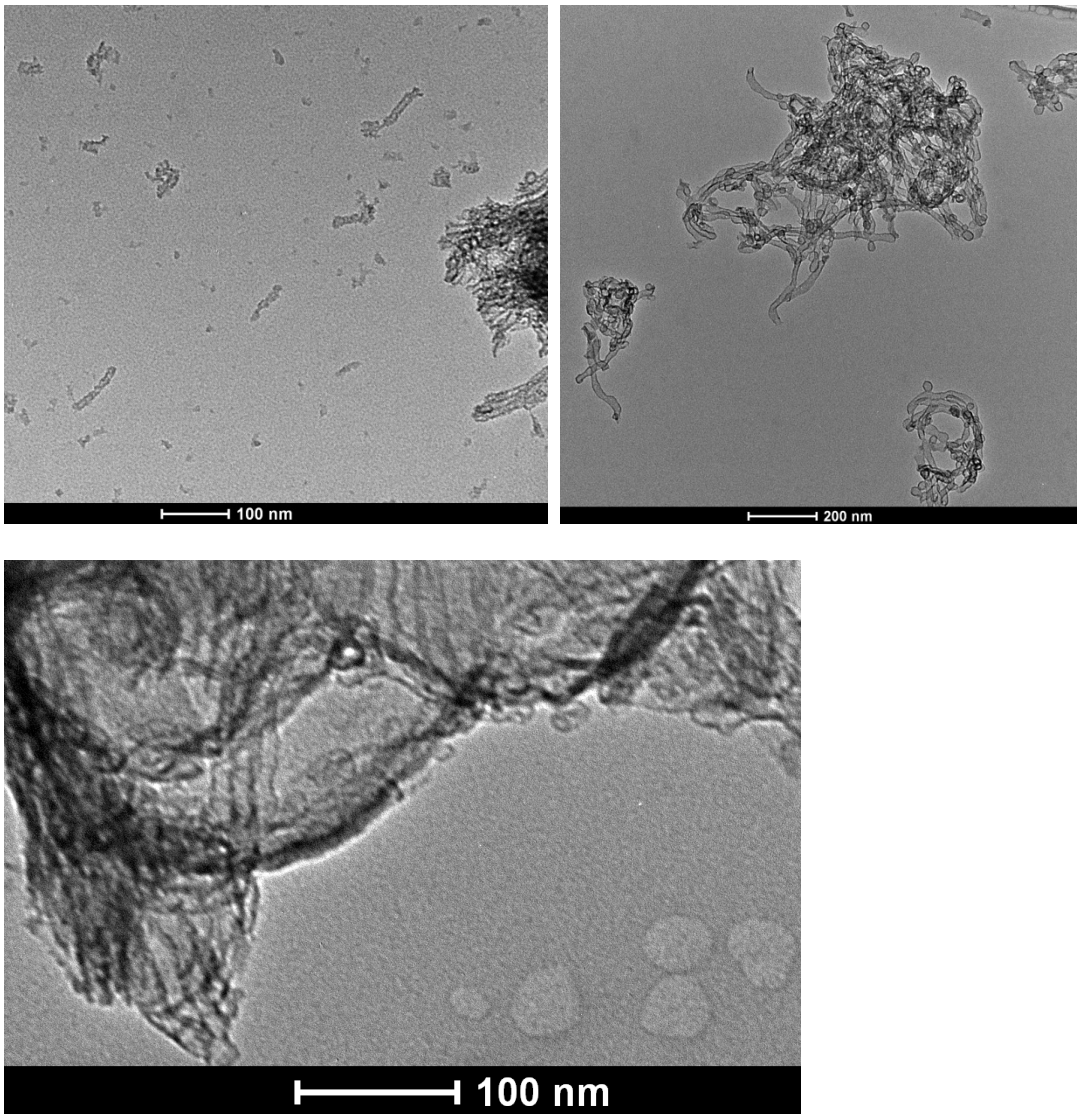

Figure 3.3.18 TEM images of organo-silica hollow nanotubules synthesized with different organic bridging groups: methylene (-CH_2-) (top left), ethylene (-CH_2CH_2-) (top right), and ethenylene (-CH=CH-) (bottom).

The orgaonosilica composed of hollow nanotubules were analyzed by nitrogen adsorption technique to further confirm their hollow structure. The materials show adsorption isotherms that revealed uniform pores and some larger secondary pores, which may reflect the space between the tubules (Figure 3.3.19). All these materials show steep capillary evaporation steps at the lower pressure limit of adsorption-desorption hysteresis

indicating that the hollow tubules (or some parts of them) have entrances or defects/pores in the walls of size below 5 nm.[201]

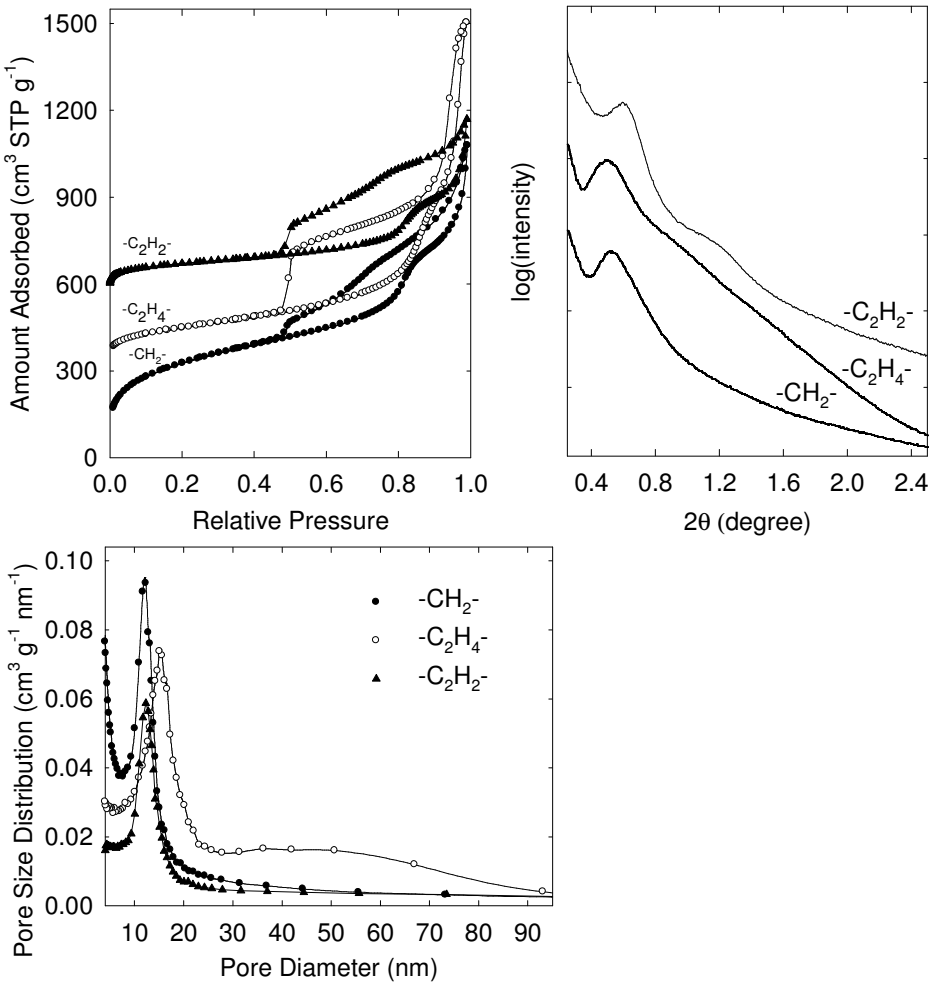

Figure 3.3.19 Nitrogen adsorption isotherms of hollow nanotubules (left), SAXS patterns (top right), and pore size distributions (bottom) with different organic bridging groups such as methylene, ethylene, and ethenylene. The adsorption isotherms were offset vertically by 350, and 600 cm^3 STP g^{-1} for hollow nanotubules synthesized using ethylene, ethenylene, and phenylene bridging groups.

The hollow nanotubule materials were further characterized by thermogravimetric analysis (Figure 3.3.20-3.3.22). The ethenylene-bridged hollow nanotubules show similar weight loss behavior to ethenylene-bridged hollow nanospheres. This indicates that the nanotubules are indeed template by the Pluronic (P123) block copolymer.

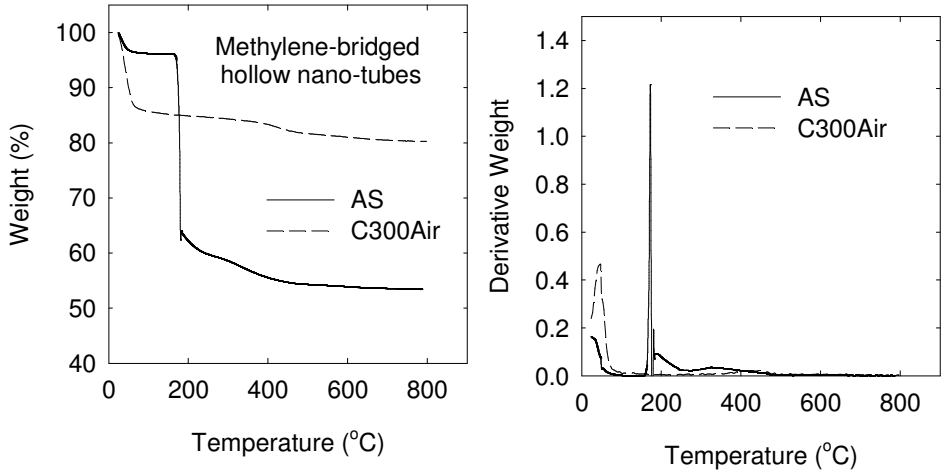

Figure 3.3.20 TGA and differential TGA of a) as-synthesized and b) calcined under air at 300 °C methylene-bridged nanotubules. The measurement was performed under air atmosphere.

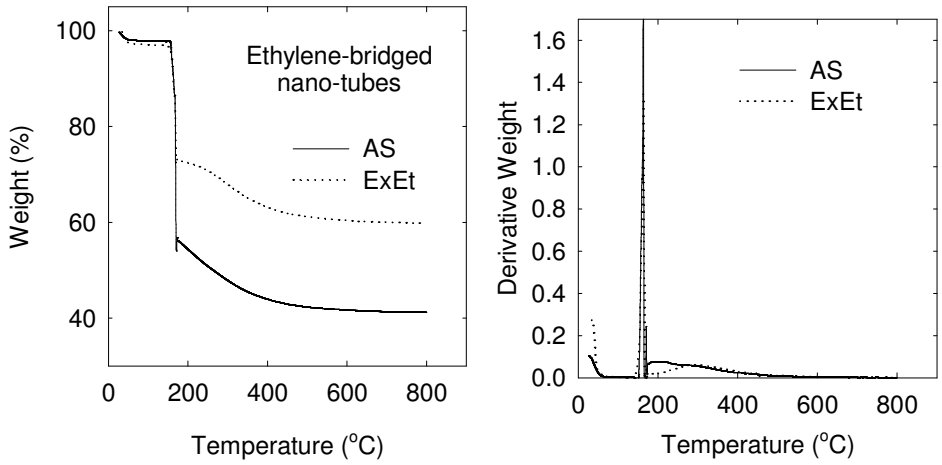

Figure 3.3.21 TGA and differential TGA of a) as-synthesized and b) ethanol-extracted ethylene-bridged nanotubules. The measurement was performed under air atmosphere.

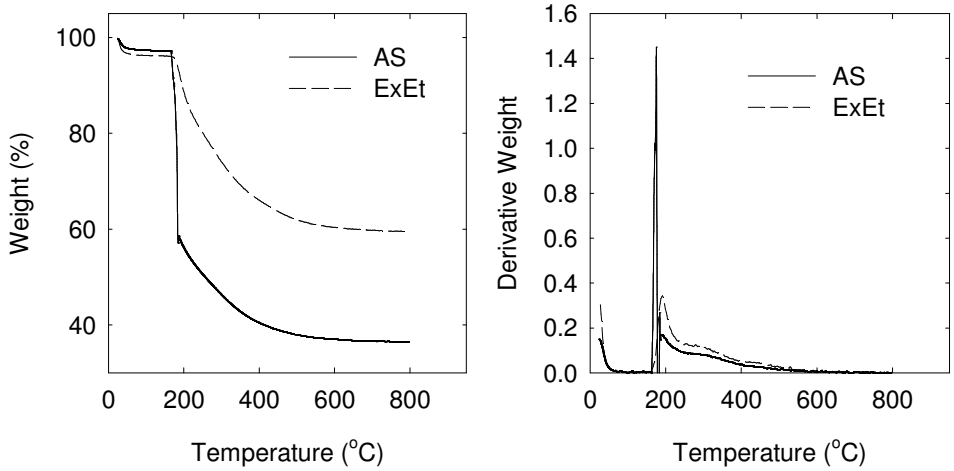

Figure 3.3.22 TGA and differential TGA of a) as-synthesized and b) ethanol-extracted ethenylene-bridged nanotubules. The measurement was performed under air atmosphere.

4. Conclusions

In the first part, we described the versatile route for the synthesis of 2-dimensional hexagonal structures with various organic bridging groups in the silica frameworks. We found that in the 10-18 ^{o}C range, the combination of Pluronic P123 triblock copolymer and cyclohexane or 1,3,5-triisopropylbenzene affords a miceller template for ultra-large-pore 2-D hexagonal periodic mesoporus organosilicas with a variety of framework compositions, including aliphatic and aromatic bridging groups. As the initial synthesis temperature decreases, the unit-cell parameter and the mesopore size tend to increase. The unit-cell enlargement is paralleled by a decrease in the degree of structural ordering and pore size uniformity, eventually reaching the temperature at which disordered materials are obtained, which in some cases still have quite uniform pore diameter. The temperature range at which the unit-cell parameter and pore size are adjustable dependents on the identity of the bridging group in the PMO precursor. The large cylindrical mesopores of the 2-D hexagonal PMOs exhibit narrow entrances or internal constrictions, which can be widened by increasing the temperature of the hydrothermal treatment, but are difficult to fully eliminate. These observations suggest that the organosilica precursor interacts with the hydrophobic domain of the micellar template (that is, with the swollen PPO domain), mediating the micelle formation or swelling process, perhaps partially cross-linking in the hydrophobic domain. The (100) interplanar spacing up to 21-26 nm achievable for 2-D hexagonal PMOs approaches the upper limit of the d_{100} range reported for SBA-15 silica synthesized using P123/TIPB combination (~26 nm).[116] On the other hand, pore diameters attainable for PMOs were somewhat smaller (up to ~ 20 nm; nominal (BJH) pore diameter up to 20-27 nm) than those

achievable for SBA-15 (up to ~26 nm; nominal (BJH) pore diameter up to ~34 nm), which is related to a larger pore wall thickness of PMOs. The proposed approach of using judiciously chosen swelling agents to mediate the formation of large-pore PMOs at low temperatures was found applicable for PMOs with both aliphatic (saturated and unsaturated) and aromatic bridging groups and is thus expected to be generally applicable for a wide variety of PMOs and related materials. It may also be generalizable for other framework compositions. The novel PMOs with the large pore size and tailorable properties open new opportunities in the many applications for which PMOs are contemplated and evaluated.

In the second part, we described the synthesis of large-pore ordered mesoporous organosilicas with spherical pores with ethylene bridging groups in the frameworks. We reported the synthesis of ethylene-bridged ordered mesoporous organosilicas with spherical pores arranged in Fm3m structure and with pore size up to ~ 17 nm. Different aromatic hydrocarbon swelling agents were systematically studied to understand the synthesis of large-pore PMOs. Swelling agents, such as xylene, toluene, and benzene, were used for the first time to synthesize large-pore PMOs with ethylene bridging groups. These swelling agents solubilize in the hydrophobic PPO core of the Pluronic block copolymer micelle more significantly compared to other larger swelling agents, such as mesitylene, triethylbenzene, and triisopropylbenzene. The quality of the materials was found to be high for some new swelling agents, such as toluene and xylene. It was found that decreasing the amount of salt in the reaction mixture increases the unit-cell parameter when xylene was used as the swelling agent. However, the quality of the materials was found to decrease as the amount of salt was lowered. Other swelling agents

did not show any clear behavior in this regard, except for high salt concentrations where smaller pore sizes were observed. This may be due to the different solubilization behavior of these swelling agents in Pluronics F127 block copolymer micelles in the presence of salt. Further, using toluene, high quality PMO was obtained without using any salt. Stirring speed was found to affect the quality of the materials. Too high or too low stirring speed did not produce highly ordered materials. Closed-pore materials were obtained by heating PMOs at 500 ^{o}C under argon atmosphere for the material synthesized using xylene as swelling agent. In general, our approach involves the judicious choice of a swelling agent for a particular surfactant template, which paves the way to large-pore PMOs with face-centered-cubic (Fm3m) structure (nominal (BJH) pore diameter approaching 20 nm) which were unattainable so far. Because of large pore size and tailorable properties, these ethylene-bridged PMOs could find applications.

In the third part of discussion, we described a versatile route through which periodic mesoporous organosilica with hollow nanospheres with different organic groups in the framework. These materials can be attained using Pluronic F127 block copolymer and bis(trialkoxysilyl)organic bridging groups at sub ambient temperature (~ 15 ^{o}C) in presence of a micelle swelling agent. The formation of the hollow nanospheres was induced by using an appreciable lower organosilica precursor/copolymer-surfactant ratio than that typically used to synthesize consolidated structures. Micelle swelling agents of different molecular size, such as benzene, toluene, xylene and trimethylbenzene were used and were found to swell micelles to different extent, which was predicted (in most cases) based on solubilization of swelling agents in block copolymers. Based on different solubilization behavior, organosilica hollow nanospheres of different pore size were

attained. Thermal studies of these nanospheres indicate that they are templated by block copolymer micelles. We were also able to convert the organosilica hollow nanospheres to pure silica nanospheres with smaller pore size. Also different calcinations temperatures can be used to tune the pore size. The pore size of the hollow nanospheres we obtained varied in 10-21 nm range. These nanospheres were also functionalized with different functional groups, such as amine ($-NH_2$), thiol (-SH), and methyl groups. Further, based on understanding of synthesis of hollow nanospheres, under conditions involving low framework-precursor/surfactant ratio, we were able to synthesize hollow nanotubules using Pluronic P123 block copolymer. Our method is quite general and we believe that this method could be extended for synthesizing other hollow nanospheres and nanotubules consisting of organosilicas possibly.

Appendix 1-Geometrical consideration of 2-dimensional hexagonal structure

A 2-D hexagonal nanostructured material has the following structure:

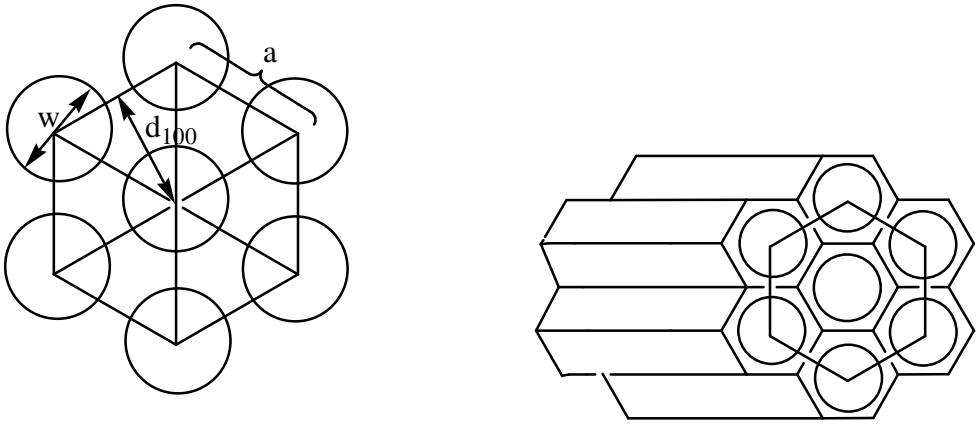

a = unit-cell parameter
w = pore diameter
d_{100} = interplanar spacing
wall thickness, b=a-w

Figure A1 Schematic representations of 2-D hexagonal nanostructured material.

Appendix 2-Geometrical consideration of face-centered cubic structure

A face-centered-cubic nanostructured material has the following structure:

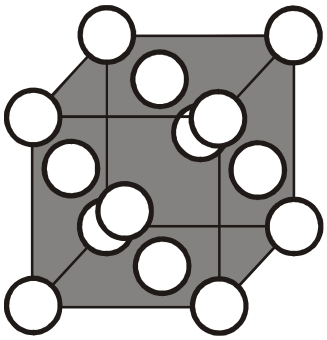

Figure A2 Schematic representation of face-centered-cubic nanostructured material.

where each corner has one pore, which contributes $1/8^{th}$ of pore per unit cell and each face has one pore, which contributes $1/2^{th}$ of pore per unit cell, making four pores per unit cell. The unit cell parameter (a) is defined by the distance between the two corner pore centers, which can be calculated from SAXS pattern.

In case of copolymer- templated nanostructured materials, each main pore may be connected to other ordered mesopores by small pores, (e.g., in the micropore range). In order to calculate the wall thickness more accurately, the following equation[156] is used to accurately determine the pore size:

$$w_d = a\left(\frac{6}{\pi v}\frac{V_{mes}\rho}{(V_{mes}\rho + V_{mic}\rho + 1)}\right)^{\frac{1}{3}} \qquad \text{A.1.1}$$

where a is unit cell parameter for the fcc structure obtained from (111) peak position on SAXS pattern, v=4 is the number of spherical pores in the unit cell, which is 4, ρ is the density of organosilica framework (assumed to be 1.52 g/cm^3),[28] V_{mes} and V_{mic} are mesopore and micropore volumes, respectively.

References

(1) Loy, D. A.; Shea, K. J. *Chem. Rev.* **1995**, *95*, 1431-1442.

(2) Boury, B.; Corriu, R. J. P. *Chem. Commun.* **2002**, 795-802.

(3) Cerveau, G.; Corriu, R. J. P. *Coord. Chem. Rev.* **1998**, *178-180*, 1051-1071.

(4) Boury, B.; Corriu, R. J. P.; Strat, V. L.; Delord, P.; Nobili, M. *Angew. Chem. Int. Ed.* **1999**, *38*, 3172-3175.

(5) Corriu, R. J. P.; Moreau, J. J. E.; Thepot, P.; Man, M. W. C. *Chem. Mater.* **1996**, *8*, 100-106.

(6) Boury, B.; Corriu, R. J. P.; Muramatsu, H. *New J. Chem.* **2002**, *26*, 981-988.

(7) Boury, B.; Corriu, R. J. P.; Delord, P.; Strat, V. L. *J. Non-Cryst. Solids* **2000**, *265*, 41-50.

(8) Ben, F.; Boury, B.; Corriu, R. J. P.; Strat, V. L. *Chem. Mater.* **2000**, *12*, 3249-3252.

(9) Corriu, R. J. P.; Moreau, J. J. E.; Thepot, P.; Man, M. W. C. *Chem. Mater.* **1992**, *4*, 1217-1224.

(10) Cerveau, G.; Corriu, R. J. P. *J. Mater. Chem.* **2001**, *11*, 713-717.

(11) Shea, K. J.; Loy, D. A.; Webster, O. *J. Am. Chem. Soc.* **1992**, *114*, 6700-6710.

(12) Shea, K. J.; Loy, D. A.; Webster, O. W. *Chem. Mater.* **1989**, *1*, 572-574.

(13) Cerveau, G.; Corriu, R. J. P.; Framery, E. *Polyhedron* **2000**, *19*, 307-313.

(14) Cerveau, G.; Corriu, R. J. P.; Fischmeister-Lepeytre, C. *J. Mater. Chem.* **1999**, *9*, 1149-1154.

(15) Loy, D. A.; Jamison, G. M.; Baugher, B. M.; Russick, E. M.; Assink, R. A.; Prabakar, S.; Shea, K. J. *J. Non-Cryst. Solids* **1995**, *186*, 44-53.

(16) Cerveau, G.; Corriu, R. J. P.; Framery, E. *Chem. Commun.* **1999**, 2081-2081.

(17) Loy, D. A.; Shea, K. J.; Russick, E. M. *Mat. Res. Soc. Symp. Proc.* **1992**, *271*, 699-704.

(18) Oviatt Jr., H. W.; Shea, K. J.; Small, J. H. *Chem. Mater.* **1993**, *5*, 943-950.

(19) Boury, B.; Chevalier, P.; Corriu, R. J. P.; Delord, P.; Moreau, J. J. E.; Chiman, M. W. *Chem. Mater.* **1999**, *11*, 281-291.

(20) Loy, D. A.; Russick, E. M.; Yamanaka, S. A.; Baugher, B. M. *Chem. Mater.* **1997**, *9*, 2264-2268.

(21) Cerveau, G.; Corriu, R. J. P.; Lepeytre, C. *J. Organomet. Chem.* **1997**, *548*, 99-103.

(22) Cerveau, G.; Corriu, R. J. P.; Framery, E.; Ghosh, S.; Mutin, H. P. *J. Mater. Chem.* **2002**, *12*, 3021-3026.

(23) Chevalier, P.; Corriu, R. J. P.; Delord, P.; Moreau, J. J. E.; Man, M. W. C. *New J. Chem.* **1998**, 423-433.

(24) Brutchey, R. L.; Goldberger, J. E.; Koffas, T. S.; Tilley, T. D. *Chem. Mater.* **2003**, *15*, 1040-1046.

(25) Chevalier, P. M.; Ou, D. L. *J. Mater. Chem.* **2002**, *12*, 3003-3009.

(26) Feng, Q.; Xu, J.; Dong, H.; Li, S.; Wei, Y. *J. Mater. Chem.* **2000**, *10*, 2490-2494.

(27) Cerveau, G.; Corriu, R. J. P.; Framery, E. *J. Mater. Chem.* **2000**, *10*, 1617-1622.

(28) Cerveau, G.; Corriu, R. J. P.; Framery, E. *J. Mater. Chem.* **2000**, *10*, 1617-1622.

(29) Shea, K. J.; Loy, D. A. *Chem. Mater.* **2001**, *13*, 3306-3319.

(30) Ben, F.; Boury, B.; Corriu, R. J. P. *Adv. Mater.* **2002**, *14*, 1081-1084.

(31) Boury, B.; Ben, F.; Corriu, R. J. P. *Angew. Chem. Int. Ed.* **2001**, *40*, 2853-2856.

(32) Liu, N.; Yu, K.; Smarsly, B.; Dunphy, D. R.; Jiang, Y.-B.; Brinker, C. J. *J. Am. Chem. Soc.* **2002**, *124*, 14540-14541.

(33) Muramatsu, H.; Corriu, R.; Boury, B. *J. Am. Chem. Soc.* **2003**, *125*, 854-855.

(34) Bellussi, G.; Carati, A.; Paola, E. D.; Millini, R.; Parker Jr., W. O. N.; Rizzo, C.; Zanardi, S. *Microporous Mesoporous Mater.* **2008**, *113*, 252-260.

(35) Beck, J. S.; Vartuli, J. C.; Roth, W. J.; Leonowicz, M. E.; Kresge, C. T.; Schmitt, K. D.; Chu, C. T. W.; Olson, D. H.; Sheppard, E. W.; McCullen, S. B.; Higgins, J. B.; Schlenker, J. L. *J. Am. Chem. Soc.* **1992**, *114*, 10834-10843.

(36) Kresge, C. T.; Leonowicz, M. E.; Roth, W. J.; Vartuli, J. C.; Beck, J. S. *Nature* **1992**, *359*, 710-712.

(37) Yanagisawa, T.; Shimizu, T.; Kuroda, K.; Kato, C. *Bull. Chem. Soc. Jpn.* **1990**, *63*, 1535-1537.

(38) Yanagisawa, T.; Shimizu, T.; Kuroda, K.; Kato, C. *Bull. Chem. Soc. Jpn.* **1990**, *63*, 988-992.

(39) Inagaki, S.; Fukushima, Y.; Kuroda, K. *J. Chem. Soc., Chem. Commun.* **1993**, 680-682.

(40) Monnier, A.; Schuth, F.; Huo, Q.; Kumar, D.; Margolese, D.; Maxwell, R. S.; Stucky, G. D.; Krishnamurthy, M.; Petroff, P.; Firouzi, A.; Janicke, M.; Chmelka, B. F. *Science* **1993**, *261*, 1299-1303.

(41) Huo, Q.; Margolese, D. I.; Ciesla, U.; Feng, P.; Gier, T. E.; Sieger, P.; Leon, R.; Petroff, P. M.; Schueth, F.; Stucky, G. D. *Nature* **1994**, *368*, 317-321.

(42) Huo, Q.; Leon, R.; Petroff, P. M.; Stucky, G. D. *Science* **1995**, *268*, 1324-1327.

(43) Huo, Q.; Margolese, D. I.; Stucky, G. D. *Chem. Mater.* **1996**, *8*, 1147-1160.

(44) Inagaki, S.; Guan, S.; Fukushima, Y.; Ohsuna, T.; Terasaki, O. *J. Am. Chem. Soc.* **1999**, *121*, 9611-9614.

(45) Asefa, T.; MacLachlan, M. J.; Coombs, N.; Ozin, G. A. *Nature* **1999**, *402*, 867-871.

(46) Melde, B. J.; Holland, B. T.; Blanford, C. F.; Stein, A. *Chem. Mater.* **1999**, *11*, 3302-3308.

(47) Yoshina-Ishii, C.; Asefa, T.; Coombs, N.; MacLachlan, M. J.; Ozin, G. A. *Chem. Commun.* **1999**, 2539-2540.

(48) Schueth, F. *Chem. Mater.* **2001**, *13*, 3184-3195.

(49) Davis, M. E. *Nature* **2002**, *417*, 813-821.

(50) Wan, Y.; Zhao, D. *Chem. Rev.* **2007**, *107*, 2821-2860.

(51) Hoffmann, F.; Cornelius, M.; Morell, J.; Froba, M. *Angew. Chem. Int. Ed.* **2006**, *45*, 3216-3251.

(52) Fujita, S.; Inagaki, S. *Chem. Mater.* **2008**, *20*, 891-908.

(53) Attard, G. S.; Glyde, J. C.; Goltner, C. G. *Nature* **1995**, *378*, 366-368.

(54) Attard, G. S.; Bartlett, P. N.; Coleman, N. R. B.; Elliott, J. M.; Owen, J. R.; Wang, J. H. *Science* **1997**, *278*, 838-840.

(55) Bagshaw, S. A.; Prouzet, E.; Pinnavaia, T. J. *Science* **1995**, *269*, 1242-1244.

(56) Zhao, D.; Huo, Q.; Feng, J.; Chmelka, B. F.; Stucky, G. D. *J. Am. Chem. Soc.* **1998**, *120*, 6024-6036.

(57) Zhao, D.; Feng, J.; Huo, Q.; Melosh, N.; Frederickson, G. H.; Chmelka, B. F.; Stucky, G. D. *Science* **1998**, *279*, 548-552.

(58) Antonietti, M.; Berton, B.; Goeltner, C.; Hentze, H. P. *Adv. Mater.* **1998**, *10*, 154-159.

(59) Goltner, C. G.; Berton, B.; Kramer, E.; Antonietti, M. *Chem. Commun.* **1998**, 2287-2288.

(60) Goltner, C. G.; Henke, S.; Weissenberger, M. C.; Antonietti, M. *Angew. Chem. Int. Ed.* **1998**, *37*, 613-616.

(61) Kramer, E.; Forster, S.; Goltner, C.; Antonietti, M. *Langmuir* **1998**, *14*, 2027-2031.

(62) Tanev, P. T.; Chibwe, M.; Pinnavaia, T. J. *Nature* **1994**, *368*, 321-323.

(63) Tanev, P. T.; Pinnavaia, T. J. *Science* **1995**, *267*, 865-867.

(64) Alexandridis, P.; Alan Hatton, T. *Colloids Surf. A: Physicochem. Engineering Aspects* **1995**, *96*, 1-46.

(65) Almgren, M.; Brown, W.; Hvidt, S. *Colloid Polym Sci.* **1995**, *273*, 2-15.

(66) Melosh, N. A.; Lipic, P.; Bates, F. S.; Wudl, F.; Stucky, G. D.; Fredrickson, G. H.; Chmelka, B. F. *Macromolecules* **1999**, *32*, 4332-4342.

(67) De Paul, S. M.; Zwanziger, J. W.; Ulrich, R.; Wiesner, U.; Spiess, H. W. *J. Am. Chem. Soc.* **1999**, *121*, 5727-5736.

(68) Mandal, M.; Kruk, M. *J. Mater. Chem.* **2010**, *20*, 7506-7516.

(69) Messinger, R.; Mandal, M.; Chmelka, B. F.; Kruk, M. **in preparation**.

(70) Ryoo, R.; Ko, C. H.; Kruk, M.; Antochshuk, V.; Jaroniec, M. *J. Phys. Chem. B* **2000**, *104*, 11465-11471.

(71) Kruk, M.; Jaroniec, M.; Ko, C. H.; Ryoo, R. *Chem. Mater.* **2000**, *12*, 1961-1968.

(72) Choi, M.; Heo, W.; Kleitz, F.; Ryoo, R. *Chem. Commun.* **2003**, 1340-1341.

(73) Jaroniec, M.; Kruk, M.; Shin, H. J.; Ryoo, R.; Sakamoto, Y.; Terasaki, O. *Microporous Mesoporous Mater.* **2001**, *48*, 127-134.

(74) Van Der Voort, P.; Ravikovitch, P. I.; De Jong, K. P.; Benjelloun, M.; Van Bavel, E.; Janseen, A. H.; Neimark, A. V.; Weckhuysen, B. M.; Vansant, E. F. *J. Phys. Chem. B* **2002**, *106*, 5873-5877.

(75) Kruk, M.; Jaroniec, M.; Joo, S. H.; Ryoo, R. *J. Phys. Chem. B* **2003**, *107*, 2205-2213.

(76) Muth, O.; Schellbach, C.; Froba, M. *Chem. Commun.* **2001**, 2032-2033.

(77) Zhu, H. G.; Jones, D. J.; Zajac, J.; Roziere, J.; Dutartre, R. *Chem. Commun.* **2001**, 2568-2569.

(78) Matos, J. R.; Kruk, M.; Mercuri, L. P.; Jaroniec, M.; Asefa, T.; Coombs, N.; Ozin, G. A.; Kamiyama, T.; Terasaki, O. *Chem. Mater.* **2002**, *14*, 1903-1905.

(79) Guo, W. P.; Kim, I.; Ha, C. S. *Chem. Commun.* **2003**, 2692-2693.

(80) Guo, W.; Li, X.; Zhao, X. S. *Microporous Mesoporous Mater.* **2006**, *93*, 285-293.

(81) Asefa, T.; MacLachlan, M. J.; Grondey, H.; Coombs, N.; Ozin, G. A. *Angew. Chem., Int. Ed.* **2000**, *39*, 1808-1811.

(82) Guan, S.; Inagaki, S.; Ohsuna, T.; Terasaki, O. *J. Am. Chem. Soc.* **2000**, *122*, 5660-5661.

(83) Ide, A.; Voss, R.; Scholz, G.; Ozin, G. A.; Antonietti, M.; Thomas, A. *Chem. Mater.* **2007**, *19*, 2649-2657.

(84) Gao, L.; Wei, F.; Zhou, Y.; Fan, X. X.; Wang, Y.; Zhu, J. H. *Chem. Eur. J.* **2009**, *15*, 8310-8318.

(85) Inagaki, S.; Guan, S.; Ohsuna, T.; Terasaki, O. *Nature* **2002**, *416*, 304-307.

(86) Kapoor, M. P.; Yang, Q. H.; Inagaki, S. *J. Am. Chem. Soc.* **2002**, *124*, 15176-15177.

(87) Kuroki, M.; Asefa, T.; Whitnal, W.; Kruk, M.; Yoshina-Ishii, C.; Jaroniec, M.; Ozin, G. A. *J. Am. Chem. Soc.* **2002**, *124*, 13886-13895.

(88) Landskron, K.; Hatton, B. D.; Perovic, D. D.; Ozin, G. A. *Science* **2003**, *302*, 266-269.

(89) Landskron, K.; Ozin, G. A. *Angew. Chem. Int. Ed.* **2005**, *44*, 2107-2109.

(90) Zhang, W.-H.; Zhang, X.; Hua, Z.; Harish, P.; Schroeder, F.; Hermes, S.; Cadenbach, T.; Shi, J.; Fischer, R. A. *Chem. Mater.* **2007**, *19*, 2663-2670.

(91) Zhang, L.; Abbenhuis, H. C. L.; Yang, Q.; Wang, Y.-M.; Magusin, P. C. M. M.; Mezari, B.; van Santen, R. A.; Li, C. *Angew. Chem. Int. Ed.* **2007**, *46*, 5003-5006.

(92) Hunks, W. J.; Ozin, G. A. *Adv. Funct. Mater.* **2005**, *15*, 259-266.

(93) Landskron, K.; Ozin, G. A. *Science* **2004**, *306*, 1529-1532.

(94) Burleigh, M. C.; Jayasundera, S.; Spector, M. S.; Thomas, C. W.; Markowitz, M. A.; Gaber, B. P. *Chem. Mater.* **2003**, *16*, 3-5.

(95) Burleigh, M. C.; Dai, S.; Hagaman, E. W.; Lin, J. S. *Chem. Mater.* **2001**, *13*, 2537-2546.

(96) Asefa, T.; Kruk, M.; MacLachlan, M. J.; Coombs, N.; Grondey, H.; Jaroniec, M.; Ozin, G. A. *J. Am. Chem. Soc.* **2001**, *123*, 8520-8530.

(97) Burleigh, M. C.; Markowitz, M. A.; Spector, M. S.; Gaber, B. P. *J. Phys. Chem. B* **2001**, *105*, 9935-9942.

(98) Grudzien, R. M.; Grabicka, B. E.; Pikus, S.; Jaroniec, M. *Chem. Mater.* **2006**, *18*, 1722-1725.

(99) Alvaro, M.; Ferrer, B.; Fornes, V.; Garcia, H. *Chem. Commun.* **2001**, 2546-2547.

(100) Alvaro, M.; Ferrer, B.; Garcia, H.; Rey, F. *Chem. Commun.* **2002**, 2012-2013.

(101) Olkhovyk, O.; Jaroniec, M. *J. Am. Chem. Soc.* **2005**, *127*, 60-61.

(102) Cho, E.-B.; Kim, D.; Gorka, J.; Jaroniec, M. *J. Phys. Chem. C* **2009**, *113*, 5111-5119.

(103) Kapoor, M. P.; Bhaumik, A.; Inagaki, S.; Kuraoka, K.; Yazawa, T. *J. Mater. Chem.* **2002**, *12*, 3078-3083.

(104) Bhaumik, A.; Kapoor, M. P.; Inagaki, S. *Chem. Commun.* **2003**, 470-471.

(105) Shylesh, S.; Singh, A. P. *Microporous Mesoporous Mater.* **2006**, *94*, 127-138.

(106) Zhao, L.; Zhu, G. S.; Zhang, D. L.; Di, Y.; Chen, Y.; Terasaki, O.; Qiu, S. L. *J. Phys. Chem. B* **2005**, *109*, 764-768.

(107) Zhou, X.; Qiao, S.; Hao, N.; Wang, X.; Yu, C.; Wang, L.; Zhao, D.; Lu, G. Q. *Chem. Mater.* **2007**, *19*, 1870-1876.

(108) Mandal, M.; Kruk, M. *J. Phys. Chem. C* **submitted**.

(109) Zhang, Z. D.; Yan, X. X.; Tian, B. Z.; Shen, S. D.; Chen, D. H.; Zhu, G. S.; Qiu, S. L.; Zhao, D. Y. *Chem. Lett.* **2005**, *34*, 182-183.

(110) Lee, H. I.; Pak, C.; Yi, S. H.; Shon, J. K.; Kim, S. S.; So, B. G.; Chang, H.; Yie, J. E.; Kwon, Y.-U.; Kim, J. M. *J. Mater. Chem.* **2005**, *15*, 4711-4717.

(111) Liang, Y.; Hanzlik, M.; Anwander, R. *J. Mater. Chem.* **2006**, *16*, 1238-1253.

(112) Kleitz, F.; Choi, S. H.; Ryoo, R. *Chem. Commun.* **2003**, 2136-2137.

(113) Matos, J. R.; Kruk, M.; Mercuri, L. P.; Jaroniec, M.; Zhao, L.; Kamiyama, T.; Terasaki, O.; Pinnavaia, T. J.; Liu, Y. *J. Am. Chem. Soc.* **2003**, *125*, 821-829.

(114) Kim, T. W.; Ryoo, R.; Kruk, M.; Gierszal, K. P.; Jaroniec, M.; Kamiya, S.; Terasaki, O. *J. Phys. Chem. B* **2004**, *108*, 11480-11489.

(115) Fan, J.; Yu, C.; Lei, J.; Zhang, Q.; Li, T.; Tu, B.; Zhou, W.; Zhao, D. *J. Am. Chem. Soc.* **2005**, *127*, 10794-10795.

(116) Cao, L.; Man, T.; Kruk, M. *Chem. Mater.* **2009**, *21*, 1144-1153.

(117) Hammoudi, H.; Yang, Y.; Moudrakovski, I. L.; Lang, S.; Sayari, A. *J. Phys. Chem. B* **2001**, *105*, 9118-9123.

(118) Rebbin, V.; Jakubowski, M.; Potz, S.; Froba, M. *Microporous Mesoporous Mater.* **2004**, *72*, 99-104.

(119) Bion, N.; Ferreira, P.; Valente, A.; Goncalves, I. S.; Rocha, J. *J. Mater. Chem.* **2003**, *13*, 1910-1913.

(120) Park, S. S.; Ha, C.-S. *Chem. Mater.* **2005**, *17*, 3519-3523.

(121) Burleigh, M. C.; Markowitz, M. A.; Spector, M. S.; Gaber, B. P. *J. Phys. Chem. B* **2002**, *106*, 9712-9716.

(122) Zhang, W.-H.; Daly, B.; O'Callaghan, J.; Zhang, L.; Shi, J.-L.; Li, C.; Morris, M. A.; Holmes, J. D. *Chem. Mater.* **2005**, *17*, 6407-6415.

(123) Bao, X. Y.; Li, X.; Zhao, X. S. *J. Phys. Chem. B* **2006**, *110*, 2656-2661.

(124) Guo, W. P.; Park, J. Y.; Oh, M. O.; Jeong, H. W.; Cho, W. J.; Kim, I.; Ha, C. S. *Chem. Mater.* **2003**, *15*, 2295-2298.

(125) Bao, X. Y.; Zhao, X. S.; Li, X.; Chia, P. A.; Li, J. *J. Phys. Chem. B* **2004**, *108*, 4684-4689.

(126) Bao, X.; Zhao, X. S.; Li, X.; Li, J. *Appl. Surf. Sci.* **2004**, *237*, 380-386.

(127) Cho, E.-B.; Char, K. *Chem. Mater.* **2004**, *16*, 270-275.

(128) Wang, W.; Xie, S.; Zhou, W.; Sayari, A. *Chem. Mater.* **2004**, *16*, 1756-1762.

(129) Vercaemst, C.; Friedrich, H.; de Jongh, P. E.; Neimark, A. V.; Goderis, B.; Verpoort, F.; Van Der Voort, P. *J. Phys. Chem. C* **2009**, *113*, 5556-5562.

(130) Goto, Y.; Inagaki, S. *Chem. Commun.* **2002**, 2410-2411.

(131) Morell, J.; Wolter, G.; Froba, M. *Chem. Mater.* **2005**, *17*, 804-808.

(132) Chan, Y.-T.; Lin, H.-P.; Mou, C.-Y.; Liu, S.-T. *Microporous Mesoporous Mater.* **2009**, *123*, 331-337.

(133) Ryoo, R.; Park, I. S.; Jun, S.; Lee, C. W.; Kruk, M.; Jaroniec, M. *J. Am. Chem. Soc.* **2001**, *123*, 1650-1657.

(134) Deng, Y.; Yu, T.; Wan, Y.; Shi, S.; Meng, Y.; Gu, D.; Zhang, L.; Huang, Y.; Liu, C.; Wu, X.; Zhao, D. *J. Am. Chem. Soc.* **2007**, *129*, 1690-1697.

(135) Huang, L.; Yan, X.; Kruk, M. *Langmuir* **submitted**.

(136) Hudson, S.; Cooney, J.; Hodnett, B. K.; Magner, E. *Chem. Mater.* **2007**, *19*, 2049-2055.

(137) Burleigh, M. C.; Markowitz, M. A.; Wong, E. M.; Lin, J. S.; Gaber, B. P. *Chem. Mater.* **2001**, *13*, 4411-4412.

(138) Liang, Y. C.; Anwander, R. *Microporous Mesoporous Mater.* **2004**, *72*, 153-165.

(139) Jiang, D.; Gao, J.; Li, J.; Yang, Q.; Li, C. *Microporous Mesoporous Mater.* **2008**, *113*, 385-392.

(140) Nakanishi, K.; Kanamori, K. *J. Mater. Chem.* **2005**, *15*, 3776-3786.

(141) Vercaemst, C.; Jongh, P. E. d.; Meeldijk, J. D.; Goderis, B.; Verpoort, F.; Voort, P. V. D. *Chem. Commun.* **2009**, 4052-4054.

(142) Li, C.; Liu, J.; Shi, X.; Yang, J.; Yang, Q. *J. Phys. Chem. C* **2007**, *111*, 10948-10954.

(143) Chung, J.-S.; Kim, D.-J.; Ahn, W.-S.; Ko, J.-H.; Cheong, W.-J. *Korean J. Chem. Eng.* **2004**, *21*, 132-139.

(144) Zhong, H.; Zhu, G.; Yang, J.; Wang, P.; Yang, Q. *Microporous Mesoporous Mater.* **2007**, *100*, 259-267.

(145) Zhang, H.; Sun, J.; Ma, D.; Weinberg, G.; Su, D. S.; Bao, X. *J. Phys. Chem. B* **2006**, *110*, 25908-25915.

(146) Sun, J.; Zhang, H.; Ma, D.; Chen, Y.; Bao, X.; Klein-Hoffmann, A.; Pfaender, N.; Su, D. S. *Chem. Commun.* **2005**, 5343-5345.

(147) Kruk, M.; Cao, L. *Langmuir* **2007**, *23*, 7247-7254.

(148) Kruk, M.; Hui, C. M. *Microporous Mesoporous Mater.* **2008**, *114*, 64-73.

(149) Schmidt-Winkel, P.; Lukens, J., W. W.; Zhao, D.; Yang, P.; Chmelka, B. F.; Stucky, G. D. *J. Am. Chem. Soc.* **1999**, *121*, 254-255.

(150) Sayari, A.; Kruk, M.; Jaroniec, M.; Moudrakovski, I. L. *Adv. Mater.* **1998**, *10*, 1376-1379.

(151) Nagarajan, R. *Colloids and Surfaces B: Biointerfaces* **1999**, *16*, 55-72.

(152) Nagarajan, R.; Barry, M.; Ruckenstein, E. *Langmuir* **1986**, *2*, 210-215.

(153) Liang, Y. C.; Hanzlik, M.; Anwander, R. *Chem. Commun.* **2005**, 525-527.

(154) Liang, Y.; Erichsen, E. S.; Hanzlik, M.; Anwander, R. *Chem. Mater.* **2008**, *20*, 1451-1458.

(155) Sayari, A.; Hamoudi, S.; Yang, Y.; Moudrakovski, I. L.; Ripmeester, J. R. *Chem. Mater.* **2000**, *12*, 3857-3863.

(156) Ravikovitch, P. I.; Neimark, A. V. *Langmuir* **2002**, *18*, 1550-1560.

(157) Lu, Y. F.; Fan, H. Y.; Doke, N.; Loy, D. A.; Assink, R. A.; LaVan, D. A.; Brinker, C. J. *J. Am. Chem. Soc.* **2000**, *122*, 5258-5261.

(158) Cho, E. B.; Kwon, K. W.; Char, K. *Chem. Mater.* **2001**, *13*, 3837-3839.

(159) Pauletti, A.; Handjani, S.; Fernandez-Martin, C.; Gervais, C.; Babonneau, F. *J. Ceram. Soc. Jpn.* **2008**, *116*, 449-453.

(160) Cho, E.-B.; Kim, D.; Gorka, J.; Jaroniec, M. *J. Mater. Chem.* **2009**, *19*, 2076-2081.

(161) Goto, Y.; Inagaki, S. *Microporous Mesoporous Mater.* **2006**, *89*, 103-108.

(162) Kruk, M.; Hui, C. M. *J. Am. Chem. Soc.* **2008**, *130*, 1528-1529.

(163) Budi Hartono, S.; Qiao, S. Z.; Jack, K.; Ladewig, B. P.; Hao, Z.; Lu, G. Q. *Langmuir* **2009**, *25*, 6413-6424.

(164) Budi Hartono, S.; Qiao, S. Z.; Liu, J.; Jack, K.; Ladewig, B. P.; Hao, Z.; Lu, G. Q. *J. Phys. Chem. C* **2010**, *114*, 8353-8362.

(165) Fan, J.; Yu, C.; Gao, F.; Lei, J.; Tian, B.; Wang, L.; Luo, Q.; Tu, B.; Zhou, W.; Zhao, D. *Angew. Chem. Int. Ed.* **2003**, *42*, 3146-3150.

(166) Yamamoto, K.; Nohara, Y.; Tatsumi, T. *Chem. Lett.* **2001**, 648-649.

(167) Fukuoka, A.; Sakamoto, Y.; Guan, S.; Inagaki, S.; Sugimoto, N.; Fukushima, Y.; Hirahara, K.; Iijima, S.; Ichikawa, M. *J. Am. Chem. Soc.* **2001**, *123*, 3373-3374.

(168) Burleigh, M. C.; Markowitz, M. A.; Spector, M. S.; Gaber, B. P. *Environ. Sci. Technol.* **2002**, *36*, 2515-2518.

(169) Remskar, M. *Adv. Mater.* **2004**, *16*, 1497-1504.

(170) Harada, M.; Adachi, M. *Adv. Mater.* **2000**, *12*, 839-841.

(171) Xiong, Y.; Mayers, B., T.; Xia, Y. *Chem. Commun.* **2005**, 5013-5022.

(172) Tenne, R. *Angew. Chem. Int. Ed.* **2003**, *42*, 5124-5132.

(173) Xia, Y.; Yang, P.; Sun, Y.; Wu, Y.; Mayers, B.; Gates, B.; Yin, Y.; Kim, F.; Yan, H. *Adv. Mater.* **2003**, *15*, 353-389.

(174) Lee, H.; Char, K. *ACS Applied Materials & Interfaces* **2009**, *1*, 913-920.

(175) Huo, Q.; Liu, J.; Wang, L.-Q.; Jiang, Y.; Lambert, T. N.; Fang, E. *J. Am. Chem. Soc.* **2006**, *128*, 6447-6453.

(176) Khanal, A.; Inoue, Y.; Yada, M.; Nakashima, K. *J. Am. Chem. Soc.* **2007**, *129*, 1534-1535.

(177) Djojoputro, H.; Zhou, X. F.; Qiao, S. Z.; Wang, L. Z.; Yu, C. Z.; Lu, G. Q. *J. Am. Chem. Soc.* **2006**, *128*, 6320-6321.

(178) Liu, J.; Yang, Q.; Zhang, L.; Yang, H.; Gao, J.; Li, C. *Chem. Mater.* **2008**, *20*, 4268-4275.

(179) Liu, J.; Bai, S.; Zhong, H.; Li, C.; Yang, Q. *J. Phys. Chem. C* **2010**, *114*, 953-961.

(180) Hao, N.; Wang, H.; Webley, P. A.; Zhao, D. *Microporous Mesoporous Mater.* **2010**, *132*, 543-551.

(181) Yuan, J.-J.; Mykhaylyk, O. O.; Ryan, A. J.; Armes, S. P. *J. Am. Chem. Soc.* **2007**, *129*, 1717-1723.

(182) Tang, J.; Zhou, X.; Zhao, D.; Lu, G. Q.; Zou, J.; Yu, C. *J. Am. Chem. Soc.* **2007**, *129*, 9044-9048.

(183) Tang, J.; Liu, J.; Wang, P.; Zhong, H.; Yang, Q. *Microporous Mesoporous Mater.* **2010**, *127*, 119-125.

(184) Yu, M.; Wang, H.; Zhou, X.; Yuan, P.; Yu, C. *J. Am. Chem. Soc.* **2007**, *129*, 14576-14577.

(185) Blas, H.; Save, M.; Pasetto, P.; Boissiere, C.; Sanchez, C.; Charleux, B. *Langmuir* **2008**, *24*, 13132-13137.

(186) Yang, J.; Lind, J. U.; Trogler, W. C. *Chem. Mater.* **2008**, *20*, 2875-2877.

(187) Du, L.; Liao, S.; Khatib, H. A.; Stoddart, J. F.; Zink, J. I. *J. Am. Chem. Soc.* **2009**, *131*, 15136-15142.

(188) Corma, A.; Diaz, U.; Arrica, M.; Fernandez, E.; Ortega, I. *Angew. Chem. Int. Ed.* **2009**, *48*, 6247-6250.

(189) Wang, J.-G.; Li, F.; Zhou, H.-J.; Sun, P.-C.; Ding, D.-T.; Chen, T.-H. *Chem. Mater.* **2009**, *21*, 612-620.

(190) Tan, L. H.; XIng, S.; Chen, T.; Chen, G.; Huang, X.; Zhang, H.; Chen, H. *ACS Nano* **2009**, *3*, 3469-3474.

(191) Agrawal, M.; Gupta, S.; Pich, A.; Zafeiropoulos, N. E.; Stamm, M. *Chem. Mater.* **2009**, *21*, 5343-5348.

(192) Sing, K. S. W.; Everett, D. H.; Haul, R. A. W.; Moscou, L.; Pierotti, R. A.; Rouquerol, J.; Siemieniewska, T. *Pure Appl. Chem.* **1985**, *57*, 603-619.

(193) Barrett, E. P.; Joyner, L. G.; Halenda, P. P. *J. Am. Chem. Soc.* **1951**, *73*, 373-380.

(194) Kruk, M.; Jaroniec, M.; Sayari, A. *Langmuir* **1997**, *13*, 6267-6273.

(195) Jaroniec, M.; Kruk, M.; Olivier, J. P. *Langmuir* **1999**, *15*, 5410-5413.

(196) Gregg, S. J.; Sing, K. S. W. *Academic Press: London* **1982**.

(197) Sayari, A.; Liu, P.; Kruk, M.; Jaroniec, M. *Chem. Mater.* **1997**, *9*, 2499-2506.

(198) Rouquerol, J.; Avnir, D.; Fairbridge, C. W.; Everett, D. H.; Haynes, J. H.; Pernicone, N.; Ramsay, J. D. F.; Sing, K. S. W.; Unger, K. K. *Pure Appl. Chem.* **1994**, *66*, 1739-1758.

(199) Cao, L.; Kruk, M. *Colloids Surf. A: Physicochem. Engineering Aspects* **2010**, *357*, 91-96.

(200) Kruk, M.; Jaroniec, M.; Sayari, A. *Chem. Mater.* **1999**, *11*, 492-500.

(201) Kruk, M.; Jaroniec, M. *Chem. Mater.* **2003**, *15*, 2942-2949.

(202) Celer, E. B.; Kruk, M.; Zuzek, Y.; Jaroniec, M. *J. Mater. Chem.* **2006**, *16*, 2824-2833.

(203) Kruk, M.; Jaroniec, M.; Sayari, A. *Microporous Mesoporous Mater.* **1999**, *27*, 217-229.

(204) Kruk, M.; Celer, E. B.; Jaroniec, M. *Chem. Mater.* **2004**, *16*, 698-707.

(205) Kapoor, M. P.; Inagaki, S.; Ikeda, S.; Kakiuchi, K.; Suda, M.; Shimada, T. *J. Am. Chem. Soc.* **2005**, *127*, 8174-8178.

(206) Jain, N. J.; Aswal, V. K.; Goyal, P. S.; Bahadur, P. *J. Phys. Chem. B* **1998**, *102*, 8452-8458.

(207) Smarsly, B.; Xomeritakis, G.; Yu, K.; Liu, N.; Fan, H.; Assink, R. A.; Drewien, C. A.; Ruland, W.; Brinker, C. J. *Langmuir* **2003**, *19*, 7295-7301.

(208) Yu, K.; Smarsly, B.; Brinker, C. J. *Adv. Funct. Mater.* **2003**, *13*, 47-52.

(209) Yu, K.; Wu, X.; Brinker, C. J.; Ripmeester, J. *Langmuir* **2003**, *19*, 7282-7288.

(210) Schmidt, W. *Microporous Mesoporous Mater.* **2009**, *117*, 372-379.